SAILING VESSEL DYNAMICS

Thesis by

Joseph David Titlow

In Partial Fulfillment of the Requirements

for the Degree of

Doctor of Philosophy

California Institute of Technology

Pasadena, California

1978

(Submitted September 30, 1977)

To my mother and father

For the scenery, so to call it, which surrounds the phenomena of rolling motion (especially when these are developed on a very large scale), is for the most part so very striking, and appeals so forcibly to the imagination, that it is almost impossible for a landsman to divest his appreciation of them from passionate colouring, even though he applies himself to the task with the most determinately prosaic intentions. While even those whose life is spent among such phenomena, and who have become familiarized to them by habit, have become accustomed chiefly to regard them under their impressive aspect, and to mould on this all the phraseology in which they describe them; so that even from nautical men it is not easy to obtain statements which can safely be reduced to measure and number.

-W. Froude (1861)

ACKNOWLEDGMENTS

I would like to thank my advisor, Professor Thomas K. Caughey, for the support and enthusiasm he has given to this project.

My wife, Marilyn, helped me a great deal with the numerical calculations and plots. She also worked with our good friend Sharon Vedrode in the preparation of the manuscript.

I am especially grateful to the Hesperides Syndicate for their financial assistance and continuing interest.

ABSTRACT

A general study has been conducted to determine how the dynamics of sailing vessels depend on speed and sailing angle. A simplified model of the forces acting on a sailing vessel has been constructed which includes all rigid body motions and uses the results of full scale tests. Numerical solutions for the steady state conditions and perturbational motions have been calculated based on limited available data. The results for performance and attitude show good agreement with full scale sailing observations; they are close to the optimum conditions reported in practice. The normal modes of sailing vessels appear to be strongly dependent on speed and sailing angle, and they are sensitive to such general parameters as displacement, stiffness, aerodynamic characteristics and rudder effectiveness. Several regions were found where unstable solutions exist.

TABLE OF CONTENTS

		Page
	ACKNOWLEDGMENTS	iv
	ABSTRACT	v
	TABLE OF CONTENTS	vi
	NOMENCLATURE	ix
	LIST OF FIGURES	xiv
	LIST OF TABLES	xx
I.	INTRODUCTION	1
	1.1 Background	1
	1.2 Previous Investigations	2
	1.3 General Objectives and Methods	5
II.	SUMMARY OF THE DYNAMICS OF RIGID BODIES IN FLUID MEDIA	9
	2.1 Reference Frames and Equations of Motion	9
	2.2 Expansion of Forces and Moments	13
	2.3 Normal Modes and Stability of Solutions	21
III.	A DYNAMIC MODEL FOR SAILING VESSELS	25
	3.1 Objectives and Assumptions	25
	3.2 Hull-Keel Forces	27
	3.3 Rudder Forces	41
	3.4 Aerodynamic Forces	46
	3.5 Summary of Elements in the Dynamic Model	52
IV.	DOWNWIND SAILING	54
	4.1 Assumptions	54
	4.2 Steady State Equations and Solutions	56

TABLE OF CONTENTS (CONTINUED)

		Page
4.3	Lateral Equations of Downwind Sailing	57
4.4	Discussion of Numerical Solutions to Lateral Equations	61
4.5	Longitudinal Equations of Downwind Sailing	74
4.6	Discussion of Numerical Solutions to Longitudinal Equations	78
V.	GENERAL SAILING CONDITIONS: STEADY STATE SOLUTIONS	87
5.1	Formulation	87
5.2	Summary of Numerical Methods	90
5.3	Numerical Solutions	93
5.4	Performance	96
5.5	Attitude and Ballasting	102
5.6	Leeway, Helm and Crossflow Angles	105
VI.	GENERAL SAILING CONDITIONS: SOLUTIONS TO PERTURBATION EQUATIONS	111
6.1	Perturbational Equations and Numerical Methods	111
6.2	Base Boat	112
6.3	Discussion of Normal Modes for Base Boat	118
6.4	Base Boat with Gottingen Foil	125
6.5	Heavy Displacement	131
VII.	SUMMARY AND CONCLUSIONS	136
7.1	General	136

TABLE OF CONTENTS (CONCLUDED)

	Page
7.2 Steady State Equations and Solutions	138
7.3 Perturbational Equations and Solutions	138
REFERENCES	141
APPENDIX A. SAILING VESSEL DATA	146
A.1 *Antiope* Data	146
A.2 Hydrodynamic Inertial and Damping Coefficients	150
A.3 Rudder Data	153
A.4 Sail Data	156
A.5 Vessel Geometry and Data	158
APPENDIX B. RESULTS OF STEADY STATE SAILING OBSERVATIONS	166
APPENDIX C. EIGENVALUE PLOTS FOR BASE BOAT	175

NOMENCLATURE

A	perturbation matrix
AR	geometric aspect ratio ($_K$...keel, $_R$...rudder)
A_w	waterplane area $\quad A'_w = \dfrac{A_w}{L^2}$
b_{kj}	normalized modal coefficients
C	damping matrix
$\underline{c}$	initial conditions
C_{K1}, C_{K2}	hull-keel resistance and sideforce coefficients
C_{R1}, C_{R2}	rudder resistance and sideforce coefficients
C_{S1}, C_{S2}	aerodynamic resistance and sideforce coefficients
DLR	displacement to length ratio
d	draft of vessel
$\underline{e}_i$	base vectors of body frame $\mathfrak{F}_B$
$\underline{e}'_i$	base vectors of inertial frame $\mathfrak{F}_I$
$\underline{F}$	force $\quad \underline{F}' = \underline{F}/\rho_{\frac{w}{2}} V_s^2 L^2$
Fr	Froude Number $\quad Fr = \dfrac{V_s}{\sqrt{gL}}$
$\underline{f}$	nondimensional force $\quad \underline{f} = \begin{Bmatrix} \underline{F}' \\ \underline{M}' \end{Bmatrix}$
$\overline{GM}$	transverse metacentric height $\quad \overline{GM}' = \dfrac{\overline{GM}}{L}$
$\overline{GM_L}$	longitudinal metacentric height $\quad \overline{GM}' = \dfrac{\overline{GM_L}}{L}$
g	acceleration of gravity

NOMENCLATURE (CONTINUED)

H	matrix of hydrodynamic inertial coefficients h_{ij}
I	identity matrix
I_{ii}, I_{ij}	moments and products of inertia $\quad I'_{ij} = \dfrac{I_{ij}}{\rho_w L^5}$
I_m	inertial matrix for vessel
K	stiffness matrix
$K(\varphi)$	righting moment
k	sidewash factor
L	waterline length
M	combined inertial matrix
$\underline{M}$	moment $\quad \underline{M}' = \dfrac{\underline{M}}{\rho_w V_s^2 L^3}$
m	mass of vessel $\quad m' = \dfrac{m}{\rho_w L^3}$
P_k	system parameters
$\underline{q}$	motion variables
$\underline{R}$	position vector in inertial frame
R_3	sinkage $\quad R'_3 = \dfrac{R_3}{L}$
$\underline{r}$	position vector in body frame $\quad \underline{r}' = \dfrac{\underline{r}}{L}$
$\underline{r}_f$	center of flotation
$\underline{r}_K$	hydrodynamic center

NOMENCLATURE (CONTINUED)

$\underline{r}_m$	center of gravity of live ballast
$\underline{r}_R$	rudder center of pressure
$\underline{r}_s$	aerodynamic center
S_A	sail area $\quad S_A' = \frac{S_A}{L^2}$
T	Euler transformation
T_j	time constant $\quad T_j' = T_j Fr \sqrt{\frac{g}{L}}$
T_j^N	natural period $\quad T_j^{N'} = T_j^N Fr \sqrt{\frac{g}{L}}$
t	time
$\underline{u}$	trans. vel. of vessel mass center $\quad \lvert \underline{u} \rvert = V_s, \ \underline{u}' = \frac{\underline{u}}{V_s}$
$\underline{V}_a$	apparent wind velocity $\quad \underline{V}_a' = \frac{\underline{V}_a}{V_s}$
$\underline{V}_T$	true wind velocity $\quad \underline{V}_T' = \frac{\underline{V}_T}{V_s}$
$\underline{x}$	independent variables
$y_{kj}(t)$	normal mode
Z	similarity transformation

$$\underline{\dot{z}} = \begin{Bmatrix} \dot{z}_1 \\ \dot{z}_2 \\ \dot{z}_3 \\ \dot{z}_4 \\ \dot{z}_5 \\ \dot{z}_6 \end{Bmatrix} = \begin{Bmatrix} \text{surge velocity} \\ \text{sway velocity} \\ \text{heave velocity} \\ \text{roll rate} \\ \text{pitch rate} \\ \text{yaw rate} \end{Bmatrix} \quad \text{perturbational variables}$$

α_j	real part of complex eigenvalue

NOMENCLATURE (CONTINUED)

α_K	hull-keel crossflow angle
α_R	rudder crossflow angle
α_S	sail crossflow angle
β_a	apparent wind angle
β_j	imaginary part of complex eigenvalue
γ	sailing angle
δ_R	helm angle
δ_S	boom angle
ϵ_K	sidewash due to keel
ζ_j	modal damping ratio
ζ_w	wave damping ratio
$\underline{\eta}_j$	imaginary part of complex eigenvector
θ	Eulerian trim angle
λ	leeway angle
λ_j	complex eigenvalues
ν_{kj}	normalized modal phase angle
$\underline{\xi}_j$	real part of complex eigenvector
ρ_a, ρ_w	densities of air and water $\rho = \frac{\rho_a}{\rho_w}$
σ	sidewash correction $\sigma = \frac{k}{2\pi AR_K}$
φ	Eulerian heel angle
ψ	Eulerian heading angle
Ω	matrix representation of $\underline{\omega}\times$

NOMENCLATURE (CONCLUDED)

$\underline{\omega}$	angular velocity of vessel
ω_j^N	natural frequency

Special Symbols

X^{-1}	inverse of the matrix X
$\underline{x} \circ \underline{y}$	anti-scalar product of vectors $\underline{x}$ and $\underline{y}$
X^T	transpose of the matrix X
$\|\underline{x}\|_2$	Euclidean norm of $\underline{x}$
$\|\underline{x}\|$	magnitude of $\underline{x}$
x'	nondimensional x
$\dot{x} = \frac{dx}{dt}$	time derivatives
x^o	steady state value or initial estimate
$\bar{x}$	complex conjugate

LIST OF FIGURES

		Page
Figure 1.1	Summary of Eigenvalues	4
Figure 2.1	Eulerian Angles and Reference Frames	11
Figure 2.2	Steady State Configuration	15
Figure 3.1	Sailing Envelope	26
Figure 3.2	Geometry of Steady State Forces in Body Frame	30
Figure 3.3	Idealized Flow Geometry at Rudder	44
Figure 3.4	Idealized Sail Geometry	48
Figure 4.1	Steady State Solution for Downwind Sailing: True Wind Speed vs. Froude Number	62
Figure 4.2	Steady State Solution for Downwind Sailing: Trim Angle vs. Froude Number	63
Figure 4.3	Solution to Lateral Equations of Downwind Sailing for Base Boat	64
Figure 4.4	Roll Natural Period and Damping Ratio for Base Boat Sailing Downwind	65
Figure 4.5	Lateral Eigenvalues with Gottingen Foil	68
Figure 4.6	Damping Ratio of Downwind Roll Mode with Gottingen Foil	68
Figure 4.7	Lateral Eigenvalues with Valiant's Rudder	69
Figure 4.8	Lateral Eigenvalues with Columbia's Rudder	70
Figure 4.9	Lateral Eigenvalues with Heavy Displacement	72
Figure 4.10	Lateral Eigenvalues with Ultra-light Displacement	72
Figure 4.11	Lateral Eigenvalues with Low $\overline{GM}$	74
Figure 4.12	Solution to Longitudinal Equations of Downwind Sailing for Base Boat	79

LIST OF FIGURES (CONTINUED)

		Page
Figure 4.13	Complex Longitudinal Eigenvalues with Wave Damping Ratio of 0.25	80
Figure 4.14	Damping Ratios for Downwind Pitch Mode	81
Figure 4.15	Longitudinal Eigenvalues with Heavy Displacement	83
Figure 4.16	Longitudinal Eigenvalues with Ultra-light Displacement	83
Figure 4.17	Steady State Solution for Downwind Sailing with Pitch-Tender Vessel	85
Figure 4.18	Complex Longitudinal Eigenvalues with Pitch-Tender Vessel	85
Figure 5.1	Sailing Envelope for Base Boat	94
Figure 5.2	Envelope of Full Scale Sailing Observations	95
Figure 5.3	Performance Data for Base Boat with Finn Sail	97
Figure 5.4	Performance Data for Base Boat with Gottingen Foil	98
Figure 5.5	Performance Data Fr ~ .26	99
Figure 5.6	Performance Data Fr ~ .34	100
Figure 5.7	Performance Data Fr ~ .40	101
Figure 5.8	Heel Angle for Base Boat with Finn Sail	102
Figure 5.9	Comparison of Heel Angle Data	103
Figure 5.10	Trim Angle for Base Boat with Gottingen Foil (Fr = .36)	104
Figure 5.11	Sinkage for Base Boat with Gottingen Foil (Fr = .36)	105
Figure 5.12	Hull-Keel Crossflow Angle for Base Boat with Gottingen Foil	106
Figure 5.13	Comparison of Calculated Leeway Angles (Fr ~ .34)	107

LIST OF FIGURES (CONTINUED)

		Page
Figure 5.14	Rudder Crossflow Angle for Base Boat with Gottingen Foil	108
Figure 5.15	Comparison of Helm Angle Data (Fr ~ .34)	109
Figure 6.1	Eigenvalues for Base Boat $\gamma = 0^{\circ}$ (Run)	114
Figure 6.2	Normal Modes for Base Boat $\gamma = 0^{\circ}$ (Run)	114
Figure 6.3	Eigenvalues for Base Boat $\gamma = -30^{\circ}$ (Broad Reach)	115
Figure 6.4	Normal Modes for Base Boat $\gamma = -30^{\circ}$ (Broad Reach)	115
Figure 6.5	Eigenvalues for Base Boat $\gamma = -70^{\circ}$ (Close Reach)	116
Figure 6.6	Normal Modes for Base Boat $\gamma = -70^{\circ}$ (Close Reach)	116
Figure 6.7	Eigenvalues for Base Boat $\gamma = -140^{\circ}$ (Beat)	117
Figure 6.8	Normal Modes for Base Boat $\gamma = -140^{\circ}$ (Beat)	117
Figure 6.9	Natural Period and Damping Ratio for Pitch Mode	119
Figure 6.10	Natural Period and Damping Ratio for HPR Mode	121
Figure 6.11	Eigenvalues for Base Boat with Gottingen Foil $\gamma = 0^{\circ}$ (Run)	126
Figure 6.12	Normal Modes for Base Boat with Gottingen Foil $\gamma = 0^{\circ}$ (Run)	126
Figure 6.13	Eigenvalues for Base Boat with Gottingen Foil $\gamma = -30^{\circ}$ (Broad Reach)	127
Figure 6.14	Normal Modes for Base Boat with Gottingen Foil $\gamma = -30^{\circ}$ (Broad Reach)	127

LIST OF FIGURES (CONTINUED)

		Page
Figure 6.15	Eigenvalues for Base Boat with Gottingen Foil $\gamma = -70^{o}$ (Close Reach)	128
Figure 6.16	Normal Modes for Base Boat with Gottingen Foil $\gamma = -70^{o}$ (Close Reach)	128
Figure 6.17	Eigenvalues for Base Boat with Gottingen Foil $\gamma = -140^{o}$ (Beat)	129
Figure 6.18	Normal Modes for Base Boat with Gottingen Foil $\gamma = -140^{o}$ (Beat)	129
Figure 6.19	Eigenvalues for Heavy Displacement $\gamma = 0^{o}$ (Run)	132
Figure 6.20	Normal Modes for Heavy Displacement $\gamma = 0^{o}$ (Run)	132
Figure 6.21	Eigenvalues for Heavy Displacement $\gamma = -30^{o}$ (Broad Reach)	133
Figure 6.22	Normal Modes for Heavy Displacement $\gamma = -30^{o}$ (Broad Reach)	133
Figure 6.23	Eigenvalues for Heavy Displacement $\gamma = -70^{o}$ (Close Reach)	134
Figure 6.24	Normal Modes for Heavy Displacement $\gamma = -70^{o}$ (Close Reach)	134
Figure 6.25	Eigenvalues for Heavy Displacement $\gamma = -140^{o}$ (Beat)	135
Figure 6.26	Normal Modes for Heavy Displacement $\gamma = -140^{o}$ (Beat)	135
Figure A.1	Antiope Resistance Coefficient for Upright Conditions	148
Figure A.2	Antiope Resistance Coefficient $C_{K1}(Fr, \alpha_K)$	149
Figure A.3	Antiope Sideforce Coefficient $C_{K2}(Fr, \alpha_K)$	149
Figure A.4	Antiope Righting Moment	150
Figure A.5	Hydrodynamic Inertial Coefficient $h_{22}(Fr)$	151

LIST OF FIGURES (CONTINUED)

		Page
Figure A.6	Hydrodynamic Inertial Coefficient $h_{26}(Fr)$	151
Figure A.7	Hydrodynamic Inertial Coefficient $h_{62}(Fr)$	152
Figure A.8	Hydrodynamic Inertial Coefficient $h_{66}(Fr)$	152
Figure A.9	Rudder Sideforce Data from Half Ton Model $C_{R2}(Fr, \alpha_R)$	154
Figure A.10	Rudder Sideforce Data from Valiant and Columbia Models $C_{R2}(\alpha_R)$	155
Figure A.11	Aerodynamic Resistance Coefficients $C_{S1}(\alpha_S)$	157
Figure A.12	Aerodynamic Sideforce Coefficients $C_{S2}(\alpha_S)$	158
Figure C.1	$\gamma = 10^{\circ}$ (By-the-lee)	176
Figure C.2	$\gamma = 0^{\circ}$ (Run)	177
Figure C.3	$\gamma = -10^{\circ}$ (Run)	178
Figure C.4	$\gamma = -20^{\circ}$ (Broad Reach)	179
Figure C.5	$\gamma = -30^{\circ}$ (Broad Reach)	180
Figure C.6	$\gamma = -40^{\circ}$ (Beam-Broad Reach)	181
Figure C.7	$\gamma = -50^{\circ}$ (Close-Beam Reach)	182
Figure C.8	$\gamma = -60^{\circ}$ (Close Reach)	183
Figure C.9	$\gamma = -70^{\circ}$ (Close Reach)	184
Figure C.10	$\gamma = -80^{\circ}$ (Beat-Close Reach)	185
Figure C.11	$\gamma = -90^{\circ}$ (Beat-Close Reach)	186
Figure C.12	$\gamma = -100^{\circ}$ (Beat)	187
Figure C.13	$\gamma = -110^{\circ}$ (Beat)	188
Figure C.14	$\gamma = -120^{\circ}$ (Beat)	189

LIST OF FIGURES (CONCLUDED)

		Page
Figure C.15	$\gamma = -130^{o}$ (Beat)	190
Figure C.16	$\gamma = -135^{o}$ (Beat)	191
Figure C.17	$\gamma = -140^{o}$ (Beat)	192
Figure C.18	$\gamma = -145^{o}$ (Beat)	193

LIST OF TABLES

		Page
Table 4.1	Lateral Time Constants for Base Boat	66
Table 4.2	Lateral Time Constants with Valiant's Rudder	70
Table 4.3	Lateral Time Constants with Variable Displacement	73
Table 4.4	Longitudinal Natural Periods and Damping Ratio for Base Boat	81
Table 4.5	Time Constant of Downwind Surge Mode for Base Boat	882
Table 4.6	Effect of Displacement on Longitudinal Modes	84
Table 4.7	Longitudinal Natural Periods and Damping Ratios for Pitch-Tender Vessel and Base Boat	86
Table 6.1	Summary of Contributions to Perturbation Matrix	113
Table 6.2	Natural Period and Damping Ratio for Roll Mode (Fr = .50, γ = -30°)	122
Table 6.3	Comparison of Modal Characteristics (γ = -70°)	123
Table 6.4	Comparison of Roll Mode Time Constants for γ = -140°, Fr = .34)	130
Table A.1	Antiope Test Variables	146
Table A.2	Vessel Geometry	159
Table B.1	Comparative Vessel Data	167
Table B.2	Comparative Data - Running	169
Table B.3	Comparative Data - Broad Reaching	170
Table B.4	Comparative Data - Beam Reaching	171

LIST OF TABLES (CONCLUDED)

		Page
Table B.5	Comparative Data - Close Reaching	172
Table B.6	Comparative Data - Beating	173
Table B.7	Comparison with Optimum Windward Solutions	174

I. INTRODUCTION

1.1 Background

Sailing vessels ceased commercial and military operations at the time when modern aeronautics and hydronautics were just developing. There is some renewed interest in commercial sailing vessels with their low fuel requirements (Woodward et al. 1975), and some work continues on military applications (Wood and Thompson 1974, Baker and Douglas 1977). But in the near future it is unlikely that many vessels except yachts will set sail.

Only in recent years have the results of aeronautical research been applied to sailing vessels, and the motivation for this work has come almost entirely from yacht racing. Most of this research effort has been devoted to improving steady state performance, especially the ability of a vessel to sail closer to the wind at higher speeds (Davidson 1956). Much less attention has been directed towards understanding dynamic behavior. The two areas where there has been active work are the motions of a vessel sailing to windward in a seaway and steering difficulties. However, the first problem has been treated largely as an extension of performance analyses (Tanner et al. 1960; Spens, De Saix and Brown 1967).

Steering has always been a concern in sailing vessel design*, but recent trends in yacht racing have led to severe control problems. These difficulties usually occur on offwind courses in moderate to heavy winds. An extreme example is that of a vessel

which "...rounded up and broached 33 times in 3 hours" (Spens et al. 1967). Less dramatic examples are provided by Milgram (1972) in a study of the course-keeping ability of several 12-meter yachts. These examples pose a fundamental question: which hydrodynamic or aerodynamic factors are responsible for the diminished course-keeping ability of the newer designs?

1.2 Previous Investigations

Ship motions have proved to be a very fertile area for research. Froude (1861) and A. N. Krilov (Blagoveshchensky 1962) studied the rolling of stationary ships in a seaway. Davidson (1936) began the experimental study of yachts with Gimcrack and later produced the first work focusing directly on the steering and control of ships (1944, 1948). These works on propeller driven ships have continued to expand with Stoker (1957), Rydill (1959), Eda and Crane (1965), Eda (1968, 1971, 1972), Mandel (1967) and Abkowitz (1969).

---

*K. C. Barnaby recalls the control schemes used on large sailing ships in the 1860's (Buchan and Flewitt 1968):

"Nathaniel Barnaby was stressing the need for a mechanical steering gear and he pointed out that it required some forty men to hold the rudder of the battleship 'Black Prince' at 28°. Ten men could grasp the concentric steering wheels, thirty more were needed to man relieving tackles.

Admiral Sir Edward Belcher ... asserted that 'the subject of this discussion is a seamen's question entirely'. It was a matter of 'trim' and when this was correct, you could 'run the flying jibboom into the eye of a needle'. He went on to add that 'the idea of steering even a boat by force of rudder is utterly repugnant to the feelings of all good seamen'."

In recent years there have been several research projects devoted to the control problem of sailing yachts. Letcher (1965) discusses the characteristics of a close-hauled yacht and in a second paper (1971) presents a static analysis of offwind sailing. These studies demonstrated that wind speed and aerodynamic resistance were strong influences on the behavior of the yacht. These results were used in a larger study of self-steering devices (Letcher 1974, 1976a). Buchan and Flewitt (1968) present an alternative analysis of yacht control systems.

Several dynamic models of sailing vessels have been presented. Newman (1967) includes vessel motions and rudder response in a speed optimization analysis of a yacht in quartering seas. Gerritsma (1968) considers the flat water behavior and wave response of a half ton yacht. Hydrodynamic data from planar motion experiments with a model are reported. This study was continued (Gerritsma and Moeyes 1973) with an analysis including aerodynamic resistance. These later studies demonstrated the importance of roll motions in the dynamic analysis of sailing vessels. This was supported by the results of Curtiss (1970).

An experimental study by Marchaj (1971, 1973) obtained wind tunnel data on a model sail which was free to rotate in roll. These experiments demonstrated that large amplitude oscillations can exist under the conditions of offwind sailing. These conditions are consistent with quasi-static analyses of other well known physical systems (Den Hartog 1956).

Milgram (1972) presents a summary paper on recent applied mechanics research on sailing vessels. Results are reported from a study of the controls-fixed behavior of sailing vessels in the absence of aerodynamic and free surface effects using the slender body theory of Wu and Newman (1972). Estimates of course-keeping ability are calculated for several 12-meter boats, but the variation between these estimates is small compared to the wide variation observed under sailing trials. Figure 1* shows these results together with those of Gerritsma and Moeyes (1973).

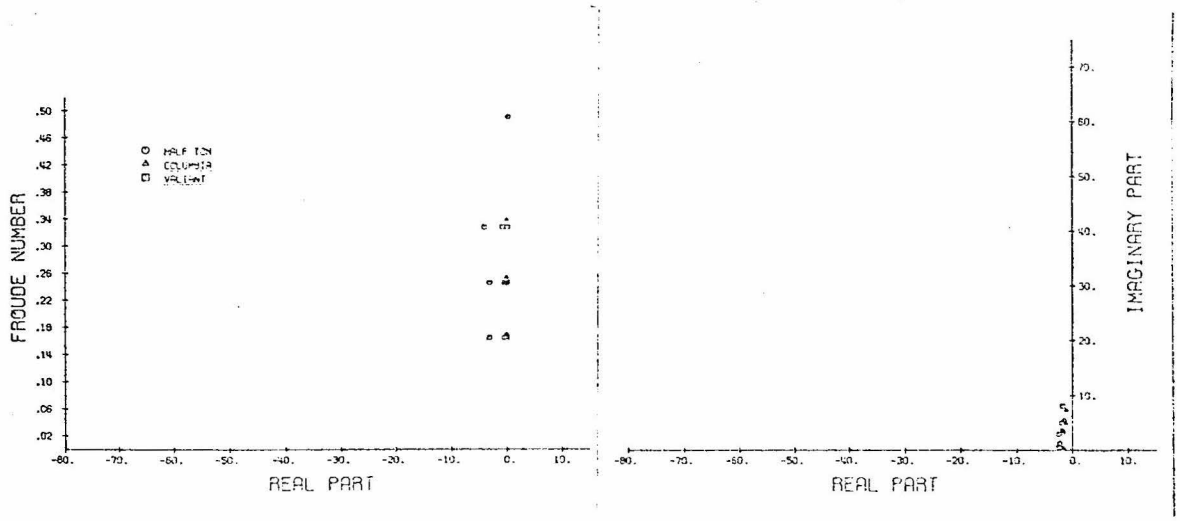


Figure 1.1. Summary of Eigenvalues

Milgram summarizes:

> The differences between theory and experiment are such that the theory would indicate substantial differences in the calculated roots if these differences were indeed the reasons for the observed differences in course-keeping ability. ...the

*The details of these eigenvalue plots are given in Appendix C.

> calculated roots do not include the effects of aerodynamic forces on the sails, nor do they include cross-coupling of sway and yaw with roll, which can be a large effect because of the center of aerodynamic force moving transversely when the vessel rolls. However, the observed variations in course-keeping ability exist in spite of rather similar sail-plans. Therefore, either the aerodynamic effects are not the reasons for the differences in course-keeping ability or the actual roots do vary between vessels when the aerodynamic effects are taken into account.

Many of the methods and assumptions of ship dynamics originate with flight dynamics, a field which has far outdistanced the study of surface vessels. This discrepancy is probably due in large to the high penalty paid for an uncontrollable aircraft. Bryan and Williams (1904) formulated and solved the dynamics problem for aerial gliders.* Useful references covering the development of airplane dynamics are Etkin (1972), Perkins and Hage (1949) and Roskam (1971a, 1971b).

1.3 General Objectives and Methods

Previous investigations and observations of sailing trials indicate that the dynamics of sailing vessels do depend on speed

---

*The timing on this work was rather remarkable. The authors begin:

> "The main difficulty connected with the attempt to fly by means of a machine heavier than air is that of longitudinal stability...
> The problem of artificial flight is hardly likely to be solved until the conditions of longitudinal stability of an aeroplane system have been reduced to a matter of pure mathematical calculation."

This paper was initially received on June 18, 1903, and published with the date January 7, 1904. On December 17, 1903, the Wright brothers flew at Kitty Hawk.

and point of sail. Steering problems are usually associated with offwind courses at moderate and high speeds, but the dynamic behavior on reaches and windward courses may be critical under some conditions. The attainable speeds and sailing angles for keelboats are described by the sailing envelope (see Figure 3.1). A basic objective of this study is to determine the way in which the gross motions of a sailing vessel depend on its location in the sailing envelope (i.e., speed and sailing angle).

The goal of considering the full range of attainable speeds and sailing angles leads to some undesirable complications. Free surface wave generation is responsible for the asymptotic limiting of the speed of displacement vessels. Additionally, fully separated aerodynamic flows are encountered on offwind courses. On windward courses at maximum speed the vessel attains extreme attitudes, e.g., heel angles may exceed 30°. Finally, a general formulation requires inclusion of all six rigid body motions.

Due to these complications, the proposed method is to replace the complex fluid flows with a discrete set of experimentally derived forces and moments. Ideally, data from full scale tests would be used; however, such data are virtually nonexistent. Of course, this method will be sufficiently general to allow for the incorporation of model test data and analytical results. This approach results in heavy emphasis on numerical techniques, but various schemes have been developed recently which can adequately handle the numerical difficulties.

Attention is focused on small perturbational motions about the steady state conditions corresponding to a point inside the sailing envelope. There are several reasons for restricting the analysis in this manner. Sailing vessels are designed and sailed with the assumption that steady state conditions will be achieved and maintained for substantial periods of time. Also the data available for use in the analysis were acquired almost entirely from steady state tests. Finally, global analyses, which permit large amplitude motions, need to account for rig and sail deformations. This exceeds the scope of this study.

A second basic objective is to attempt to provide insight into the steering difficulties of keelboats. Specifically, under what conditions are the solutions to the helm-fixed equations of motion for a sailing vessel Liapunov asymptotically unstable? Of course, the results of the perturbation analysis are valid for the full nonlinear equations under some rather mild conditions, and, further, this analysis forms the backbone for future work with nonautonomous and forced equations.

A third objective is to present the results of some preliminary numerical calculations to demonstrate the efficacy of the method. Due to the scarcity of data, the results are tenuous; however, they may give a coarse indication of what may be expected in the way of the stability properties and normal modes of sailing vessels. The sensitivity to several gross parameters (e.g., mass and aerodynamic sideforce) is briefly explored.

Several items are specifically ignored in this study. A comprehensive treatment of sailing vessel dynamics would necessarily include unsteady fluid forces*, dynamic response in waves and working control systems. This study assumes quasi-static fluid flows, flat water and fixed controls. Using discrete forces to model the complex pressure distributions on the hull and sails avoids the necessity of establishing the details of the fluid flows. Similarly, the steady state and perturbational solutions are not fine tuned through any optimization schemes.

---

*"For the theoretical aerodynamicist, the most interesting unsolved problem concerning sails is that of unsteady sail aerodynamics," Milgram (1972).

II. SUMMARY OF THE DYNAMICS OF RIGID BODIES IN FLUID MEDIA

This chapter briefly sketches the development of the equations of motion and solutions for a rigid body in fluid media. Detailed treatments are given in Abkowitz (1969) for ships and Etkin (1972) for airplanes.

2.1 Reference Frames and Equations of Motion

The six degrees of freedom for a rigid body with fixed controls are specified as follows: a reference frame fixed in the body is defined by

$$\mathfrak{F}_B = \{\underline{o}; \underline{e}_1, \underline{e}_2, \underline{e}_3\} \tag{2.1}$$

where

$\underline{o}$	...origin of $\mathfrak{F}_B$ coincident with body center of mass
$(\underline{e}_1, \underline{e}_2, \underline{e}_3)$	...base vectors of right-handed, cartesian frame
$\underline{e}_1$	...towards bow
$\underline{e}_2$	...to starboard
$\underline{e}_3$	...towards keel .

The location of any point in the body is given by

$$\underline{r} = \begin{Bmatrix} r_1 \\ r_2 \\ r_3 \end{Bmatrix} . \tag{2.2}$$

Similarly, an inertial frame $\mathfrak{F}_I$ is specified by

$(\underline{e}_1', \underline{e}_2', \underline{e}_3')$ ...base vectors for inertial frame

$(\underline{e}_1', \underline{e}_2')$ ...parallel to the free surface with $\underline{e}_1'$ coincident with the ambient or true wind direction

$\underline{e}_3'$ ...vertically down .

The location of the center of mass of the body with respect to the inertial frame is given by

$$\underline{R} = \begin{Bmatrix} R_1 \\ R_2 \\ R_3 \end{Bmatrix} \tag{2.3}$$

Nautical Eulerian angles (Blagoveshchensky, 1962) are chosen to specify the orientation of the body with respect to the inertial frame. The relationship between $\mathfrak{F}_B$, $\mathfrak{F}_I$ and the Eulerian angles is sketched in Figure 2.1. These angles are called:

φ ...heel angle

θ ...trim angle

ψ ...heading angle .

The Eulerian angles describe a series of rotations from the inertial frame $\mathfrak{F}_I$ to the body frame $\mathfrak{F}_B$. These rotations are expressed analytically by the Euler transformation.

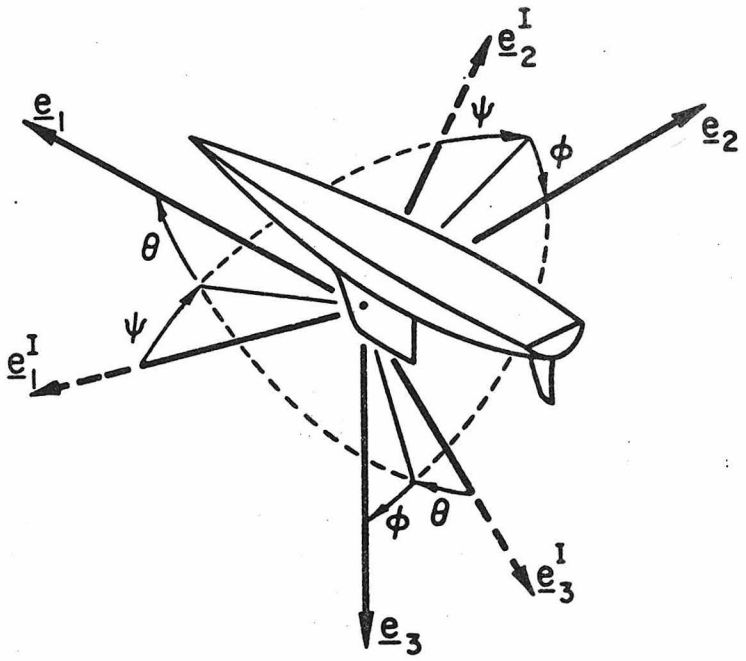


Figure 2.1. Eulerian Angles and Reference Frames

$$T(\varphi,\theta,\psi) = \begin{bmatrix} \cos\theta\cos\psi & \cos\theta\sin\psi & -\sin\theta \\ (\sin\varphi\sin\theta\cos\psi - \cos\varphi\sin\psi) & (\sin\varphi\sin\theta\sin\psi + \cos\varphi\cos\psi) & \sin\varphi\cos\theta \\ (\cos\varphi\sin\theta\cos\psi + \sin\varphi\sin\psi) & (\cos\varphi\sin\theta\sin\psi - \sin\varphi\cos\psi) & \cos\varphi\cos\theta \end{bmatrix} \tag{2.4}$$

This transformation has several useful properties including orthogonality,

$$T^T T = T^{-1} T = I \ . \tag{2.5}$$

The translational and angular velocities of the body are

$$\underline{u} = \begin{Bmatrix} u_1 \\ u_2 \\ u_3 \end{Bmatrix} , \qquad \underline{\omega} = \begin{Bmatrix} \omega_1 \\ \omega_2 \\ \omega_3 \end{Bmatrix} , \tag{2.6}$$

and the angular velocity is related to the Eulerian angles by

$$\underline{\omega} = \begin{Bmatrix} \omega_1 \\ \omega_2 \\ \omega_3 \end{Bmatrix} = \begin{Bmatrix} \dot{\varphi} - \dot{\psi} \sin\theta \\ \dot{\theta} \cos\varphi + \dot{\psi} \cos\theta \sin\varphi \\ \dot{\psi} \cos\theta \cos\varphi - \dot{\theta} \sin\varphi \end{Bmatrix} . \tag{2.7}$$

The rigid body equations of motion in this notation are

$$\left.\begin{aligned} m(\dot{\underline{u}} + \underline{\omega} \times \underline{u}) &= \underline{F} \\ I_m \dot{\underline{\omega}} + \underline{\omega} \times I_m \underline{\omega} &= \underline{M} \end{aligned}\right\} , \tag{2.8}$$

where

m ... mass of the body

$$I_m = \begin{bmatrix} I_{11} & -I_{12} & -I_{13} \\ -I_{12} & I_{22} & -I_{23} \\ -I_{13} & -I_{23} & I_{33} \end{bmatrix} \quad \text{... inertial matrix of the body} \tag{2.9}$$

$$I_{ii} = \int_m \left(r_j^2 + r_k^2\right) dm , \quad i \neq j \neq k \quad \text{... moments of inertia} \tag{2.10}$$

$$I_{ij} = \int_m r_i r_j dm , \quad i \neq j \quad \text{... products of inertia} \tag{2.11}$$

$\underline{F}, \underline{M}$ ... external forces and moments acting on body .

It is convenient to combine these equations and work in a generalized space of the six motion variables. First, equations (2.8) are nondimensionalized by dividing by a reference force and moment (namely, $\frac{\rho_w}{2} V_s^2 L^2$ and $\frac{\rho_w}{2} V_s^2 L^3$). Then adopting the matrix representation for the vector cross product

$$\Omega = \underline{\omega}\times = \begin{bmatrix} 0 & -\omega_3 & \omega_2 \\ \omega_3 & 0 & -\omega_1 \\ -\omega_2 & \omega_1 & 0 \end{bmatrix} , \qquad (2.12)$$

the equations of motion become

$$\begin{bmatrix} m'I & 0 \\ 0 & I'_m \end{bmatrix} \begin{Bmatrix} \dot{\underline{u}}' \\ \dot{\underline{\omega}}' \end{Bmatrix} + \begin{bmatrix} m'\Omega' & \\ & \Omega' I'_m \end{bmatrix} \begin{Bmatrix} \underline{u}' \\ \underline{\omega}' \end{Bmatrix} = \begin{Bmatrix} \underline{F}' \\ \underline{M}' \end{Bmatrix} . \qquad (2.13)$$

The primes in this equation denote nondimensional quantities (see Nomenclature). Throughout the remainder of this study only nondimensional quantities will be considered unless explicitly noted. Henceforth, all primes are omitted.

2.2 Expansion of Forces and Moments

Calculation of the forces and moments acting on a rigid body in arbitrary motion at the interface between two fluid media is an extremely difficult problem. The classical procedure dating back to Bryan and Williams (1904) is to assume the existence of a Taylor Series expansion of the forces and moments about some

steady state condition*. The validity of this assumption is discussed in detail by Abkowitz (1969) for ships and Etkin (1972) for airplanes. Further, as noted in Chapter I, the fluid flows are assumed to be quasi-static. These assumptions are sufficient to reduce equation (2.13) to a system of autonomous, ordinary differential equations with constant coefficients.

For sailing vessels the steady state condition of primary interest is uniform translation across the free surface. This is specified in $\mathfrak{F}_1$ by

$$\underline{\dot{R}} = V_S \begin{Bmatrix} \cos\gamma \\ \sin\gamma \\ 0 \end{Bmatrix} \tag{2.14}$$

where

$$V_S = |\underline{u}^o| \quad \ldots \quad \text{steady state speed of vessel} \tag{2.15}$$

$$\gamma \quad \ldots \quad \text{sailing angle}^{**} \quad .$$

The steady state configuration is shown projected onto the free surface in Figure 2.2 with

---

*Adopting this method prohibits investigating some practical cases of interest for sailing vessels, e.g., it is a relatively common event to observe the apparent wind speed drop to zero on a vessel surfing downwind. Of course, this is usually accompanied with large sail deformations.

**The conventional true wind angle is related to the sailing angle by $\beta_T = 180^\circ - |\gamma|$.

V_T ... true wind velocity

$\lambda = \gamma - \psi^o$ ... steady state leeway angle , (2.16)

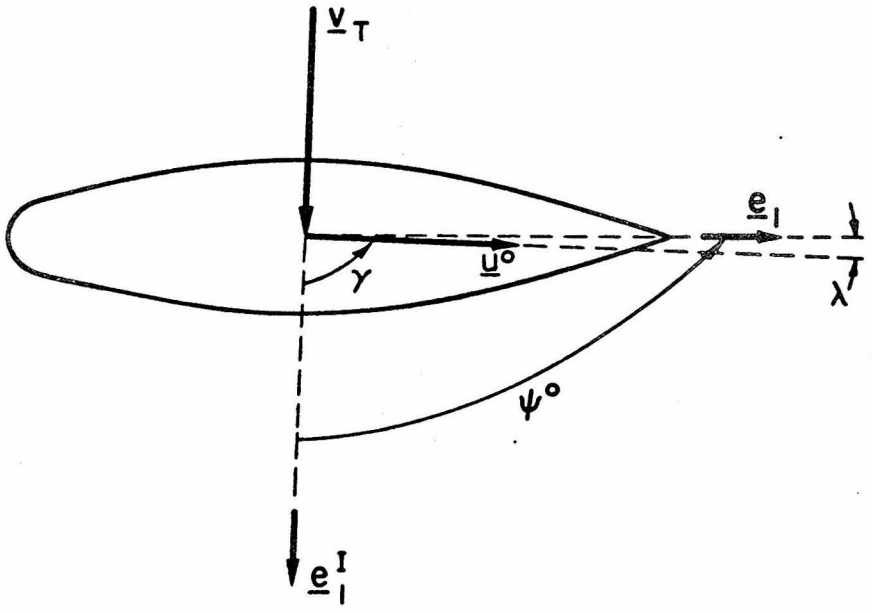


Figure 2.2. Steady State Configuration

Then the Euler transformation can be used to relate the steady state velocity to the orientation of the body:

$$\underline{u}^o = V_s T(\varphi^o, \theta^o, \psi^o) \begin{Bmatrix} \cos\gamma \\ \sin\gamma \\ 0 \end{Bmatrix} . \quad (2.17)$$

The nondimensional forces on the right hand side of equation (2.13) are functions of the motion variables, i.e.

$$\begin{Bmatrix} \underline{F} \\ \underline{M} \end{Bmatrix} = \underline{f} = \underline{f}(\underline{u}, \dot{\underline{u}}, \underline{\omega}, \dot{\underline{\omega}}, \varphi, \theta, \psi, \underline{R}; P_k) \tag{2.18}$$

where P_k represents any system parameters. The vector defining the perturbations in the motion variables in six-space is

$$\underline{q} = \begin{Bmatrix} \delta u_1 \\ \delta u_2 \\ \delta u_3 \\ \delta \omega_1 \\ \delta \omega_2 \\ \delta \omega_3 \end{Bmatrix} = \begin{Bmatrix} u_1 - u_1^o \\ u_2 - u_2^o \\ u_3 - u_3^o \\ \omega_1 \\ \omega_2 \\ \omega_3 \end{Bmatrix} . \tag{2.19}$$

However, for computational and interpretational ease it is convenient to carry out the expansion in a modified set of variables. These are defined in the following way: when all quantities are small, the linearized version of equation (2.7) is

$$\underline{\omega} = \begin{Bmatrix} \delta\dot{\varphi} \\ \delta\dot{\theta} \\ \delta\dot{\psi} \end{Bmatrix} . \tag{2.20}$$

However, since the steady state heel and trim angles are relatively large for some sailing conditions, a similarity transformation $Z(\varphi^o, \theta^o, \psi^o)$ is defined by

$$\dot{\underline{z}} = \begin{Bmatrix} \dot{z}_1 \\ \dot{z}_2 \\ \dot{z}_3 \\ \dot{z}_4 \\ \dot{z}_5 \\ \dot{z}_6 \end{Bmatrix} = \begin{bmatrix} 1 & 0 & 0 & 0 & 0 & 0 \\ 0 & 1 & 0 & 0 & 0 & 0 \\ 0 & 0 & 1 & 0 & 0 & 0 \\ 0 & 0 & 0 & 1 & 0 & -\sin\theta^{\circ} \\ 0 & 0 & 0 & 0 & \cos\varphi^{\circ} & \sin\varphi^{\circ}\cos\theta^{\circ} \\ 0 & 0 & 0 & 0 & -\sin\varphi^{\circ} & \cos\varphi^{\circ}\cos\theta^{\circ} \end{bmatrix} \begin{Bmatrix} \delta u_1 \\ \delta u_2 \\ \delta u_3 \\ \delta\dot{\varphi} \\ \delta\dot{\theta} \\ \delta\dot{\psi} \end{Bmatrix} . \quad (2.21)$$

Here the perturbational velocities are called

$$\dot{z}_1 = \delta u_1 \quad \ldots \quad \text{surge}$$
$$\dot{z}_2 = \delta u_2 \quad \ldots \quad \text{sway}$$
$$\dot{z}_3 = \delta u_3 \quad \ldots \quad \text{heave} \quad .$$

The perturbational quantities (z_4, z_5, z_6) correspond to a second set of Eulerian angles, and they are called

$$z_4 \quad \ldots \quad \text{roll angle}$$
$$z_5 \quad \ldots \quad \text{pitch angle}$$
$$z_6 \quad \ldots \quad \text{yaw angle} \quad .$$

These angles describe a series of rotations from the steady state configuration to the perturbed state. This is stated explicitly by

$$\underline{e}_j = T(z_4, z_5, z_6)\, T(\varphi^{\circ}, \theta^{\circ}, \psi^{\circ})\, \underline{e}_j' \quad , \qquad \forall\, j \in (1,3) \quad , \qquad (2.22)$$

and since the z_i are perturbational quantities,

$$T(z_4, z_5, z_6) = \begin{bmatrix} 1 & z_6 & -z_5 \\ -z_6 & 1 & z_4 \\ z_5 & -z_4 & 1 \end{bmatrix} + O(\|\underline{z}\|^2) \quad . \qquad (2.23)$$

The Z-transformation is singular for $\theta^\circ = \frac{\pi}{2}$; this configuration is of no practical significance for sailing vessels and is excluded from consideration. For $\theta^\circ \neq \frac{\pi}{2}$ the inverse transformation is

$$Z^{-1}(\varphi^\circ, \theta^\circ, \psi^\circ) = \begin{bmatrix} 1 & 0 & 0 & 0 & 0 & 0 \\ 0 & 1 & 0 & 0 & 0 & 0 \\ 0 & 0 & 1 & 0 & 0 & 0 \\ 0 & 0 & 0 & 1 & \sin\varphi^\circ \tan\theta^\circ & \cos\varphi^\circ \tan\theta^\circ \\ 0 & 0 & 0 & 0 & \cos\varphi^\circ & -\sin\varphi^\circ \\ 0 & 0 & 0 & 0 & \sin\varphi^\circ \sec\theta^\circ & \cos\varphi^\circ \sec\theta^\circ \end{bmatrix} \qquad (2.24)$$

Since all the perturbational quantities are represented by $\underline{z}$ and its derivatives, it is not necessary to explicitly indicate the steady state values, e.g., φ°. Henceforth, the steady state value will be implied.

Making use of equations (2.19), (2.20), (2.21) and (2.23), the nondimensional forces can be written in a form suitable for the Taylor Series expansion:

$$\underline{f} = \underline{f}(\underline{u}, \varphi, \theta, \psi, \underline{R}; \underline{z}, \dot{\underline{z}}, \ddot{\underline{z}}; P_k)$$

$$= \underline{f}(\underline{u}, \varphi, \theta, \psi, \underline{R}; P_k) + \left(\frac{\partial \underline{f}}{\partial \underline{z}}\right)\underline{z} + \left(\frac{\partial \underline{f}}{\partial \dot{\underline{z}}}\right)\dot{\underline{z}} + \left(\frac{\partial \underline{f}}{\partial \ddot{\underline{z}}}\right)\ddot{\underline{z}} + O(\|\underline{z}\|^2) \quad . \qquad (2.25)$$

The left-hand side of equation (2.13) is also expanded:

$$\begin{bmatrix} mI & 0 \\ 0 & I_m \end{bmatrix} Z^{-1} \ddot{\underline{z}} + \begin{bmatrix} 0 & mU \\ 0 & 0 \end{bmatrix} Z^{-1} \dot{\underline{z}} + O(\|\underline{z}\|^2) = \underline{f} \qquad (2.26)$$

where

$$U = \begin{bmatrix} 0 & u_3 & -u_2 \\ -u_3 & 0 & u_1 \\ u_2 & -u_1 & 0 \end{bmatrix} . \qquad (2.27)$$

Equating terms of similar order in equations (2.25) and (2.26) yields

$$\underline{f}(\underline{u}, \varphi, \theta, \psi, \underline{R}; P_k) = \underline{0} \qquad (2.28)$$

and

$$\left\{ \begin{bmatrix} mI & 0 \\ 0 & I_m \end{bmatrix} Z^{-1} - \left(\frac{\partial \underline{f}}{\partial \ddot{\underline{z}}} \right) \right\} \ddot{\underline{z}} + \left\{ \begin{bmatrix} 0 & mU \\ 0 & 0 \end{bmatrix} Z^{-1} - \left(\frac{\partial \underline{f}}{\partial \dot{\underline{z}}} \right) \right\} \dot{\underline{z}} - \left(\frac{\partial \underline{f}}{\partial \underline{z}} \right) \underline{z} = \underline{0} \qquad (2.29)$$

Equation (2.28) is the vector form of the Steady State Equations. These are a system of six nonlinear, transcendental equations which are solved for the translational velocities ($\underline{u}$) and orientation ($\varphi, \theta, \psi, \underline{R}$). Their solution is the subject of Chapter V.

Equation (2.29) is a form of the Perturbation Equations; in standard form they are represented as a system of 12 first order differential equations:

$$\frac{d\underline{x}}{dt} = A\underline{x} \ , \quad \underline{x}(0) = \underline{c} \tag{2.30}$$

where

$$\underline{x} = \begin{Bmatrix} \underline{z} \\ \dot{\underline{z}} \end{Bmatrix} \tag{2.31}$$

$$A = \begin{bmatrix} 0 & I \\ -Z M^{-1} K & -Z M^{-1} C \end{bmatrix} \quad \ldots \quad \text{perturbation matrix} \tag{2.32}$$

$$M = \begin{bmatrix} mI & 0 \\ 0 & I_m \end{bmatrix} - \left(\frac{\partial \underline{f}}{\partial \dot{\underline{q}}} \right) \quad \ldots \quad \text{inertial matrix} \tag{2.33}$$

$$C = \begin{bmatrix} 0 & mU \\ 0 & 0 \end{bmatrix} Z^{-1} - \left(\frac{\partial \underline{f}}{\partial \dot{\underline{z}}} \right) \quad \ldots \quad \text{damping matrix} \tag{2.34}$$

$$K = -\left(\frac{\partial \underline{f}}{\partial \underline{z}} \right) \quad \ldots \quad \text{stiffness matrix} \ , \tag{2.35}$$

and $\underline{c}$ is the vector of initial conditions.

The inertial matrix M is composed on the vessel's inertial properties (m and I_m) and the fluid-dynamic force coefficients of the acceleration terms. These are sometimes called the added or virtual masses of the system and have the following useful interpretation. For a rigid body moving in an unbounded ideal fluid, Blagoveshchensky (1962) shows that the kinetic energy of the fluid medium can be expressed as a quadratic form:

$$E_f = \tfrac{1}{2}(\underline{q}, H\underline{q}) > 0 \qquad \forall\ \underline{q} \neq \underline{0} \tag{2.36}$$

where the elements of H are

$$h_{ij} = h_{ji} = -\frac{\partial f_i}{\partial q_j} \quad , \qquad \forall\ i,j \in (1,6) \tag{2.37}$$

But the kinetic energy of the vessel is

$$E_v = \tfrac{1}{2}\left(\underline{q}, \begin{bmatrix} mI & 0 \\ 0 & I_m \end{bmatrix}\underline{q}\right) > 0 \qquad \forall\ \underline{q} \neq 0 \ . \tag{2.38}$$

Then the total kinetic energy associated with the perturbational motions is

$$E = \tfrac{1}{2}\left(\underline{z}(Z^{-1})^T\left[\begin{bmatrix} mI & 0 \\ 0 & I_m \end{bmatrix} + H\right]Z^{-1}\underline{z}\right) > 0 \qquad \forall\ \underline{z} \neq 0 \ . \tag{2.39}$$

This equation shows that the inertial matrix is symmetric, positive definite and thus possesses an inverse ($\theta \neq \frac{\pi}{2}$).

2.3 Normal Modes and Stability of Solutions

Assuming the matrix A has a full set of ordinary eigenvectors, the solution to the Perturbation Equations can be expressed as

$$\underline{x}(t) = X e^{\Lambda t} X^{-1}\underline{c} \tag{2.40}$$

where

$$\Lambda = X^{-1} A X \quad \ldots \quad \text{eigenvalue matrix of A} \tag{2.41}$$

$$X \quad \ldots \quad \text{eigenvector matrix of A} \ .$$

The real and imaginary parts of the elements of these matrices are denoted by

$$\left.\begin{aligned} \lambda_j &= \alpha_j + i\beta_j \\ \underline{x}_j &= \underline{\xi}_j + i\underline{\eta}_j \end{aligned}\right\} \quad \forall\, j \in (1, 12) \ . \tag{2.42}$$

When discussing numerical solutions to the Perturbation Equations, it is convenient to express the solution in terms of the normal modes of the vessel. They are defined by:

Real Eigenvalues ($\beta_j = 0$)

$$y_{kj}(t) = b_{kj} e^{-t/T_j} \quad \ldots \quad k^{th} \text{ element of the } j^{th} \text{ normal mode} \tag{2.43}$$

$$T_j = -\frac{1}{\alpha_j} \quad \ldots \quad \text{time constant for } j^{th} \text{ normal mode} \tag{2.44}$$

$$b_{kj} = \frac{\xi_{kj}}{b_j^*} \quad \ldots \quad k^{th} \text{ normalized modal coefficient for } j^{th} \text{ mode} \tag{2.45}$$

$$b_j^* = \operatorname{sgn}(\xi_{kj}) \max |\xi_{kj}| \quad \ldots \quad \text{normalization criterion} \tag{2.46}$$

$$\forall\, k \in (1, 12)$$

Complex Conjugate Eigenvalues ($\lambda_j = \overline{\lambda_{j+1}}$)

$$y_{kj}(t) = b_{kj} e^{-\omega_j \zeta_j t} \cos\left(\omega_j \sqrt{1 - \zeta_j^2}\ t - \nu_{kj}\right)$$

$$\ldots \quad k^{th} \text{ element of the } j^{th} \text{ normal mode} \tag{2.47}$$

$$\omega_j = (\alpha_j^2 + \beta_j^2)^{\frac{1}{2}} \quad \ldots \quad \text{natural frequency of } j^{th} \text{ mode} \tag{2.48}$$

$$T_j^N = \frac{2\pi}{\omega_j} \quad \ldots \quad \text{natural period of } j^{th} \text{ mode} \tag{2.49}$$

$$\zeta_j = \frac{-\alpha_j}{(\alpha_j^2 + \beta_j^2)^{\frac{1}{2}}} \quad \ldots \quad \text{damping ratio of } j^{th} \text{ mode} \tag{2.50}$$

$$b_{kj} = \frac{(\xi_{kj}^2 + \eta_{kj}^2)^{\frac{1}{2}}}{b_j^*} \quad \ldots \quad k^{th} \text{ normalized modal coefficient for } j^{th} \text{ mode} \tag{2.51}$$

$$b_j^* = \max (\xi_{kj}^2 + \eta_{kj}^2)^{\frac{1}{2}} \quad \ldots \quad \text{amplitude normalization criterion} \tag{2.52}$$

$$\forall\, k \in (1, 12)$$

$$\nu_{kj} = \tan^{-1}\left(-\frac{\eta_{kj}}{\xi_{kj}}\right) - \nu_j^* \quad \ldots \quad \text{normalized phase angle of } k^{th} \text{ element of } j^{th} \text{ mode} \tag{2.53}$$

$$\nu_j^* = \nu_{kj}\,, \quad k \ni b_j^* = b_{kj} \quad \ldots \quad \text{phase angle normalization criterion} \tag{2.54}$$

The normalization criteria make the amplitude of the largest modal coefficient unity with zero phase, and phase lags are indicated by $\nu_{kj} > 0$.

Since the stability of the steady state solutions is of concern in sailing vessel dynamics, it is worthwhile to re-state the basic theorems. Detailed proofs of these theorems are given in slightly different form in Coddington and Levinson (1955).

Theorem 1 (Liapunov - Poincare Stability)

Given that

(1) the Taylor Series expansion of equation (2.13) exists with

(a) $\underline{f}(\underline{u}, \varphi, \theta, \psi, \underline{R}; P_k) = \underline{0}$ [equation (2.28) is satisfied]

(b) $\frac{d\underline{x}}{dt} = A\underline{x} + \underline{g}(\underline{x}) \quad , \quad \underline{x}(0) = \underline{c}$

where

$$\underline{g}(\underline{x}) = O(\|\underline{x}\|^2) \quad ,$$

(2) all eigenvalues of A have negative real parts, i.e.,

$$\alpha_j < 0 \qquad \forall\ j \in (1, 12) \quad , \tag{2.55}$$

(3) $\underline{c}$ is sufficiently small,

then the steady state solution to equation (2.28) is Liapunov asympotically stable, i.e.,

$$\lim_{t \to \infty} \|\underline{x}(t)\| = 0 \quad . \tag{2.56}$$

Theorem 2 (General Instability Theorem)

Given that

(1) as in Theorem 1,

(2) there exists at least one eigenvalue of A with positive real part, i.e.,

$$\alpha_j > 0 \quad \text{for some} \quad j \in (1, 12) \quad , \tag{2.57}$$

then the steady state solution to equation (2.28) is Liapunov unstable.

III. A DYNAMIC MODEL FOR SAILING VESSELS

The major piece of unfinished business of Chapter II is a detailed description of the forces in the equations of motion (2.13). This chapter sketches the development of these forces and gives a detailed formulation for use in the Steady State and Perturbational Equations.

3.1 Objectives and Assumptions

The general objectives of this study were given in Section 1.3. The model presented here is intended only to be a workable scheme for calculating the gross behavior of sailing vessels, not a fine tuned analysis of the fluid mechanics of sailing vessels.

A key question in this study is how do the dynamics of the vessel depend on speed and sailing angle? Figure 3.1 shows a probable envelope of steady state conditions for vessels sailing on port tack. The radial coordinate is the Froude Number based on waterline length

$$Fr = \frac{V_s}{\sqrt{gL}} \quad , \tag{3.1}$$

and Υ is the sailing angle. Specifically, the objective is to determine the eigenvalues and normal modes as functions of these parameters:

$$\left.\begin{aligned} \Lambda &= \Lambda(Fr, \Upsilon) \\ \underline{Y}_j &= \underline{Y}_j(Fr, \Upsilon) \end{aligned}\right\} \tag{3.2}$$

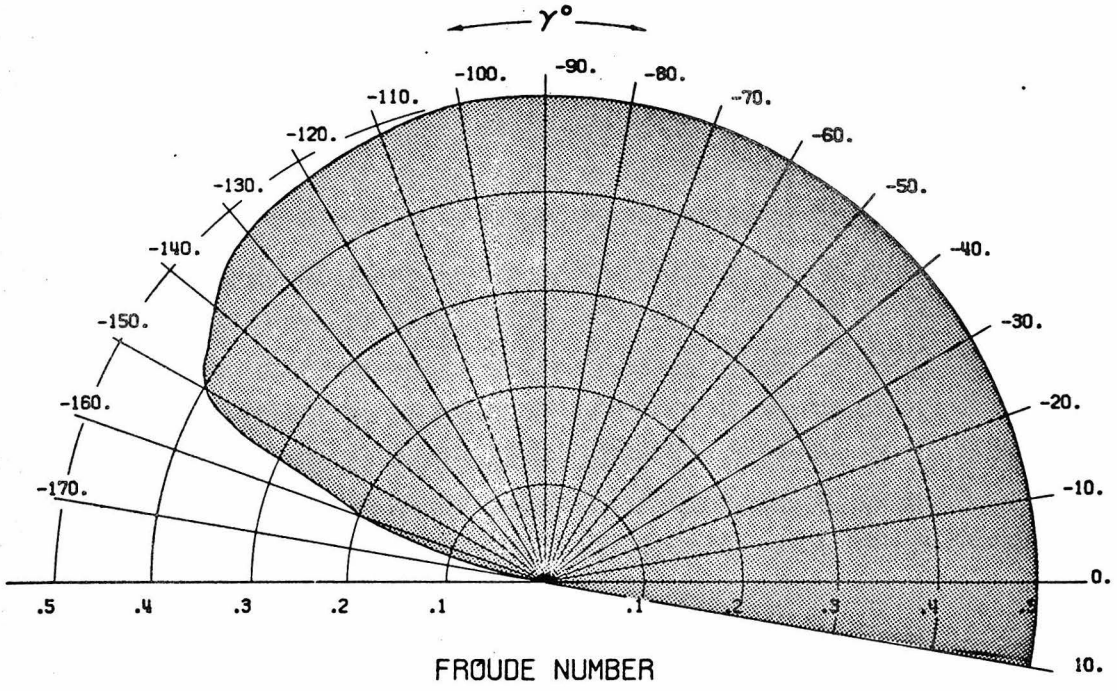


Figure 3.1. Sailing Envelope

The model developed in the following sections is primarily an attempt to provide insight into this question. Numerous assumptions are required; for reference some of the broader assumptions are listed here:

1. Flat water
2. The bare vessel has port-starboard symmetry
3. The controls (rudder and sails) are adjusted to achieve a steady state condition, then fixed

4. Quasi-static fluid flows
5. Complex pressure distributions can be replaced by discrete forces (resistance and sideforce) acting at specified points
6. There are no spanwise sideforces
7. Righting moments can be calculated with sufficient accuracy by the transverse and longitudinal metacentric heights
8. Rudder effects can be separated from the hull-keel
9. Except for sidewash from the keel, wake effects can be neglected
10. An equivalent sail can be used, i.e., no sail interaction

Finally, it is assumed that the forces can be separated into these groups: hull-keel forces, rudder forces and aerodynamic forces.

3.2 Hull-Keel Forces

Ideally the complex distribution of hydrodynamic pressures acting on the hull of a sailing vessel could be directly resolved into a system of forces similar to equation (2.25), i.e.,

$$\underline{f} = \underline{f}(\underline{u}, \varphi, \theta, \psi, \underline{R}; \underline{z}, \dot{\underline{z}}, \ddot{\underline{z}}; P_k) \quad . \tag{3.3}$$

However, there is insufficient analytical and experimental work on sailing vessels to permit such a formulation for general motions. The alternative method used here is to approximate these forces with a set of nondimensional coefficients. These can be calculated from full scale tests, such as the Antiope data in Appendix A.1, from model tests or analytical results.

Hydrodynamic lift and drag are the basic measurements on sailing hulls. To date results are available in the literature from tank tests on only one full scale vessel, namely, the 5.5 meter Antiope (Herreshoff and Newman 1967, Kirkman and Pedrick 1974, Letcher 1975). However, it appears that more full scale data may soon be available, e.g., Clauser 1975. The data from these tests have been used as a guide in the development of the hydrodynamic coefficients. If new tests indicate significantly different behavior from the Antiope results, modifications in this formulation may be required.

The results from the Antiope tests suggest the following minimal formulation for the hydrodynamic forces:

$$\underline{F}_K = \underline{F}_K(Fr, \alpha_K) \tag{3.4}$$

where α_K is the effective angle of incidence of the keel. Specifically, the nondimensional forces in the body frame $\mathfrak{F}_B$ are assumed to be of the form

$$\underline{F}_{K1} = -C_{K1} |\underline{u}_K| \underline{u}_K \tag{3.5}$$

$$\underline{F}_{K2} = -C_{K2} |\underline{u}_K| \underline{e}_3 \times \underline{u}_K \tag{3.6}$$

where

$$C_{K1} = C_{K1}(Fr, \alpha_K) \quad \ldots \quad \text{hull-keel resistance coefficient} \tag{3.7}$$

$$C_{K2} = C_{K2}(Fr, \alpha_K) \quad \ldots \quad \text{hull-keel sideforce coefficient} \tag{3.8}$$

$$\tan \alpha_K = \frac{u_2^K}{u_1^K} \quad \ldots \quad \text{hull-keel crossflow angle} \tag{3.9}$$

and

$$\underline{u}_K = T(z_4, z_5, z_6)\left[\underline{u} + \begin{Bmatrix} \dot{z}_1 \\ \dot{z}_2 \\ \dot{z}_3 \end{Bmatrix}\right] + \Omega \underline{r}_K \tag{3.10}$$

with

$$\underline{r}_K \quad \ldots \quad \text{hydrodynamic center} \quad . \tag{3.11}$$

This formulation is much simpler than some previous studies (Herreshoff 1964, Kerwin 1975) and requires some discussion. Froude Number dependence of the resistance coefficient is well established and is responsible for the asymptotic limiting of speed for displacement vessels. The dependence of sideforce on Froude Number is not well established*, and the results for Antiope at moderate speeds ($Fr \leq .36$) suggest a weak dependence (Letcher 1975). However, recent theoretical and experimental work (Chapman 1976) indicates that the generation of sideforce may show a significant dependence on Froude Number in the range of interest for sailing vessels ($Fr \leq .5$).

Since these coefficients are defined in the body frame, conventional lift and drag coefficients (based on tank axes similar to $\mathfrak{F}_1$) can be derived via the Euler transformation. This provides the dependence of resistance and sideforce on heel similar to that

---

*Davidson (1936) presents an interesting discussion with Von Karman on sideforce and wave generation.

reported by Letcher (1975). Heel is also considered in the calculation of the crossflow angle in equations (3.9) and (3.10). However, these are purely geometric effects; at large heel and heading angles the effect of heel on the hydrodynamics may be much more complicated. Figure 3.2 shows the geometry in the body frame of all the steady state forces for a vessel sailing close-hauled on port tack.

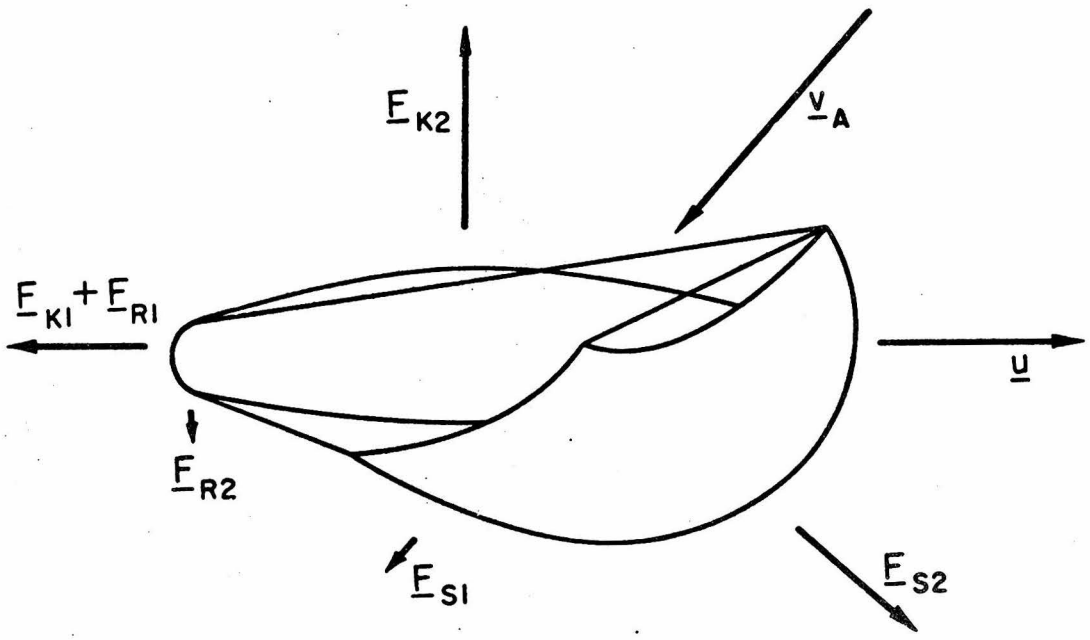


Figure 3.2. Geometry of Forces in Body Frame

The Taylor Series expansion of the hydrodynamic resistance and sideforce in the motion variables is straightforward but tedious. The steady state forces in $\mathfrak{F}_B$ are simply

$$\underline{F}_{K1} = -C_{K1}(Fr, \alpha_K)\,\underline{u} \tag{3.12}$$

$$\underline{F}_{K2} = -C_{K2}(Fr, \alpha_K)\begin{Bmatrix} -u_2 \\ u_1 \\ 0 \end{Bmatrix} \tag{3.13}$$

where

$$\tan \alpha_K = \frac{u_2}{u_1} = -\cos\varphi \tan\psi \tag{3.14}$$

and the moments are given by

$$\left.\begin{aligned} \underline{M}_{K1} &= \underline{r}_K \times \underline{F}_{K1} \\ \underline{M}_{K2} &= \underline{r}_K \times \underline{F}_{K2} \end{aligned}\right\} \tag{3.15}$$

Equation (3.15) uses the assumption of port-starboard symmetry such that there is no moment at zero sideforce.

The linear terms in the expansion are presented in the form of 3×6 matrices, which are related to equation (2.25) by

$$\begin{bmatrix} \left(\frac{\partial \underline{F}_{Ki}}{\partial \underline{z}}\right) \\ \left(\frac{\partial \underline{M}_{Ki}}{\partial \underline{z}}\right) \end{bmatrix} = \left(\frac{\partial \underline{f}_{Ki}}{\partial \underline{z}}\right) \quad , \qquad i \in (1,2) \quad . \tag{3.16}$$

The linear force terms are

$$\left(\frac{\partial \underline{F}_{K1}}{\partial \underline{z}}\right) = -\frac{\partial C_{K1}}{\partial \alpha_K}\left(\underline{u} \circ \frac{\partial \alpha_K}{\partial \underline{z}}\right) - C_{K1}\frac{\partial \underline{u}_K}{\partial \underline{z}} \tag{3.17}$$

$$\left(\frac{\partial \underline{F}_{K1}}{\partial \dot{\underline{z}}}\right) = -\frac{\partial C_{K1}}{\partial \alpha_K}\left(\underline{u} \circ \frac{\partial \alpha_K}{\partial \dot{\underline{z}}}\right) - \frac{\partial C_{K1}}{\partial Fr}\, Fr\left(\underline{u} \circ \frac{\partial |\underline{u}|}{\partial \dot{\underline{z}}}\right)$$

$$- C_{K1}\left[\left(\underline{u} \circ \frac{\partial |\underline{u}_K|}{\partial \dot{\underline{z}}}\right) + \left(\frac{\partial \underline{u}_K}{\partial \dot{\underline{z}}}\right)\right] \qquad (3.18)$$

$$\left(\frac{\partial \underline{F}_{K2}}{\partial \underline{z}}\right) = -\frac{\partial C_{K2}}{\partial \alpha_K}\left(\underline{u}_{K2} \circ \frac{\partial \alpha_K}{\partial \underline{z}}\right) - C_{K2}\left(\frac{\partial \underline{u}_{K2}}{\partial \underline{z}}\right) \qquad (3.19)$$

$$\left(\frac{\partial \underline{F}_{K2}}{\partial \dot{\underline{z}}}\right) = -\frac{\partial C_{K2}}{\partial \alpha_K}\left(\underline{u}_{K2} \circ \frac{\partial \alpha_K}{\partial \dot{\underline{z}}}\right) - \frac{\partial C_{K2}}{\partial Fr}\, Fr\left(\underline{u}_{K2} \circ \frac{\partial |\underline{u}|}{\partial \dot{\underline{z}}}\right)$$

$$- C_{K2}\left[\left(\underline{u}_{K2} \circ \frac{\partial |\underline{u}_K|}{\partial \dot{\underline{z}}}\right) + \left(\frac{\partial \underline{u}_{K2}}{\partial \dot{\underline{z}}}\right)\right] \quad , \qquad (3.20)$$

where

$$\underline{u}_{K2} = \underline{e}_3 \times \underline{u} \qquad (3.21)$$

$$\frac{\partial \alpha_K}{\partial \underline{z}} = \frac{1}{(u^*)^2}\begin{Bmatrix} 0 \\ 0 \\ 0 \\ u_1 u_3 \\ u_2 u_3 \\ -(u_1^2 + u_2^2) \end{Bmatrix} \qquad (3.22)$$

$$\frac{\partial \alpha_K}{\partial \dot{\underline{z}}} = \frac{1}{(u^*)^2}\begin{Bmatrix} -u_2 \\ u_1 \\ 0 \\ -u_1 r_3^K \\ -u_2 r_3^K \\ u_1 r_1^K + u_2 r_2^K \end{Bmatrix} \qquad (3.23)$$

$$\frac{\partial |\underline{u}|}{\partial \dot{\underline{z}}} = \begin{Bmatrix} u_1 \\ u_2 \\ u_3 \\ 0 \\ 0 \\ 0 \end{Bmatrix} \tag{3.24}$$

$$\frac{\partial |\underline{u}_K|}{\partial \dot{\underline{z}}} = \begin{Bmatrix} u_1 \\ u_2 \\ u_3 \\ u_3 r_2^K - u_2 r_3^K \\ u_1 r_3^K - u_3 r_1^K \\ u_2 r_1^K - u_1 r_2^K \end{Bmatrix} \tag{3.25}$$

$$\frac{\partial \underline{u}_K}{\partial \underline{z}} = \begin{bmatrix} 0 & 0 & 0 & 0 & -u_3 & u_2 \\ 0 & 0 & 0 & u_3 & 0 & -u_1 \\ 0 & 0 & 0 & -u_2 & u_1 & 0 \end{bmatrix} \tag{3.26}$$

$$\frac{\partial \underline{u}_K}{\partial \dot{\underline{z}}} = \begin{bmatrix} 1 & 0 & 0 & 0 & r_3^K & -r_2^K \\ 0 & 1 & 0 & -r_3^K & 0 & r_1^K \\ 0 & 0 & 1 & r_2^K & -r_1^K & 0 \end{bmatrix} \tag{3.27}$$

$$\frac{\partial \underline{u}_{K\beta}}{\partial \underline{z}} = \begin{bmatrix} 0 & 0 & 0 & -u_3 & 0 & u_1 \\ 0 & 0 & 0 & 0 & -u_3 & u_2 \\ 0 & 0 & 0 & 0 & 0 & 0 \end{bmatrix} \tag{3.28}$$

$$\frac{\partial \underline{u}_{K2}}{\partial \underline{\dot{z}}} = \begin{bmatrix} 0 & -1 & 0 & r_3^K & 0 & -r_1^K \\ 1 & 0 & 0 & 0 & r_3^K & -r_2^K \\ 0 & 0 & 0 & 0 & 0 & 0 \end{bmatrix} \tag{3.29}$$

$$u^* = (u_1^2 + u_2^2)^{\frac{1}{2}} \tag{3.30}$$

The moment terms are simply

$$\frac{\partial \underline{M}_{Ki}}{\partial \underline{z}} = (\underline{r}_K \times) \frac{\partial \underline{F}_{Ki}}{\partial \underline{z}} \quad , \qquad i \in (1,2), \text{ etc.} \tag{3.31}$$

where

$$(\underline{r}_K \times) = \begin{bmatrix} 0 & -r_3^K & r_2^K \\ r_3^K & 0 & -r_1^K \\ -r_2^K & r_1^K & 0 \end{bmatrix} \tag{3.32}$$

Test data indicate that the hydrodynamic center is not fixed but may vary with speed and crossflow angle, e.g., Letcher (1975). Accounting for these effects necessitates including terms of the form

$$\frac{\partial \underline{r}_K}{\partial \alpha_K} \quad , \quad \frac{\partial \underline{r}_K}{\partial \underline{\dot{z}}} \quad , \quad \text{etc.},$$

but there are insufficient data to justify this. However, since the analysis focusses only on small perturbations about steady state, it is always possible to choose an appropriate hydrodynamic center for each condition in the sailing envelope.

Hydrostatics

The attitude of a vessel for specified sailing conditions is largely determined by its buoyant properties. Following classical procedures (Blagoveshchensky 1962) the hydrostatic forces are divided into the principal part (constant displacement with ballast shifts) and the incremental buoyancy.

There is some concern whether the results of hydrostatic measurements can be used in dynamic calculations. Stephens (Herreshoff 1964) reports cases where the righting moment measured during tank tests on models was reduced by up to 25 percent compared with static values. Kerwin (1975) and Gerritsma, Kerwin and Moeyes (1975) incorporate terms in their formulations to account for this reduction in righting moment with speed. However, the full scale tests of Antiope revealed (Letcher 1975):

> Heel angles can be accurately predicted from static stability figures, with little evident dependence of stability on forward speed.

The results and interpretations from these full scale tests are adopted here, but again it should be acknowledged that these results may not be valid for hull forms significantly different than Antiope.

The moments due to the principal part of the buoyancy are calculated from the transverse and longitudinal metacentric heights. However, live ballast (usually crew weight) is shifted to provide additional righting moment. On the newer, light displacement vessels this is an important consideration. Of course, shifting ballast means

that the center of gravity of the system moves. This not only complicates the equations by changing the origin of the body coordinate system $\mathfrak{F}_B$, it also implies that the center of gravity may no longer be located on the vessel's centerline. The following notation is used for the change in the location of the center of gravity due to ballast shifts:

$$\underline{r}_m = \left\{ \begin{matrix} r_1^m \\ r_2^m \\ r_3^m \end{matrix} \right\} , \quad \left. \begin{matrix} r_1^m > 0 \Leftrightarrow \text{c.g. moves aft } (-\underline{e}_1) \\ r_2^m > 0 \Leftrightarrow \text{c.g. moves to port } (-\underline{e}_2) \\ r_3^m > 0 \Leftrightarrow \text{c.g. moves up } (-\underline{e}_3) \end{matrix} \right\} \tag{3.33}$$

For small angles of heel and trim, linear righting moment equations give adequate results; at large angles of heel ($\varphi \sim 30^o$) the righting moment curve has significant nonlinear behavior. The standard formulation of naval architecture (Moore 1967) is adopted here. Appendix A.1 gives some evidence of the validity of this assumption for Antiope.

In terms of the Eulerian angles the nondimensional steady state moments due to the principal part of the buoyancy (including ballast shifts) are

$$\underline{M}_{P_B} = \frac{m}{Fr^2} \left\{ \begin{matrix} -\overline{GM} \sin\varphi \cos\theta - r_2^m \cos\varphi \cos\theta \\ -\overline{GM}_L \sin\theta + r_1^m \cos\varphi \cos\theta \\ (\overline{GM}_L - \overline{GM}) \tan\varphi \sin\theta - r_1^m \sin\varphi \cos\theta - r_2^m \sin\theta \end{matrix} \right\} \tag{3.34}$$

where

$$\overline{GM} = \hat{\overline{GM}} - r_3^m, \quad \hat{\overline{GM}} \quad \ldots \quad \text{transverse metacentric without live ballast} \tag{3.35}$$

$$\overline{GM_L} = \hat{\overline{GM_L}} - r_3^m, \quad \hat{\overline{GM}} \quad \ldots \quad \text{longitudinal metacentric without live ballast} \tag{3.36}$$

The linear terms from the expansion are

$$\frac{\partial f_4^{PB}}{\partial z_4} = -\frac{m}{Fr^2}\left(\overline{GM}\cos\varphi\cos\theta - r_2^m \sin\varphi\cos\theta\right) \tag{3.37}$$

$$\frac{\partial f_4^{PB}}{\partial z_5} = -\frac{m}{Fr^2} r_2^m \sin\theta \tag{3.38}$$

$$\frac{\partial f_4^{PB}}{\partial z_6} = -\frac{m}{Fr^2}\overline{GM}\sin\theta \tag{3.39}$$

$$\frac{\partial f_5^{PB}}{\partial z_4} = -\frac{m}{Fr^2} r_1^m \sin\varphi\cos\theta \tag{3.40}$$

$$\frac{\partial f_5^{PB}}{\partial z_5} = -\frac{m}{Fr^2}\left(\overline{GM_L}\cos\varphi\cos\theta + r_1^m \sin\theta\right) \tag{3.41}$$

$$\frac{\partial f_5^{PB}}{\partial z_6} = \frac{m}{Fr^2}\overline{GM_L}\sin\varphi\cos\theta \tag{3.42}$$

$$\frac{\partial f_6^{PB}}{\partial z_4} = \frac{m}{Fr^2}\left[\left(\overline{GM_L} - \overline{GM}\right)\sec^2\varphi\sin\theta - r_1^m\cos\varphi\cos\theta\right] \tag{3.43}$$

$$\frac{\partial f_6^{PB}}{\partial z_5} = \frac{m}{Fr^2}[(\overline{GM}_L - \overline{GM}) \sin\varphi \sec\theta (1 + \tan^2\varphi \sin^2\theta) - r_2^m \cos\varphi \cos\theta] \quad (3.44)$$

$$\frac{\partial f_6^{PB}}{\partial z_6} = \frac{m}{Fr^2}[(\overline{GM}_L - \overline{GM}) \sec\varphi \sec\theta (\sin^2\theta - \sin^2\varphi \cos^2\theta) - r_1^m \sin\theta - r_2^m \sin\varphi \cos\theta] \quad (3.45)$$

Equation (3.34) is readily recognizable for the special case of zero trim ($\theta = 0$). In dimensional form it reduces to the standard equation for righting moment with a shifted center of gravity (Moore 1967)

$$K(\varphi) = -\underline{M}_{PB}\big|_{\theta=0} = mg(\overline{GM} \sin\varphi + r_2^m \cos\varphi) \quad . \quad (3.46)$$

The roll stiffness (or tenderness) of the vessel is given by

$$\frac{dK}{d\varphi} = mg(\overline{GM} \cos\varphi - r_2^m \sin\varphi) \quad , \quad (3.47)$$

which is of the same form as equation (3.37). This last equation is rather surprising: it states that transverse shifts in ballast to achieve lower heel angles reduce the roll stiffness, i.e., with crew weight on the rail the vessel is more tender to perturbations in roll.

Incremental Buoyancy

The incremental buoyancy force corresponds to a change in the submerged volume of the hull. The standard dimensional formulation from hydrostatics (Blagoveshchensky 1962) is

$$\underline{F}_{BI} = -\rho_w g A_w R_3 \underline{e}_3' \quad (3.48)$$

where

A_w ... waterplane area

R_3 ... amount c.g. moves perpendicular to free surface

Then the nondimensional steady state forces in $\mathfrak{F}_B$ are

$$\underline{F}_{B1} = -\frac{2A_w R_3}{Fr^2}\begin{Bmatrix} -\sin\theta \\ \sin\varphi\cos\theta \\ \cos\varphi\cos\theta \end{Bmatrix} \tag{3.49}$$

where for consistent notation

$$R_3 = R_3^o \quad \text{...} \quad \text{steady state sinkage} \ .$$

Since the incremental buoyancy acts at the center of flotation, the moment due to this force is just

$$\underline{M}_{B1} = (\underline{r}_f \times)\,\underline{F}_{B1} \ . \tag{3.50}$$

The linear terms from the expansion are given by the partitioned 3×6 matrix

$$\frac{\partial \underline{F}_{B1}}{\partial \underline{z}} = -\frac{2A_w}{Fr^2}\left[\begin{array}{c|ccc} \underline{T}_3 \circ \underline{T}_3 & 0 & -R_3\cos\varphi\cos\theta & R_3\sin\varphi\cos\theta \\ & R_3\cos\varphi\cos\theta & 0 & R_3\sin\theta \\ & -R_3\sin\varphi\cos\theta & -R_3\sin\theta & 0 \end{array}\right] \tag{3.51}$$

where

$$\underline{T}_3 = \begin{Bmatrix} -\sin\theta \\ \sin\varphi\cos\theta \\ \cos\varphi\cos\theta \end{Bmatrix} \quad \ldots \quad \text{third column of Euler transformation} \tag{3.52}$$

and the moment terms are similarly given by

$$\frac{\partial \underline{M}_{BI}}{\partial \underline{z}} = (\underline{r}_f \times) \frac{\partial \underline{F}_{BI}}{\partial \underline{z}} \quad . \tag{3.53}$$

Hydrodynamic Inertial and Wave Damping Forces

The hydrodynamic inertial forces were introduced in Chapter II. There has been considerable attention devoted to calculating these coefficients for ships (Blagoveshchensky 1962) or from experiments (Vugts 1968). Under standard assumptions, e.g., port-starboard symmetry, it can be shown by potential theory that for general motions these coefficients exhibit the following structure:

$$H = \begin{bmatrix} h_{11} & 0 & h_{13} & 0 & h_{15} & 0 \\ 0 & h_{22} & 0 & h_{24} & 0 & h_{26} \\ h_{31} & 0 & h_{33} & 0 & h_{35} & 0 \\ 0 & h_{24} & 0 & h_{44} & 0 & h_{46} \\ h_{15} & 0 & h_{35} & 0 & h_{55} & 0 \\ 0 & h_{26} & 0 & h_{46} & 0 & h_{66} \end{bmatrix} \tag{3.54}$$

Additionally, experimental studies on sailing hulls (Gerritsma 1968) and geometric cylinders have indicated that at least some of these coefficients are strongly dependent on Froude Number and oscillation frequency.

For the purposes of this study, experimental data are used to estimate these coefficients (Appendix A.2). The resulting non-zero coefficients are

$$H = H(Fr) = \begin{bmatrix} h_{11} & 0 & 0 & 0 & 0 & 0 \\ 0 & h_{22} & 0 & 0 & 0 & h_{26} \\ 0 & 0 & h_{33} & 0 & 0 & 0 \\ 0 & 0 & 0 & h_{44} & 0 & 0 \\ 0 & 0 & 0 & 0 & h_{55} & 0 \\ 0 & h_{62} & 0 & 0 & 0 & h_{66} \end{bmatrix} \tag{3.55}$$

Vugts (1968) also presents damping data for cylinders oscillating in heave. Since the analysis presented so far has no wave damping mechanism, these data are used in Appendix A.2 to give a rough estimate of damping in heave and pitch due to wave generation, i.e.,

$$\frac{\partial f_3^w}{\partial \dot{z}_3} \quad \text{and} \quad \frac{\partial f_5^w}{\partial \dot{z}_5} \quad .$$

3.3 Rudder Forces

Rudders serve two functions on sailing vessels. Their conventional role is as a control surface. Under typical sailing conditions the rudder is used in combination with sail adjustments to achieve and maintain a steady course. This function is taken account of in the Steady State Equations where the helm angle is calculated as part of the solution. Then in the perturbation

analysis, the helm is fixed at this steady state value. During these motions the rudder acts as a second keel and usually generates a substantial contribution to the total sideforce.

A thorough analysis of rudder behavior on sailing vessels is lacking, although much use has been made of airfoil data (e.g., Letcher 1974, Hammitt 1975). Appendix A.3 summarizes some experimental data on rudder sideforce. These data indicate that flow separation and wake effects can be critical. Detailed consideration of these fluid phenomena are beyond the objectives of this study, but it seems prudent to include some simple mechanisms in an attempt to crudely model the physical situation. Although prediction of sidewash due to the keel is very complex, airfoil theory can be used for a rough estimate of the change in angle of incidence at the rudder (Gerritsma 1968, Hoerner 1975). This is given by

$$\epsilon_K = \frac{kC_L}{2\pi AR_K} \sim \frac{kC_{K2}}{2\pi d^2} \quad \ldots \quad \text{sidewash estimate} \tag{3.56}$$

where

C_L ... conventional lift coefficient for keel

$$AR_K = \frac{d^2}{A_K} \quad \ldots \quad \text{geometric aspect ratio of the keel} \tag{3.57}$$

d ... draft of vessel

A_K ... keel area

Hoerner (1975) gives the following values for the sidewash factor:

$$k = \begin{cases} \sim 1.6 & \ldots \quad \text{experimental data on airfoils} \\ 2.0 & \ldots \quad \text{airfoil with elliptic lift distribution} \end{cases} \tag{3.58}$$

The angle of incidence of the rudder is given by

$$\alpha_R = \tan^{-1}\left(\frac{u_2^R}{u_1^R}\right) - \epsilon_K - \delta_R \tag{3.59}$$

where

$$\underline{u}_R = T(z_4, z_5, z_6)\left[\underline{u} + \begin{Bmatrix} \dot{z}_1 \\ \dot{z}_2 \\ \dot{z}_3 \end{Bmatrix}\right] + \Omega \underline{r}_R \tag{3.60}$$

$$\begin{aligned} \delta_R &\ldots \quad \text{helm angle} \\ \underline{r}_R &\ldots \quad \text{effective rudder center of pressure} \end{aligned} \tag{3.61}$$

Figure 3.3 shows the idealized steady state flow geometry at the rudder. For a vessel sailing on port tack, weather helm is indicated by negative values of δ_R.

There is little data describing rudder resistance. At zero sideforce ($\alpha_R = 0$) any resistance due to the rudder is assumed to be combined in the hull-keel resistance. Up to very large rudder angles where flow separation occurs, it seems consistent with the sidewash estimates to include the induced resistance due to the generation of sideforce. Then following the same procedure used

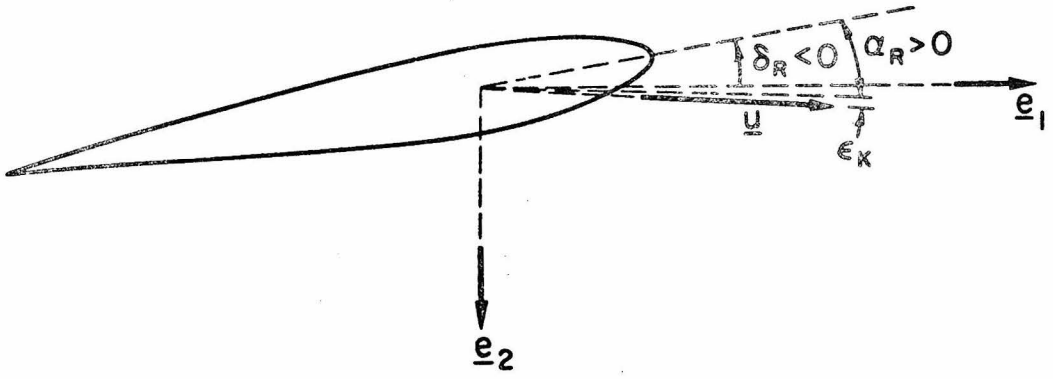


Figure 3.3. Idealized Flow Geometry at Rudder

for the hull-keel hydrodynamic forces, the steady state rudder forces are

$$\underline{F}_{R1} = -C_{R1}(Fr, \alpha_R)\,\underline{u} \tag{3.62}$$

$$\underline{F}_{R2} = -C_{R2}(Fr, \alpha_R) \begin{Bmatrix} -u_2 \\ u_1 \\ 0 \end{Bmatrix} \tag{3.63}$$

where

$$\alpha_R = \alpha_K - \epsilon_K - \delta_R \tag{3.64}$$

$$C_{R1} = \frac{C_{R2}^2}{2\pi AR_R} \,. \tag{3.65}$$

These forces are diagramed on Figure 3.2.

The linear terms from the expansion of the rudder sideforce are

$$\frac{\partial \underline{F}_{R2}}{\partial \underline{z}} = - \frac{\partial C_{R2}}{\partial \alpha_R} \left(1 - \sigma \frac{\partial C_{K2}}{\partial \alpha_K} \right) \left(\underline{u}_{R2} \circ \frac{\partial \alpha_K}{\partial \underline{z}} \right) - C_{R2} \left(\frac{\partial \underline{u}_{R2}}{\partial \underline{z}} \right) \tag{3.66}$$

$$\begin{aligned} \frac{\partial \underline{F}_{R2}}{\partial \dot{\underline{z}}} = & - \frac{\partial C_{R2}}{\partial \alpha_R} \left[\underline{u}_{R2} \circ \left(\frac{\partial \chi}{\partial \dot{\underline{z}}} - \sigma \frac{\partial C_{K2}}{\partial \alpha_K} \frac{\partial \alpha_K}{\partial \dot{\underline{z}}} \right) \right] \\ & - \left(\frac{\partial C_{R2}}{\partial Fr} - \sigma \frac{\partial C_{R2}}{\partial \alpha_R} \frac{\partial C_{K2}}{\partial Fr} \right) Fr \left(\underline{u}_{R2} \circ \frac{\partial |\underline{u}|}{\partial \dot{\underline{z}}} \right) \\ & - C_{R2} \left[\left(\underline{u}_{R2} \circ \frac{\partial |\underline{u}_R|}{\partial \dot{\underline{z}}} \right) + \left(\frac{\partial \underline{u}_{R2}}{\partial \dot{\underline{z}}} \right) \right] \end{aligned} \tag{3.67}$$

where

$$\underline{u}_{R2} = \underline{e}_3 \times \underline{u} \tag{3.68}$$

$$\sigma = \frac{k}{2\pi AR_K} \tag{3.69}$$

$$\frac{\partial \chi}{\partial \dot{\underline{z}}} = \frac{1}{(u^*)^2} \begin{Bmatrix} -u_2 \\ u_1 \\ 0 \\ -u_1 r_3^R \\ -u_2 r_3^R \\ (u_1 r_1^R + u_2 r_2^R) \end{Bmatrix} \tag{3.70}$$

$$\frac{\partial}{\partial \dot{\underline{z}}} \left| \underline{u}_R \right| = \begin{Bmatrix} u_1 \\ u_2 \\ u_3 \\ u_3 r_2^R - u_2 r_3^R \\ u_1 r_3^R - u_3 r_1^R \\ u_2 r_1^R - u_1 r_2^R \end{Bmatrix} \tag{3.71}$$

$$\frac{\partial \underline{u}_{R2}}{\partial \underline{z}} = \begin{bmatrix} 0 & 0 & 0 & -u_3 & 0 & u_1 \\ 0 & 0 & 0 & 0 & -u_3 & u_2 \\ 0 & 0 & 0 & 0 & 0 & 0 \end{bmatrix} \tag{3.72}$$

$$\frac{\partial \underline{u}_{R2}}{\partial \dot{\underline{z}}} = \begin{bmatrix} 0 & -1 & 0 & r_3^R & 0 & -r_1^R \\ 1 & 0 & 0 & 0 & r_3^R & -r_2^R \\ 0 & 0 & 0 & 0 & 0 & 0 \end{bmatrix} \tag{3.73}$$

Numerical estimates show that the linear terms from the expansion of the induced rudder resistance are quite small; therefore, they are omitted. The moment terms due to sideforce are given by

$$\frac{\partial \underline{M}_{R2}}{\partial \underline{z}} = (\underline{r}_R \times) \frac{\partial \underline{F}_{R2}}{\partial \underline{z}} , \quad \text{etc.} \tag{3.74}$$

3.4 Aerodynamic Forces

The aerodynamics of sailing vessels has received considerable attention as part of the development of aeronautics (Milgram 1972). Consistent with the objectives of this study, only a simple model of

the forces acting on the sails, rig and above water portions of the hull is assumed. However, methods have been developed to provide fine tuned estimates of these forces in performance predictions (Bradfield and Griswold 1977).

The model assumes that an equivalent sail can be constructed from wind tunnel data to include any gross effects of sail interaction, rigging, etc. Sail deformation, aerodynamic inertial effects and any moments at zero aerodynamic sideforce are neglected. The effects of heel are assumed to be purely geometric as suggested by Milgram (1968), but there is some evidence that the dependence may be more complicated (Kerwin, Oppenheim and Mays 1974). Consistent with the hydrodynamic forces, it is assumed that no spanwise sideforce is generated (Gerritsma, Kerwin and Moeyes 1975).

The steady state geometry of the idealized sail projected on to the $(\underline{e}_1, \underline{e}_2)$ plane is shown in Figure 3.4, where the apparent wind velocity is

$$\underline{V}_a = T(z_4, z_5, z_6)\left[T(\varphi, \theta, \psi)\underline{V}_T - \underline{u} - \begin{Bmatrix} \dot{z}_1 \\ \dot{z}_2 \\ \dot{z}_3 \end{Bmatrix}\right] - \Omega \underline{r}_3 \qquad (3.75)$$

and

$$\alpha_s = \tan^{-1}\left(\frac{V_1^a}{V_2^a}\right) + \frac{\pi}{2} - \delta_s \quad \ldots \text{ crossflow angle of sail}^* \qquad (3.76)$$

*To avoid numerical difficulties, variations of this equation are used on different points of sail.

δ_s ... boom angle (3.77)

$\underline{r}_s$ ... aerodynamic center (3.78)

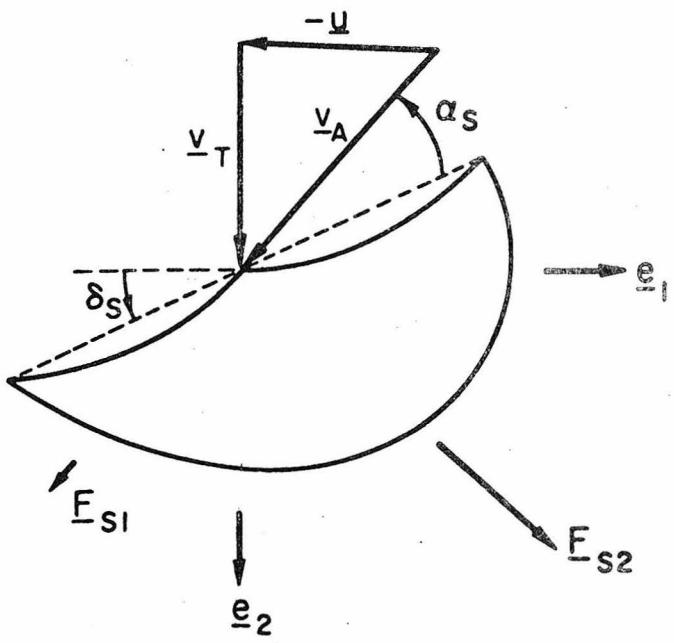


Figure 3.4. Idealized Sail Geometry

The aerodynamic force coefficients are assumed to depend only on the crossflow angle; explicit dependence on Reynolds Number is neglected. Appendix A.4 presents estimates of these coefficients for two data sets. The steady state aerodynamic forces based on these coefficients are given by

$$\underline{F}_{s1} = \rho C_{s1}(\alpha_s) V_a \underline{V}_a \quad \ldots \quad \text{aerodynamic resistance} \tag{3.79}$$

$$\underline{F}_{s2} = \rho C_{s2}(\alpha_s) V_a \underline{V}_{a2} \quad \ldots \quad \text{aerodynamic sideforce} \tag{3.80}$$

where

$$\rho = \frac{\rho_a}{\rho_w} \quad \ldots \quad \text{ratio of fluid densities} \tag{3.81}$$

$$\underline{V}_{a2} = -\underline{e}_3 \times \underline{V}_a \tag{3.82}$$

$$V_a = |\underline{V}_a^{\circ}| = |\underline{V}_T - \underline{u}| \quad . \tag{3.83}$$

The geometry of these forces is shown in Figure 3.2, and the corresponding moments are just

$$\underline{M}_{s1} = (\underline{r}_s \times) \underline{F}_{s1} \ , \quad \text{etc.} \tag{3.84}$$

The linear terms from the expansion are

$$\frac{\partial \underline{F}_{s1}}{\partial \underline{z}} = \rho V_a \left[\frac{dC_{s1}}{d\alpha_s} \left(\underline{V}_a \circ \frac{\partial \alpha_s}{\partial \underline{z}} \right) + C_{s1} \frac{\partial \underline{V}_a}{\partial \underline{z}} \right] \tag{3.85}$$

$$\frac{\partial \underline{F}_{s1}}{\partial \dot{\underline{z}}} = \rho \left[V_a \frac{dC_{s1}}{d\alpha_s} \left(\underline{V}_a \circ \frac{\partial \alpha_s}{\partial \dot{\underline{z}}} \right) + C_{s1} \left(\underline{V}_a \circ \frac{\partial |\underline{V}_a|}{\partial \dot{\underline{z}}} + V_a \frac{\partial \underline{V}_a}{\partial \dot{\underline{z}}} \right) \right] \tag{3.86}$$

$$\frac{\partial \underline{F}_{s2}}{\partial \underline{z}} = \rho V_a \left[\frac{dC_{s2}}{d\alpha_s} \left(\underline{V}_{a2} \circ \frac{\partial \alpha_s}{\partial \underline{z}} \right) + C_{s2} \frac{\partial \underline{V}_{a2}}{\partial \underline{z}} \right] \tag{3.87}$$

$$\frac{\partial \underline{F}_{s2}}{\partial \dot{\underline{z}}} = \rho \left[V_a \frac{dC_{s2}}{d\alpha_s} \left(\underline{V}_{a2} \circ \frac{\partial \alpha_s}{\partial \dot{\underline{z}}} \right) + C_{s2} \left(\underline{V}_{a2} \circ \frac{\partial |\underline{V}_a|}{\partial \dot{\underline{z}}} + V_a \frac{\partial \underline{V}_{a2}}{\partial \dot{\underline{z}}} \right) \right] \tag{3.88}$$

where

$$\frac{\partial \alpha_s}{\partial \underline{z}} = \frac{1}{(V_a^*)^2} \begin{Bmatrix} 0 \\ 0 \\ 0 \\ -V_1^a V_3^a \\ -V_2^a V_3^a \\ (V_a^*)^2 \end{Bmatrix} \tag{3.89}$$

$$\frac{\partial \alpha_s}{\partial \dot{\underline{z}}} = \frac{1}{(V_a^*)^2} \begin{Bmatrix} V_2^a \\ V_1^a \\ 0 \\ -V_1^a r_3^s \\ -V_2^a r_3^s \\ V_1^a r_1^s + V_2^a r_2^s \end{Bmatrix} \tag{3.90}$$

$$\frac{\partial |\underline{V}_a|}{\partial \dot{\underline{z}}} = \frac{1}{V_a} \begin{Bmatrix} -V_1^a \\ -V_2^a \\ -V_3^a \\ V_2^a r_3^s - V_3^a r_2^s \\ V_3^a r_1^s - V_1^a r_3^s \\ V_1^a r_2^s - V_2^a r_1^s \end{Bmatrix} \tag{3.91}$$

$$\frac{\partial \underline{V}_a}{\partial \underline{z}} = \begin{bmatrix} 0 & 0 & 0 & 0 & -V_3^a & V_2^a \\ 0 & 0 & 0 & V_3^a & 0 & -V_1^a \\ 0 & 0 & 0 & -V_2^a & V_1^a & 0 \end{bmatrix} \tag{3.92}$$

$$\frac{\partial \underline{V}_a}{\partial \dot{\underline{z}}} = \begin{bmatrix} -1 & 0 & 0 & 0 & -r_3^s & r_2^s \\ 0 & -1 & 0 & r_3^s & 0 & -r_1^s \\ 0 & 0 & -1 & -r_2^s & r_1^s & 0 \end{bmatrix} \tag{3.93}$$

$$\frac{\partial \underline{V}_{a2}}{\partial \underline{z}} = \begin{bmatrix} 0 & 0 & 0 & V_3^a & 0 & -V_1^a \\ 0 & 0 & 0 & 0 & V_3^a & -V_2^a \\ 0 & 0 & 0 & 0 & 0 & 0 \end{bmatrix} \tag{3.94}$$

$$\frac{\partial \underline{V}_{a2}}{\partial \dot{\underline{z}}} = \begin{bmatrix} 0 & -1 & 0 & r_3^s & 0 & -r_1^s \\ 1 & 0 & 0 & 0 & r_3^s & -r_2^s \\ 0 & 0 & 0 & 0 & 0 & 0 \end{bmatrix} \tag{3.95}$$

$$V_a^* = [(V_1^a)^2 + (V_2^a)^2]^{\frac{1}{2}} \quad , \tag{3.96}$$

and the moments are

$$\frac{\partial \underline{M}_{s1}}{\partial \underline{z}} = [\underline{r}_s \times] \frac{\partial \underline{F}_{s1}}{\partial \underline{z}} \quad , \quad \text{etc.} \tag{3.97}$$

3.5 Summary of Elements in the Dynamic Model

The objective has been to construct a simplified model of the fluid dynamic forces acting on a sailing vessel. The forces are expanded about the steady state condition in a Taylor Series; only the steady state and linear terms are retained. The model assumes that nondimensional force coefficients can be calculated from experimental data, and typical calculations are presented in the Appendices. The following elements describe the dynamic model:

Hydrodynamic

$$C_{K1}(Fr, \alpha_K) \quad , \quad \frac{\partial C_{K1}}{\partial \alpha_K}(Fr, \alpha_K) \quad , \quad \frac{\partial C_{K1}}{\partial Fr}(Fr, \alpha_K)$$

$$C_{K2}(Fr, \alpha_K) \quad , \quad \frac{\partial C_{K2}}{\partial \alpha_K}(Fr, \alpha_K) \quad , \quad \frac{\partial C_{K2}}{\partial Fr}(Fr, \alpha_K)$$

$$\underline{r}_K$$

Hydrostatic

$$\overline{GM} \quad , \quad \overline{GM}_L \quad , \quad \underline{r}_m$$

$$A_w \quad , \quad \underline{r}_f$$

Hydrodynamic Inertial and Wave Damping

$$H(Fr) \quad , \quad \frac{\partial f_3^w}{\partial \dot{z}_3} \quad , \quad \frac{\partial f_5^w}{\partial \dot{z}_5}$$

Rudder

$C_{R2}(Fr, \alpha_R)$, $\frac{\partial C_{R2}}{\partial \alpha_R}(Fr, \alpha_R)$, $\frac{\partial C_{R2}}{\partial Fr}(Fr, \alpha_R)$

δ_R

$\underline{r}_R$, AR_R , d

k

Aerodynamic

$C_{S1}(\alpha_S)$, $\frac{dC_{S1}}{d\alpha_S}(\alpha_S)$

$C_{S2}(\alpha_S)$, $\frac{dC_{S2}}{d\alpha_S}(\alpha_S)$

δ_S

$\underline{r}_S$

IV. DOWNWIND SAILING

This chapter presents a special model for the case when a vessel sails directly before the wind. Several assumptions are made on the form of the force coefficients of Chapter III. These assumptions produce two very useful simplifications: (1) the solution to the Steady State Equations can be expressed in closed form and (2) the Perturbation Equations decouple into longitudinal and lateral groups. This decoupling permits comparison with the standard equations of ship motions (Abkowitz 1969) and airplane dynamics (Etkin 1972). Downwind sailing is of interest in its own right, since steering difficulties are usually more pronounced on this point of sail. Some of the results of this chapter have been previously published (Titlow 1977).

4.1 Assumptions

Downwind sailing is characterized by the vessel's steady state trajectory being coincident with the true wind direction. Assuming the vessel sails upright, this configuration is specified by

$$\underline{u} = V_s \underline{e}_1' \tag{4.1}$$

$$\gamma = \psi = 0 \tag{4.2}$$

$$\varphi = 0 \ . \tag{4.3}$$

Port-starboard symmetry is assumed throughout: specifically

$$r_2 = 0 \quad \ldots \quad \text{all force centers on centerline of vessel} \tag{4.4}$$

$$\delta_S = \frac{\pi}{2} \quad \ldots \quad \text{sail squared off} \tag{4.5}$$

$$\delta_R = 0 \quad \ldots \quad \text{neutral helm} \; . \tag{4.6}$$

These assumptions, together with the downwind configuration, yield the following steady state conditions:

$$\alpha_K = \alpha_R = 0 \tag{4.7}$$

$$\lambda = 0 \tag{4.8}$$

$$\alpha_S = \frac{\pi}{2} \; . \tag{4.9}$$

Appendix A summarizes experimental data on the force coefficients. For downwind sailing these coefficients at steady state are assumed to have the following special form:

$$\frac{\partial C_{K1}}{\partial \alpha_K} = \frac{\partial C_{R1}}{\partial \alpha_R} = 0 \quad \ldots \quad \text{hydrodynamic resistances are a minimum} \tag{4.10}$$

$$C_{K2} = C_{R2} = 0 \quad \ldots \quad \text{no hydrodynamic sideforce} \tag{4.11}$$

$$\frac{\partial C_{K2}}{\partial Fr} = \frac{\partial C_{R2}}{\partial Fr} = 0 \quad \ldots \quad \text{hydrodynamic sideforces independent of Froude Number} \tag{4.12}$$

$$k = 0 \quad \ldots \quad \text{sidewash is neglected} \tag{4.13}$$

$$\frac{dC_{S1}}{d\alpha_S} = 0 \quad \ldots \quad \text{aerodynamic resistance is a maximum} \tag{4.14}$$

$$C_{S2} = 0 \quad \ldots \quad \text{no aerodynamic sideforce} \tag{4.15}$$

4.2 Steady State Equations and Solutions

The Steady State Equations (2.28) with the force coefficients of Chapter III and the assumptions of downwind sailing, i.e., equations (4.1 - 4.15), reduce to the following simple form:

$$C_{K1}(Fr,0) - \rho(V_T - 1)^2 C_{S1}(\tfrac{\pi}{2}) = 0 \tag{4.16}$$

$$\tan\theta = \frac{(m/Fr^2)r_1^m + \rho(V_T - 1)^2 C_{S1}(r_3^s - r_3^K)}{(m/Fr^2)\overline{GM}_L + \rho(V_T - 1)^2 C_{S1}(r_1^s - r_1^K)} \tag{4.17}$$

$$R_3 = 0 \ . \tag{4.18}$$

Equation (4.18) states that there is no steady state sinkage*, i.e., the displacement is unchanged from the stationary condition. Equation (4.16) is a re-statement of the familiar balance of thrust and drag. For fixed Froude Number this equation is easily solved for the nondimensional true wind speed

$$V_T = 1 + \sqrt{\frac{C_{K1}(Fr,0)}{\rho\, C_{S1}(\pi/2)}} \tag{4.19}$$

Obtaining the solution in this manner is contrary to the physical situation where the ambient wind speed (V_T) is given and a particular boat speed (V_S) results. However, solving the inverse problem

---

*In this study sinkage is a consequence of the force balance required to achieve steady state. It should not be confused with dynamic sinkage, e.g., Herreshoff and Newman (1967).

reduces the computational effort substantially. With the results of equation (4.16), equation (4.17) can be solved directly.

To summarize, the complete steady state solution for Downwind Sailing is given by equations (4.1) - (4.3), (4.5), (4.6) and (4.17) - (4.19). Typical solutions are described in section 4.4.

4.3 Lateral Equations of Downwind Sailing

The conditions and assumptions of Downwind Sailing are sufficient to cause the Perturbation Equations (2.29) to decouple into two sets of three equations. One group is commonly termed the Lateral Equations (Etkin 1972) and is composed solely of sway, roll and yaw motions. The detailed structure of these equations is shown in their scalar representation:

$$(m + h_{22})\ddot{z}_2 + h_{26} \sec\theta\, \ddot{z}_6 + \left[C_K + \frac{\partial C_{R2}}{\partial \alpha_R} + \rho(V_T - 1)C_S \right] \dot{z}_2$$

$$- \left[C_K r_3^K + \frac{\partial C_{R2}}{\partial \alpha_R} r_3^R + \rho(V_T - 1)C_S r_3^S + m \sin\theta \right] \dot{z}_4$$

$$+ \left[C_K r_1^K + \frac{\partial C_{R2}}{\partial \alpha_R} r_1^R + \rho(V_T - 1)C_S r_1^S + m(1 - \sin\theta \tan\theta) \right] \dot{z}_6$$

$$+ \left[\frac{\partial C_{K2}}{\partial \alpha_K} + \frac{\partial C_{R2}}{\partial \alpha_R} - \rho(V_T - 1)^2 \frac{dC_{S2}}{d\alpha_S} \right] \sin\theta\, z_4$$

$$- \left[\frac{\partial C_{K2}}{\partial \alpha_K} + \frac{\partial C_{R2}}{\partial \alpha_R} - \rho(V_T - 1)^2 \frac{dC_{S2}}{d\alpha_S} \right] \cos\theta\, z_6 = 0 \quad . \qquad (4.20)$$

$$(I_x + h_{44})\ddot{z}_4 + [(I_x + h_{44}) \tan\theta - I_{xz} \sec\theta]\ddot{z}_6$$

$$- [C_K r_3^K + \frac{\partial C_{R2}}{\partial \alpha_R} r_3^R + \rho(V_T - 1)C_S r_3^S]\dot{z}_2$$

$$+ [C_K (r_3^K)^2 + \frac{\partial C_{R2}}{\partial \alpha_R} (r_3^R)^2 + \rho(V_T - 1)C_S (r_3^S)^2]\dot{z}_4$$

$$- [C_K r_1^K r_3^K + \frac{\partial C_{R2}}{\partial \alpha_R} r_1^R r_3^R + \rho(V_T - 1)C_S r_1^S r_3^S]\dot{z}_6$$

$$+ [-C_K r_3^K - \frac{\partial C_{R2}}{\partial \alpha_R} r_3^R + \rho(V_T - 1)^2 C_S r_3^S + \frac{m}{Fr^2} \overline{GM} \cot\theta] \sin\theta z_4$$

$$+ [C_K r_3^K + \frac{\partial C_{R2}}{\partial \alpha_R} r_3^R - \rho(V_T - 1)^2 C_S r_3^S + \frac{m}{Fr^2} \overline{GM} \tan\theta] \cos\theta z_6$$

$$= 0 \quad . \tag{4.21}$$

$$h_{62}\ddot{z}_2 - I_{xz}\ddot{z}_4 + [(I_z + h_{66}) \sec\theta - I_{xz} \tan\theta]\ddot{z}_6$$

$$+ [C_K r_1^K + \frac{\partial C_{R2}}{\partial \alpha_R} r_1^R + \rho(V_T - 1)C_S r_1^S]\dot{z}_2$$

$$- [C_K r_1^K r_3^K + \frac{\partial C_{R2}}{\partial \alpha_R} r_1^R r_3^R + \rho(V_T - 1)C_S r_1^S r_3^S]\dot{z}_4$$

$$+ [C_K (r_1^K)^2 + \frac{\partial C_{R2}}{\partial \alpha_R} (r_1^R)^2 + \rho(V_T - 1)C_S (r_1^S)^2]\dot{z}_6$$

$$+ \{C_K r_1^K + \frac{\partial C_{R2}}{\partial \alpha_R} r_1^R - \rho(V_T - 1)^2 C_S r_1^S + \frac{m}{Fr^2} [-(\overline{GM}_L - \overline{GM})$$

$$+ r_1^m \cot\theta]\} \sin\theta z_4 - \{C_K r_1^K + \frac{\partial C_{R2}}{\partial \alpha_R} r_1^R - \rho(V_T - 1)^2 C_S r_1^S$$

$$- \frac{m}{Fr^2} [-(\overline{GM}_L - \overline{GM}) \tan^2\theta + r_1^m \tan\theta]\} \cos\theta z_6 = 0 \quad . \tag{4.22}$$

where

$$C_K = C_{K1} + \frac{\partial C_{K2}}{\partial \alpha_K} \tag{4.23}$$

$$C_S = C_{S1} + \frac{dC_{S2}}{d\alpha_S} \tag{4.24}$$

The structure of the Lateral Equations is basically the same as used in previous dynamic models of sailing vessels, e.g., Curtiss (1970), Milgram (1972) and Gerritsma and Moeyes (1973). Some of those results were summarized in Figure 1.1. The observed steering difficulties of yachts are usually attributed to the stability properties of these equations.

The Lateral Equations have no z_2 terms; this is a consequence of the general assumption of no dependence on position in the plane of the free surface. Noting this, it is convenient to re-define the eigenvalue problem for the Lateral Equations as a system of five, first order equations. Let

$$\underline{x} = \begin{Bmatrix} z_4 \\ z_6 \\ \dot{z}_2 \\ \dot{z}_4 \\ \dot{z}_6 \end{Bmatrix} , \tag{4.25}$$

then in matrix form, the Lateral Equations are

$$\frac{d\underline{x}}{dt} = ZM^{-1}A\underline{x} , \quad \underline{x}(0) = \underline{c} \tag{4.26}$$

$$M = \begin{bmatrix} 1 & 0 & 0 & 0 & 0 \\ 0 & 1 & 0 & 0 & 0 \\ 0 & 0 & (m+h_{22}) & 0 & h_{26} \\ 0 & 0 & 0 & (I_x+h_{44}) & -I_{xz} \\ 0 & 0 & h_{62} & -I_{xz} & (I_z+h_{66}) \end{bmatrix} \tag{4.27}$$

$$Z = \begin{bmatrix} 1 & -\sin\theta & 0 & 0 & 0 \\ 0 & \cos\theta & 0 & 0 & 0 \\ 0 & 0 & 1 & 0 & 0 \\ 0 & 0 & 0 & 1 & -\sin\theta \\ 0 & 0 & 0 & 0 & \cos\theta \end{bmatrix}, \tag{4.28}$$

and

$$A = \begin{bmatrix} 0 & 0 & 0 & 1 & 0 \\ 0 & 0 & 0 & 0 & 1 \\ \frac{\partial f_2}{\partial z_4} & \frac{\partial f_2}{\partial z_6} & \frac{\partial f_2}{\partial \dot{z}_2} & \left(\frac{\partial f_2}{\partial \dot{z}_4}+m\sin\theta\right) & \left[\frac{\partial f_2}{\partial \dot{z}_6}-m(1-\sin\theta\tan\theta)\right] \\ \frac{\partial f_4}{\partial z_4} & \frac{\partial f_4}{\partial z_6} & \frac{\partial f_4}{\partial \dot{z}_2} & \frac{\partial f_4}{\partial \dot{z}_4} & \frac{\partial f_4}{\partial \dot{z}_6} \\ \frac{\partial f_6}{\partial z_6} & \frac{\partial f_6}{\partial z_6} & \frac{\partial f_6}{\partial \dot{z}_2} & \frac{\partial f_6}{\partial \dot{z}_4} & \frac{\partial f_6}{\partial \dot{z}_6} \end{bmatrix} \tag{4.29}$$

The elements in the last three rows of the matrix A correspond to the coefficients in the scalar equations (4.20) - (4.22). The solution of the Lateral Equations can be expressed in the notation of section

2.3 with the indices restricted to

$$k, j \in (1,5) \quad . \tag{4.30}$$

4.4 Discussion of Numerical Solutions to the Lateral Equations

The Steady State and Lateral Equations of Downwind Sailing can be readily solved using the data in the appendices and standard numerical techniques (see Chapter VI). The motivation for these calculations is to demonstrate how the eigenvalues and normal modes are affected by the system parameters. The data have been collected from tests on vessels of various description, and they were extrapolated to provide all the necessary input data. This process will not yield a fine tuned estimate of the steady state solutions and normal modes for any particular vessel, but it is intended that the results should be representative of the type of dynamic behavior which can be expected of sailing vessels. Of course, this can be determined as soon as appropriate full scale dynamic experiments are made.

Base Boat

Appendix A.5 defines the Base Boat. Its geometry and inertial properties are typical of a light displacement keelboat with a waterline length of 20 feet (6.1 meters). Data from the full scale tests of Antiope are developed in Appendix A.1 for the hull-keel coefficients. The rudder and inertial coefficients are calculated from the half ton model test data of Gerritsma (1968) and Gerritsma and Moeyes (1973) in Appendices A.2 and A.3. Sail coefficients

based on the wind tunnel tests of a soft model Finn sail (Marchaj 1973) are computed in Appendix A.4.

The solution to the Steady State Equations of Downwind Sailing (4.17) and (4.19) for the Base Boat are shown in Figures 4.1 and 4.2.

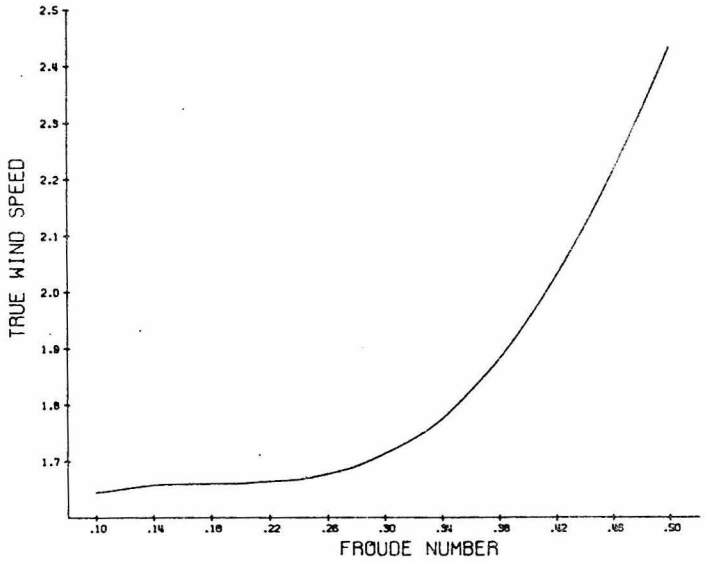


Figure 4.1. Steady State Solution for Downwind Sailing: True Wind Speed vs. Froude Number

At moderate to high speeds the effect of hull drag due to wave generation is evident with the rapid increase of true wind speed. Comparison with sailing observations (Appendix B) indicates that the calculated true wind speeds may be somewhat low. The trim angle at low speed is positive (bow up) due to the aft location of live ballast (Appendix A.5). The trim angle decreases rapidly at high speed, but since the Base Boat is rather stiff in trim

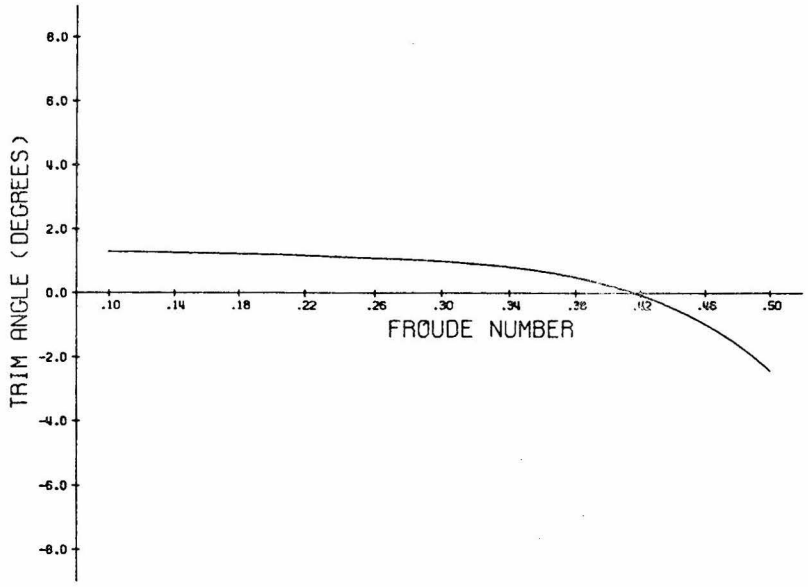


Figure 4.2. Steady State Solution for Downwind Sailing: Trim Angle vs. Froude Number

($\overline{GM}_L$ = 1.4), it remains small. Figure 4.3 summarizes the solution to the Lateral Equations of Downwind Sailing for the Base Boat, i.e., equations (4.26) and (2.40). A detailed description of these plots is given in Appendix C.

There are several interesting features from the results for the Base Boat:

1. Since the order of the Lateral Equations (4.26) is odd, there always exists at least one real eigenvalue. The calculations show that in general there are three real eigenvalues and only one complex conjugate pair.

2. The modal coefficients indicate that at low speed the complex eigenvalues correspond to almost a pure oscillation in roll

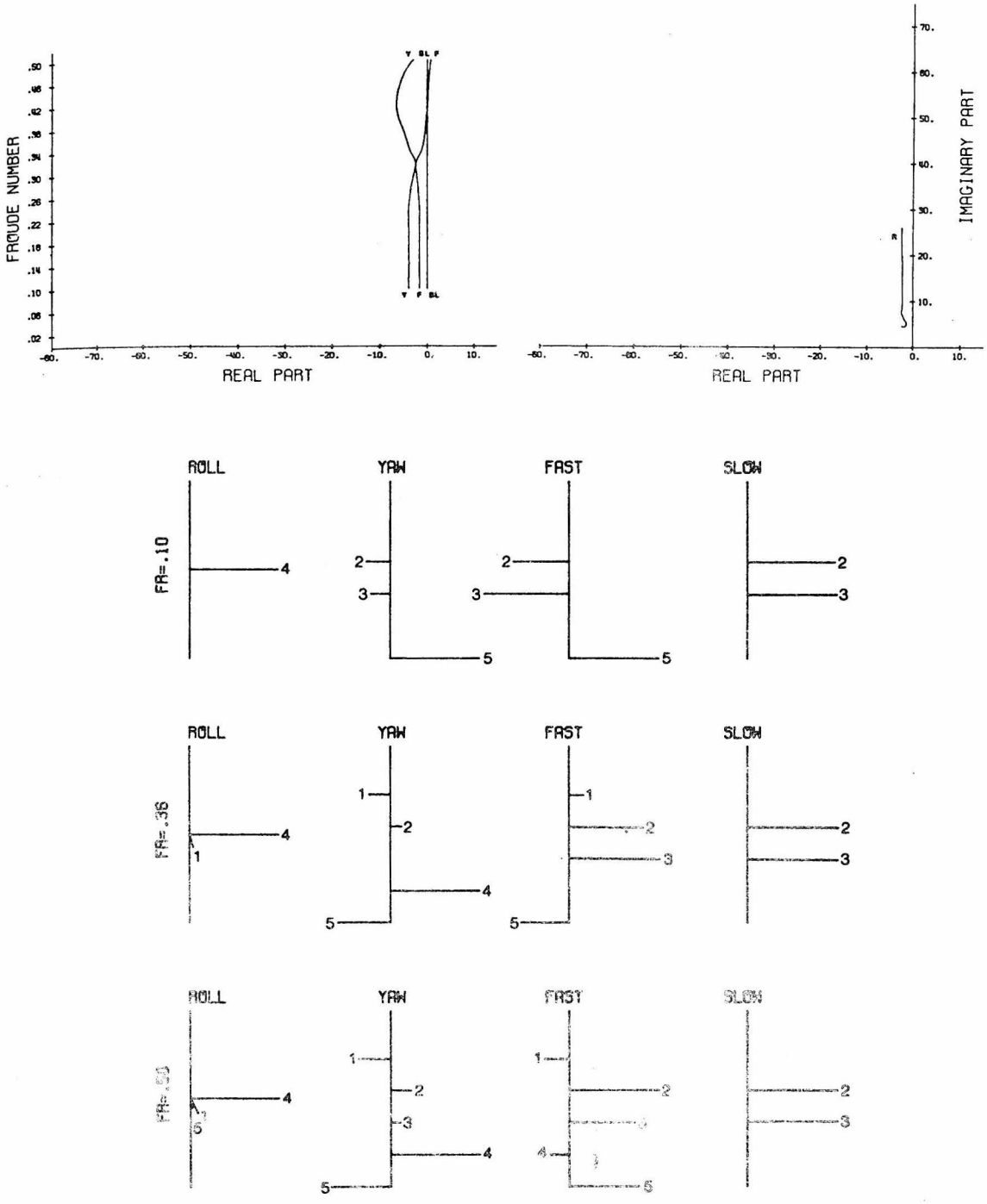


Figure 4.3. Solution to Lateral Equations of Downwind Sailing for Base Boat

($x_4 = \dot{z}_4$). At higher speeds there is some motion in yaw ($x_5 = \dot{z}_6$). Due to this dominant characteristic, this is termed the Roll Mode. Figure 4.4 shows some of the same data for the Roll Mode replotted in the form of the dimensional natural

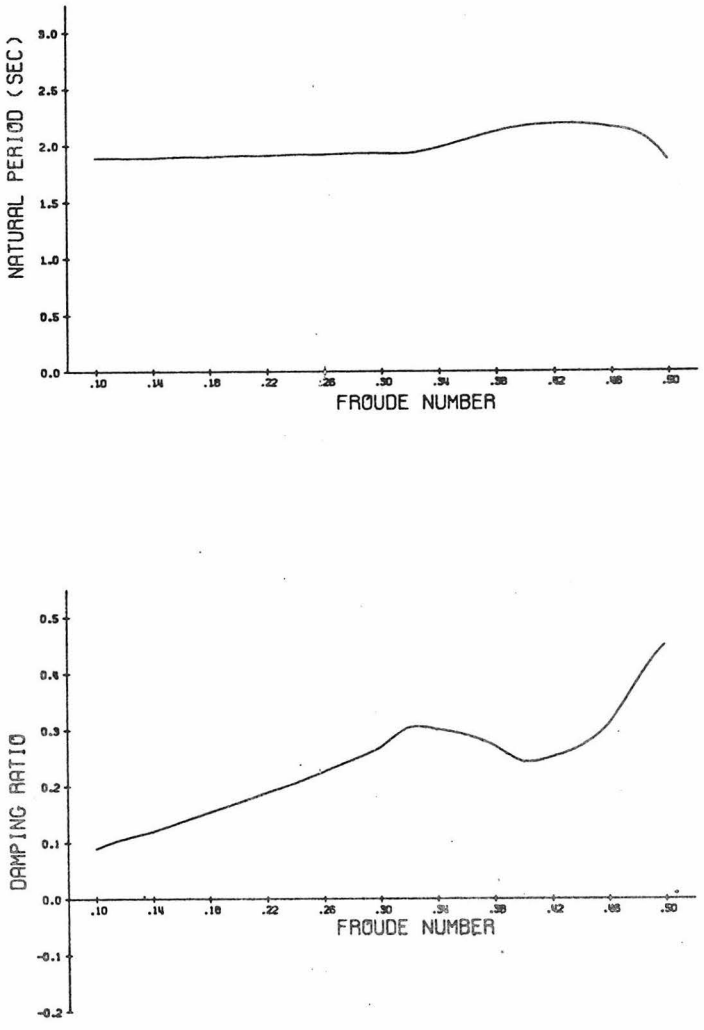


Figure 4.4. Roll Natural Period and Damping for Base Boat Sailing Downwind

period and damping ratio, i.e., equations (2.49) and (2.50). As before all dimensional quantities correspond to a vessel with waterline length of 20 feet. The natural period is relatively constant for $Fr \leq .32$ but shows some variation at high speed. The damping increases linearly in the low and high speed ranges. Near hull speed the damping has local extrema, which can also be seen on Figure 4.3.

3. There is always one real eigenvalue close to the boundary of unstable solutions, i.e.,

$$\Re e(\lambda_j) = 0 \quad , \tag{4.31}$$

and the mode is dominated by sway motions ($x_3 = \dot{z}_2$). The time constant given by equation (2.44) for this mode is always large, and hence, it is called the Slow Mode. Typical dimensional values of the time constant are given in Table 4.1. This is a weak mode which may be stable ($T_j > 0$) or unstable ($T_j < 0$) (Titlow 1977).

Table 4.1. Lateral Time Constants for Base Boat (sec.)

Froude No.	.10	.36	.50
Slow Mode	-530.	-100.	-51.
Fast Mode	4.9	3.3	-2.0
Yaw Mode	2.0	0.5	0.5

4. The two remaining real eigenvalues correspond to complicated sway-yaw-roll motions. At low speeds they are relatively constant, but they coalesce at Fr = .32 to form a complex mode. One eigenvalue becomes positive at high speed. This is called the Fast Mode, and Table 4.1 indicates that it has a relatively short time constant. Since the roll and yaw motions are 180° out of phase, this instability is interpreted as a broach to leeward. The remaining eigenvalue is always negative and is usually dominated by yawing motions; it is called the Yaw Mode.

This completes the discussion of the important results from the calculations for the Base Boat. Additional insight can be obtained by systematically varying the input data. This will be done for a few simple cases to demonstrate the sensitivity of the method. Only one parameter will be changed from the Base Boat in each case. Except for the case of Pitch-Tender Vessels, the steady state solutions are identical with those for the Base Boat given in Figures 4.1 and 4.2.

Aerodynamic Sideforce

The aerodynamic coefficients from the rigid, Gottingen foil (Appendix A.4) were used in place of the Finn sail data. The only change in this case is the slope of the sideforce curve, i.e.,

$$\left.\frac{dC_{S2}}{d\alpha_S}\right|_{\alpha_S = \frac{\pi}{2}}$$

The eigenvalues for this case are plotted in Figure 4.5, and the damping ratio of the Roll Mode is shown in Figure 4.6.

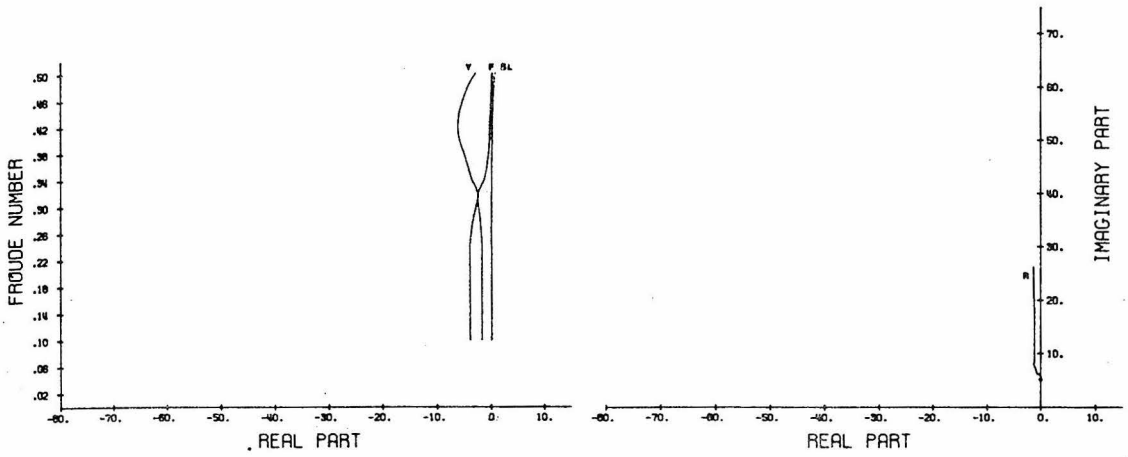


Figure 4.5. Lateral Eigenvalues with Gottingen Foil

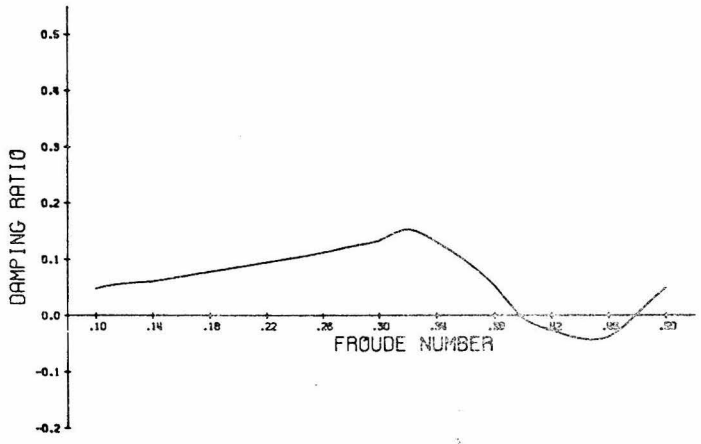


Figure 4.6. Damping Ratio of Downwind Roll Mode with Gottingen Foil

These plots show that with the Gottingen foil the Roll Mode has a critical region above hull speed where divergent oscillations occur. This case seems to correlate with the wind tunnel tests of Marchaj (1971), where it was demonstrated that under the conditions of Downwind Sailing large amplitude roll oscillations could develop. The real eigenvalues are similar to those of the Base Boat, except at high speed both the Slow and Fast Modes correspond to broaches to weather. The time constants are 6.3 and 1.9 seconds.

Rudder Sideforce

Gerritsma and Moeyes (1973) provide rudder sideforce data from model tests of the 12-meter yachts Valiant and and Columbia (Appendix A.3). These data were used in place of the half ton coefficients of the Base Boat. Figures 4.7 and 4.8 summarize the results of the calculations.

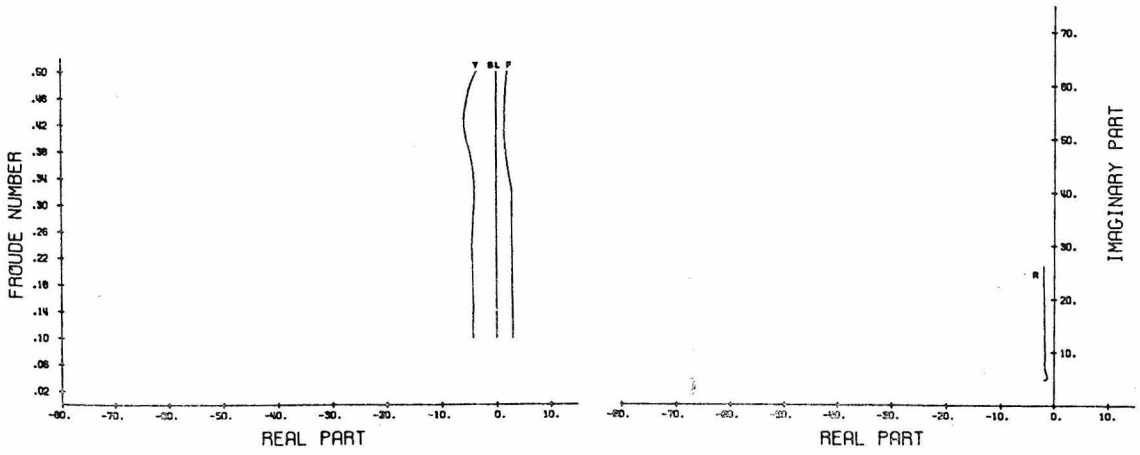


Figure 4.7. Lateral Eigenvalues with Valiant's Rudder

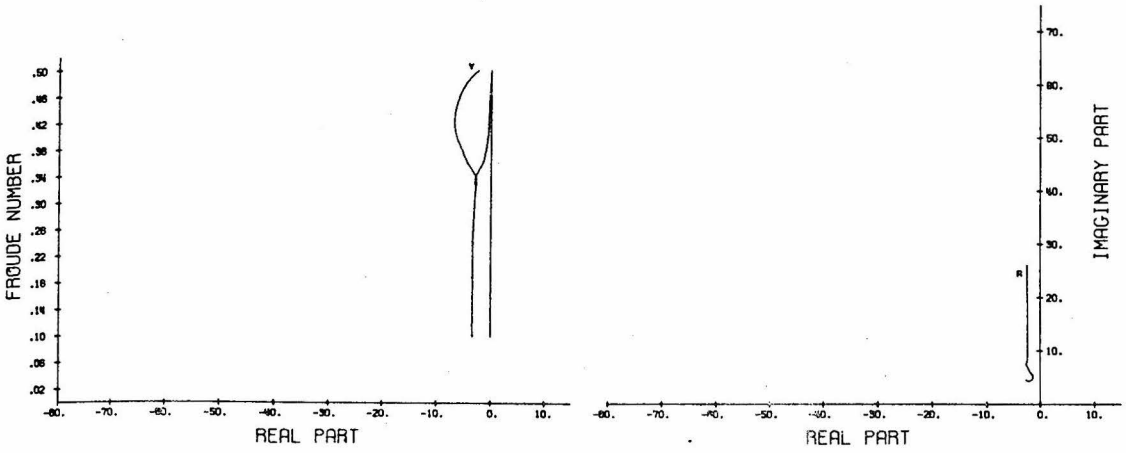


Figure 4.8. Lateral Eigenvalues with Columbia's Rudder

The Fast Mode with Valiant's rudder has a positive eigenvalue throughout the speed range and corresponds to a broach to leeward. The time constants for this mode are much shorter than for the Base Boat; they are summarized in Table 4.2.

Table 4.2. Lateral Time Constants with Valiant's Rudder (sec.)

Froude No.	.10	.36	.50
Slow Mode	3500.	1500.	-130.
Fast Mode	-2.6	-1.1	-.76
Yaw Mode	1.8	.50	.46

With Columbia's rudder data the character of the solution has changed. There are two complex modes at low and high speeds. For Fr < .36 the Fast and Yaw Modes coalesce to form a heavily

damped complex mode, whose natural period varies from 15 seconds at low speed to about 5 seconds at Fr = .34. As speed increases the complex mode degenerates into two real modes, but at high speed the Fast and Slow roots coalesce to form a long period (60 seconds) unstable mode. The Roll Mode for these two cases is essentially the same as for the Base Boat.

Previous studies of Valiant and Columbia were summarized in Figure 1.1. The eigenvalues fall in the same general range as calculated here except for the Fast Mode. It is tempting to speculate that the large difference in course-keeping ability between Valiant and Columbia reported by Milgram (1972) was largely due to rudder effectiveness.

Displacement

The Base Boat is typical of a light displacement keelboat with displacement-to-length ratio (DLR*) of about 150. The effect of displacement on the eigenvalues is shown first for a heavy displacement vessel (DLR ~ 360) in Figure 4.9, then for an ultra-light displacement craft (DLR ~ 70) in Figure 4.10. Only the mass of the vessel and the hydrodynamic inertial coefficients derived from it are changed. This is somewhat unrealistic, since displacement changes of this magnitude would be accompanied by other parameter changes, e.g., I_{ij}, $\overline{GM}$, $\underline{r}_s$, etc. However, the intent is only to demonstrate the method and indicate the sensitivity to some gross

*See Appendix A.5.

parameters. Table 4.3 summarizes the time constants for these cases.

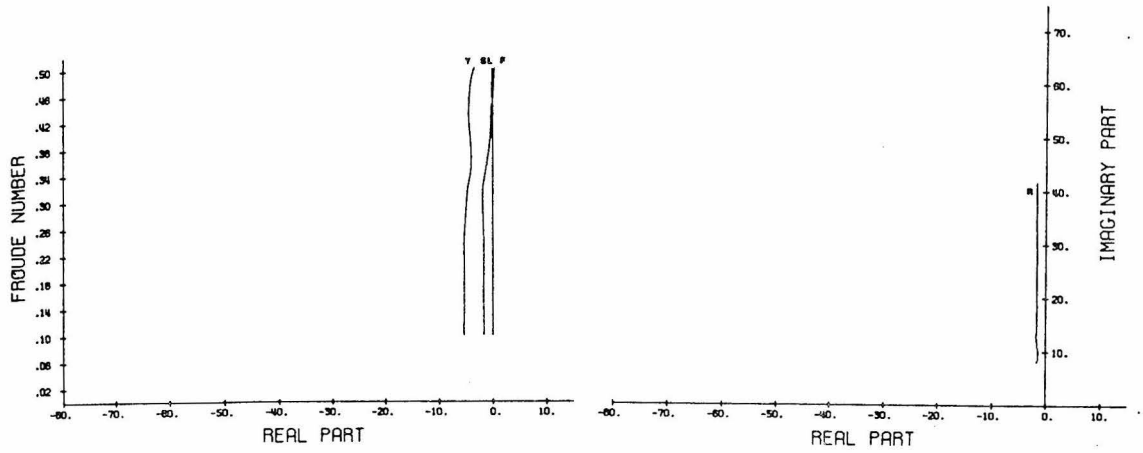


Figure 4.9. Lateral Eigenvalues with Heavy Displacement

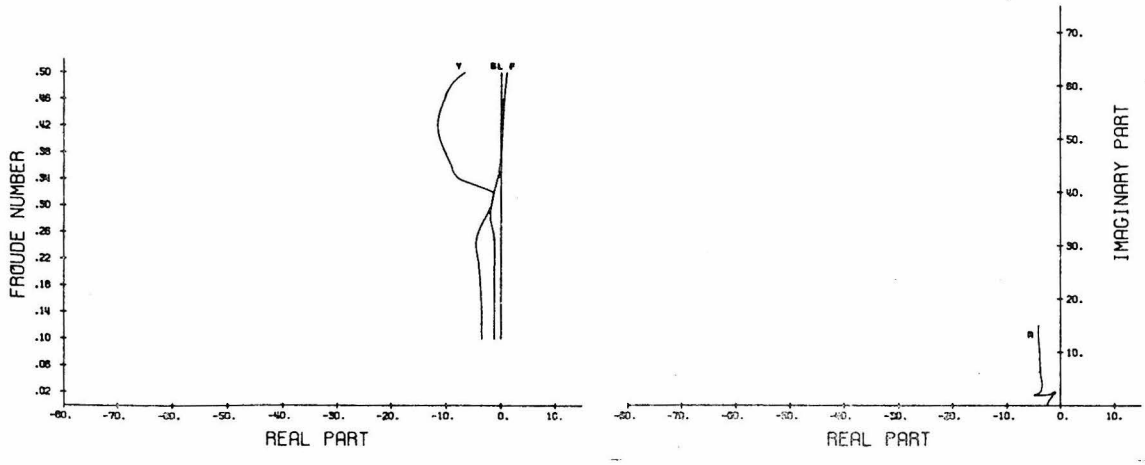


Figure 4.10. Lateral Eigenvalues with Ultra-Light Displacement

Table 4.3. Lateral Time Constants with Variable Displacement

Froude No.	.10	.36	.50
Heavy			
Slow Mode	-850.	-160.	64.
Fast Mode	4.9	2.2	-4.2
Yaw Mode	1.5	.55	.47
Ultra-Light			
Slow Mode	-270.	-100.	-16.
Fast Mode	6.7	14.	-1.5
Yaw Mode	2.3	.24	.24

These figures show that the Froude Number effects demonstrated in earlier cases are very sensitive to displacement. Increased displacement tends to attenuate the variations with speed, while Figure 4.10 shows a dramatic amplification for ultra-light displacement craft. The Fast Mode is unstable at high speed for both cases, but the time constant is substantially shorter for the lighter craft.

Roll-Tender Vessels

The Base Boat is rather stiff in roll with $\overline{GM} = .125$. To demonstrate the effect of transverse metacentric height on the eigenvalues, the calculations were repeated with $\overline{GM} = .05$. The results are shown in Figure 4.11. The results are similar to the ultra-light displacement case shown in Figure 4.10. The

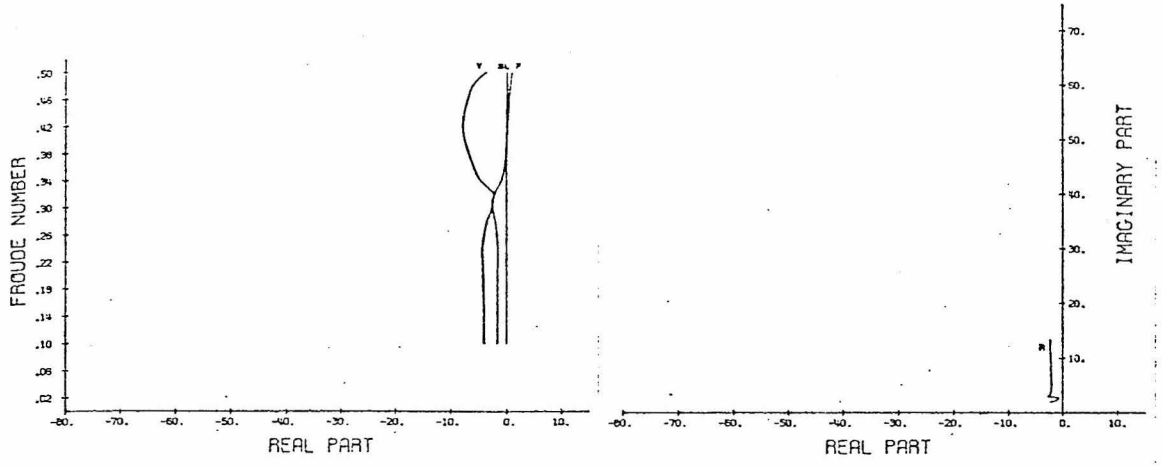


Figure 4.11. Lateral Eigenvalues with Low $\overline{GM}$

sensitivity to Froude Number is amplified, and the time constant for the Fast Mode at high speed is shortened 1.5 seconds.

4.5 Longitudinal Equations of Downwind Sailing

The Longitudinal Equations are the second group decoupled from the full Perturbation Equations under the assumptions and conditions of Downwind Sailing. These equations describe motions in surge, heave and pitch ($\dot{z}_1, \dot{z}_3, z_5$). These motions are usually considered of secondary importance on offwind courses unless surfing occurs (Letcher 1977), which is not permitted here by the assumption of flat water. There have been some previous studies of pitch and heave motions (Spens et al. 1967 and Gerritsma 1968), but these have been concerned only with windward performance in a seaway.

The Longitudinal Equations in scalar form are

$$(m+h_{11})\ddot{z}_1 + \left[\frac{\partial C_{K1}}{\partial Fr} Fr \cos\theta \sin\theta + \rho C_{S1}(V_T - 1)V_T(1+\cos^2\theta)\right]\dot{z}_1$$

$$+ \left[\frac{\partial C_{K1}}{\partial Fr} Fr + \rho C_{S1}(V_T - 1)V_T\right]\cos\theta \sin\theta \dot{z}_3$$

$$+ \left[\left[\rho C_{S1}(V_T - 1)\{[(V_T - 1)r_3^K + r_3^S](1+\cos^2\theta) - [(V_T - 1)r_1^K\right.\right.$$

$$\left.\left. + r_1^S]\cos\theta \sin\theta\} + m \sin\theta\right]\right]\dot{z}_5 + \frac{2A_w}{Fr^2} \sin^2\theta z_1$$

$$- \frac{2A_w}{Fr^2} \cos\theta \sin\theta z_3 = 0 \qquad (4.32)$$

$$(m+h_{33})\ddot{z}_3 + \left[C_{K1} + \frac{\partial C_{K1}}{\partial Fr} Fr + \rho C_{S1}(V_T - 1)\right]\cos\theta \sin\theta \dot{z}_1$$

$$+ \left[C_{K1}(1+\sin^2\theta) + \frac{\partial C_{K1}}{\partial Fr} Fr \sin^2\theta + \rho C_{S1}(V_T - 1)(1+\sin^2\theta) + \frac{\partial f_3^w}{\partial \dot{z}_3}\right]\dot{z}_3$$

$$+ \{C_{K1}[r_3^K \cos\theta \sin\theta - (1+\sin^2\theta)r_1^K] + \rho C_{S1}(V_T - 1)[r_3^S \cos\theta \sin\theta$$

$$- r_1^S(1+\sin^2\theta)] - m\cos\theta\}\dot{z}_5 - \frac{2A_w}{Fr^2} \cos\theta \sin\theta z_1$$

$$+ \frac{2A_w}{Fr^2} \cos^2\theta z_3 = 0 \qquad (4.33)$$

$$(I_y+h_{55})\ddot{z}_5 + \{C_{K1}[r_3^K(1+\cos^2\theta) - r_1^K\cos\theta\sin\theta]$$

$$+ \frac{\partial C_{K1}}{\partial Fr} Fr[r_3^K\cos^2\theta - r_1^K\cos\theta\sin\theta]$$

$$+ \rho C_{S1}(V_T - 1)[r_3^S(1+\cos^2\theta) - r_1^S\cos\theta\sin\theta]\}\dot{z}_1$$

$$+ \{C_{K1}[r_3^K\cos\theta\sin\theta - r_1^K(1+\sin^2\theta)] + \frac{\partial C_{K1}}{\partial Fr}Fr[r_3^K\cos\theta\sin\theta - r_1^K\sin^2\theta]$$

$$+ \rho C_{S1}(V_T - 1)[r_3^S\cos\theta\sin\theta - r_1^S(1+\sin^2\theta)]\}\dot{z}_3$$

$$+ \Big\{C_{K1}[(r_1^K)^2 + (r_3^K)^2 + (r_1^K\sin\theta - r_3^K\cos\theta)^2]$$

$$+ \rho C_{S1}(V_T - 1)[(r_1^S)^2 + (r_3^S)^2 + (r_1^S\sin\theta - r_3^S\cos\theta)^2] + \frac{\partial f_5^W}{\partial \dot{z}_5}\Big\}\dot{z}_5$$

$$+ \frac{2A_W}{Fr^2}(r_3^f\sin^2\theta + r_1^f\cos\theta\sin\theta)z_1 - \frac{2A_W}{Fr^2}(r_1^f\cos^2\theta + r_3^f\cos\theta\sin\theta)z_3$$

$$+ \left[\frac{m\overline{GM}_L}{Fr^2} + \rho C_{S1}(V_T - 1)^2(r_1^S - r_1^K)\right]\sec\theta\, z_5 = 0 \qquad (4.34)$$

The Longitudinal Equations can be re-cast in matrix form similar to the Lateral Equations. A system of six, first order equations is defined by letting

$$\underline{x} = \begin{Bmatrix} z_1 \\ z_3 \\ z_5 \\ \dot{z}_1 \\ \dot{z}_3 \\ \dot{z}_5 \end{Bmatrix} \qquad (4.35)$$

Then the Longitudinal Equations become

$$\frac{d\underline{x}}{dt} = M^{-1}A\underline{x} \ , \quad \underline{x}(0) = \underline{c} \tag{4.36}$$

where

$$M = \begin{bmatrix} 1 & 0 & 0 & 0 & 0 & 0 \\ 0 & 1 & 0 & 0 & 0 & 0 \\ 0 & 0 & 1 & 0 & 0 & 0 \\ 0 & 0 & 0 & (m+h_{11}) & 0 & 0 \\ 0 & 0 & 0 & 0 & (m+h_{33}) & 0 \\ 0 & 0 & 0 & 0 & 0 & (m+h_{55}) \end{bmatrix} \tag{4.37}$$

$$A = \begin{bmatrix} 0 & 0 & 0 & 0 & 0 & 0 \\ 0 & 0 & 0 & 0 & 0 & 0 \\ 0 & 0 & 0 & 0 & 0 & 0 \\ \frac{\partial f_1}{\partial z_1} & \frac{\partial f_1}{\partial z_3} & \frac{\partial f_1}{\partial z_5} & \frac{\partial f_1}{\partial \dot{z}_1} & \frac{\partial f_1}{\partial \dot{z}_3} & \left(\frac{\partial f_1}{\partial \dot{z}_5} - m\sin\theta\right) \\ \frac{\partial f_3}{\partial z_1} & \frac{\partial f_3}{\partial z_3} & \frac{\partial f_3}{\partial z_5} & \frac{\partial f_3}{\partial \dot{z}_1} & \frac{\partial f_3}{\partial \dot{z}_3} & \left(\frac{\partial f_3}{\partial \dot{z}_5} + m\cos\theta\right) \\ \frac{\partial f_5}{\partial z_1} & \frac{\partial f_5}{\partial z_5} & \frac{\partial f_5}{\partial z_5} & \frac{\partial f_5}{\partial \dot{z}_1} & \frac{\partial f_5}{\partial \dot{z}_3} & \frac{\partial f_5}{\partial \dot{z}_5} \end{bmatrix} \tag{4.38}$$

The Z-transformation has reduced to the identity matrix for this case. The solution can be expressed as in Chapter II with

$$k, j \in (1,6) \ . \tag{4.39}$$

4.6 Discussion of Numerical Solutions to Longitudinal Equations

This discussion follows the method and format of section 4.4

Base Boat

Figure 4.12 shows the eigenvalues and normal modes of Longitudinal Equations for the Base Boat. There are several interesting features of these results:

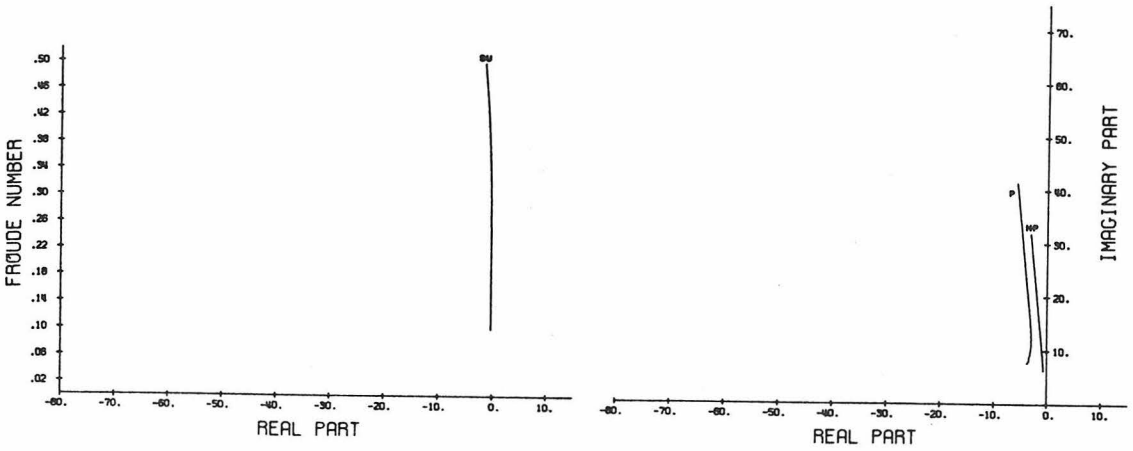
1. There is always one zero eigenvalue, i.e.,

$$\lambda_1 = 0 \quad . \tag{4.40}$$

Again this is a consequence of the general assumption of no dependence on position in the plane of the free surface. Unlike the Lateral Equations where z_2 did not appear explicitly, both z_1 and z_3 appear in the body frame representation of the Longitudinal Equations. All zero eigenvalues are omitted from the figures.

2. There are two complex modes. The modal coefficients indicate that one mode is virtually a pure oscillation in pitch ($x_3 = z_5$); this is termed the Pitch Mode. The second complex mode corresponds to a coupled heave-pitch motion; this is called the HP Mode. These modes are sensitive to the wave damping coefficients

$$\frac{\partial f_3^w}{\partial \dot{z}_3} \quad , \quad \frac{\partial f_5^w}{\partial \dot{z}_5} \quad .$$



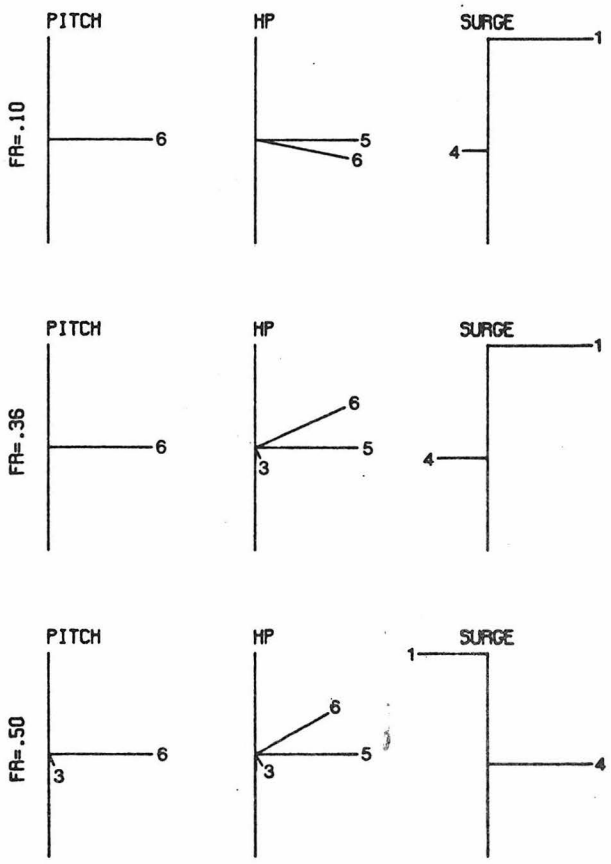


Figure 4.12. Solution to Longitudinal Equations of Downwind Sailing for Base Boat

In Figure 4.12 a wave damping ratio of 0.10 was assumed, i.e.,

$$\zeta_w = 2\left(\frac{\partial f_3^w}{\partial \dot{z}_3}\right)\left[\frac{\partial f_3}{\partial z_3}(m+h_{33})\right]^{\frac{1}{2}} = 2\left(\frac{\partial f_5^w}{\partial \dot{z}_5}\right)\left[\frac{\partial f_5}{\partial z_5}(I_{22}+h_{55})\right]^{\frac{1}{2}} \quad . \quad (4.41)$$

Figure 4.13 shows the complex eigenvalues when the assumed wave damping ratio is 0.25.

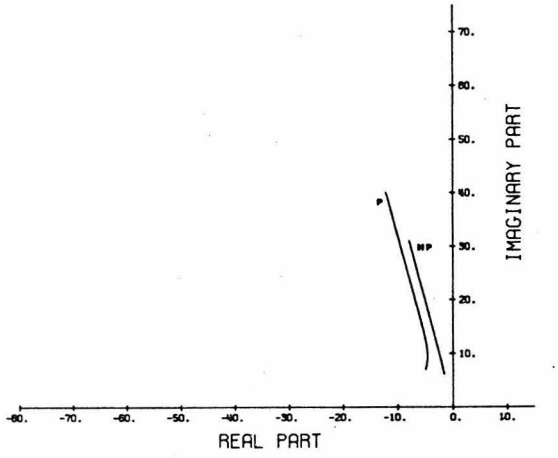


Figure 4.13. Complex Longitudinal Eigenvalues with Wave Damping Ratio of 0.25

Comparison of the figures shows that changes in wave damping shift the loci in the complex plane without any major modifications in shape. The effect is demonstrated more clearly by plotting the Pitch Mode damping ratio for these two cases. This is done in Figure 4.14. The natural period of the Pitch Mode, and the natural period and damping ratio of the HP Mode remain relatively constant with variations in speed and wave

damping. Table 4.4 summarizes these results in dimensional form.

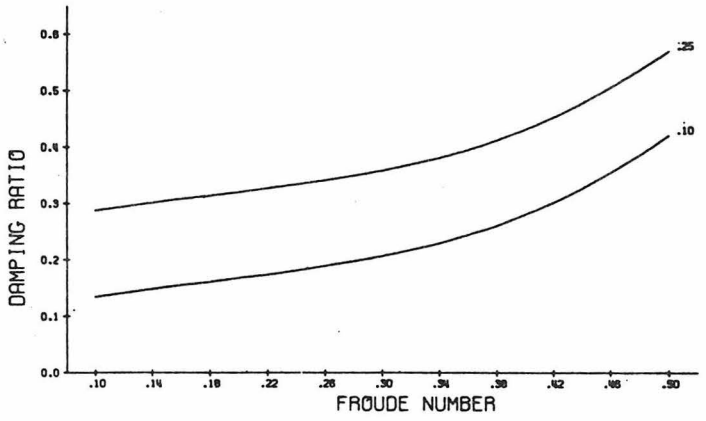


Figure 4.14. Damping Ratios for Downwind Pitch Mode

Table 4.4. Longitudinal Natural Periods and Damping Ratio for Base Boat

ζ_w	.10	.25
Pitch Mode		
T^N (sec)	1.17	1.17
HP Mode		
T^N (sec)	1.55	1.55
ζ	.09	.24

3. There is one real, nonzero eigenvalue, and it consists predominantly of surge motions ($x_4 = \dot{z}_1$). The range of time constants in dimensional form is shown in Table 4.5.

Table 4.5. Time Constant of Downwind Surge Mode for Base Boat

	Fr	T (sec)
Low Speed	.10	34.
~Hull Speed	.36	4.7
High Speed	.50	1.0

Displacement

The effect on the lateral eigenvalues due to changes in displacement were discussed in section 4.4. The effect on the longitudinal eigenvalues for the heavy displacement case is shown in Figure 4.15, and Figure 4.16 shows the results for the ultra-light displacement craft. Table 4.6 summarizes the dimensional data for these cases and the Base Boat.

The Pitch Mode natural period decreases with displacement. This is again due to holding the moments of inertia fixed and only varying the mass and related hydrodynamic inertial coefficients. The natural period of the HP Mode increases with displacement, and the modal coefficients indicate that the mode is predominantly motions in heave ($x_2 = z_3$). The Surge Mode time constant decreases rapidly with displacement; at most speeds there is a five-fold reduction between the heavy displacement vessel and the ultra-light craft.

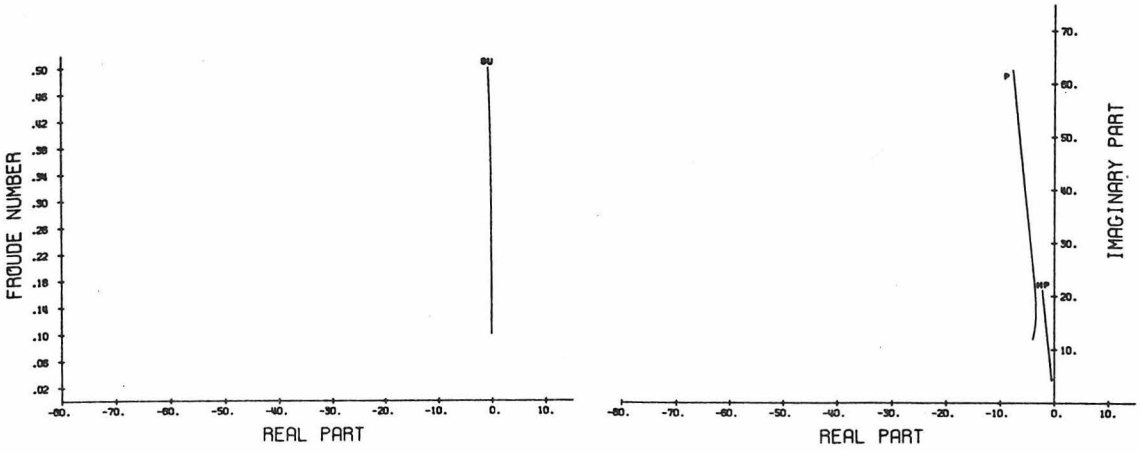


Figure 4.15. Longitudinal Eigenvalues with Heavy Displacement

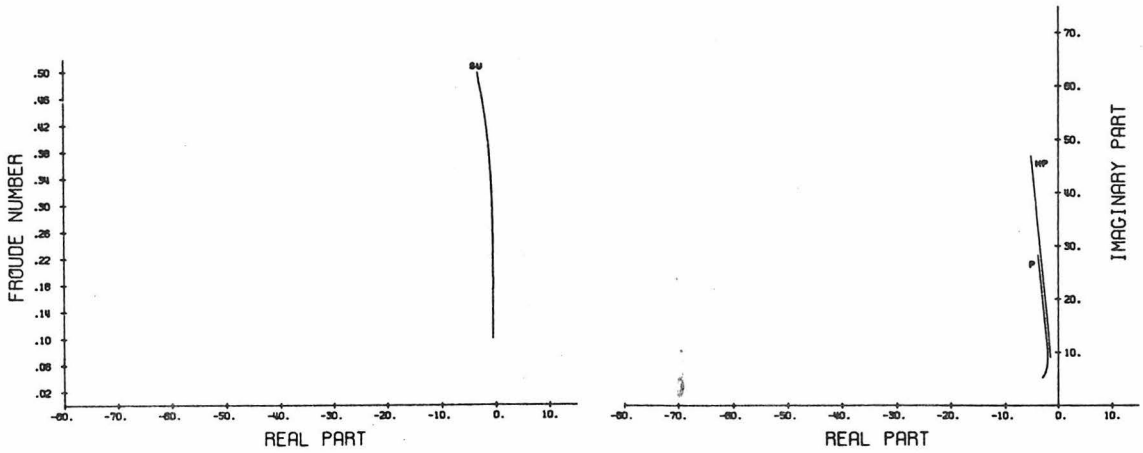


Figure 4.16. Longitudinal Eigenvalues with Ultra-light Displacement

Table 4.6. Effect of Displacement on Longitudinal Modes

DLR		70 (UL)	150 (BB)	360 (H)
Pitch Mode				
T^N (sec)		1.70	1.17	.78
ζ: Fr =	.10	.13	.14	.12
	.36	.25	.25	.19
	.50	.47	.42	.31
HP				
T^N (sec)		1.05	1.55	2.33
ζ		.13	.09	.10
Surge				
T: Fr = (sec)	.10	16.	34.	81.
	.36	2.1	4.7	11.
	.50	.48	1.0	2.4

Pitch-Tender Vessels

The longitudinal metacentric for the Base Boat is 1.4. This was reduced to 0.5 to demonstrate the dependence of the eigenvalues on pitch stiffness. For this case the Steady State Solution changes; Figure 4.17 shows the solution to equation (4.17) for this case. At high speed the trim angle approaches a moderately large value of -7° (bow down). The complex eigenvalues for this case are shown in Figure 4.18. Table 4.7 summarizes the dimensional data for this case and the Base Boat.

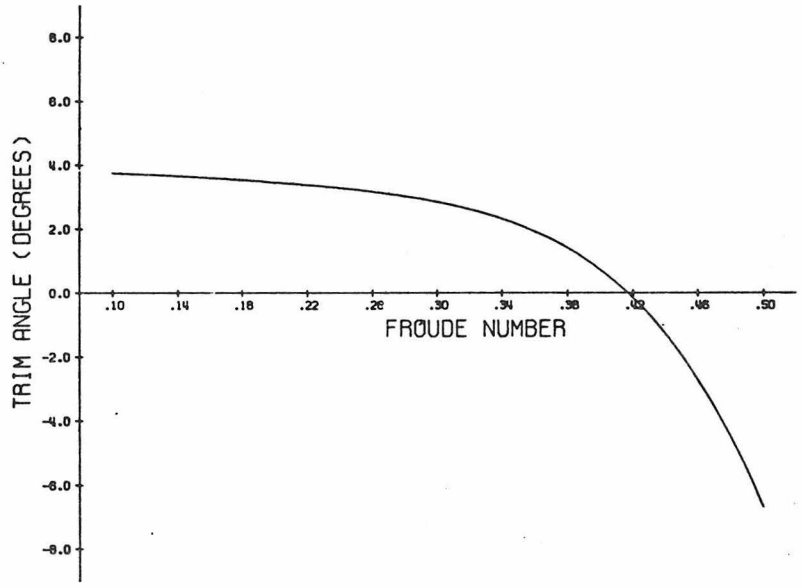


Figure 4.17. Steady State Solution for Downwind Sailing with Pitch-Tender Vessel

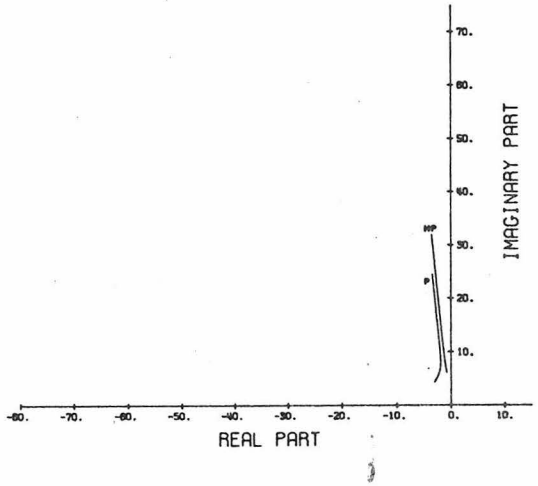


Figure 4.18. Complex Longitudinal Eigenvalues with Pitch-Tender Vessel

Table 4.7. Longitudinal Natural Periods and Damping Ratios with Pitch-Tender Vessel and Base Boat

$\overline{GM_L}$	0.5	1.4
Pitch Mode		
T^N (sec)	2.00	1.17
ζ: Fr = .10	.14	.14
ζ: Fr = .36	.29	.25
ζ: Fr = .50	.57	.42
HP Mode		
T^N (sec)	1.57	1.55
ζ	.12	.09

Figure 4.17 indicates that $\overline{GM_L}$ does not amplify Froude Number sensitivity in a manner similar to effect of $\overline{GM}$ on the lateral eigenvalues. The Pitch Mode natural period increases with reduced $\overline{GM_L}$, but it is relatively constant with variations in speed. There is some change in the damping ratio of the HP Mode, but there is little amplification in Froude Number dependence.

V. GENERAL SAILING CONDITIONS: STEADY STATE SOLUTIONS

This chapter returns to the general equations of Chapters II and III. The Steady State Equations are formulated, and numerical solutions are presented.

5.1 Formulation

The Steady State Equations (2.28) were derived in Chapter II. The steady state terms from the Taylor Series expansion in Chapter III are collected into the following nondimensional scalar form:

$$\rho V_a C_{S1} V_1^a + \rho V_a C_{S2} V_2^a - (C_{K1} + C_{R1})u_1 + (C_{K2} + C_{R2})u_2 + \frac{2A_w}{Fr^2} R_3 \sin\theta = 0 \tag{5.1}$$

$$\rho V_a C_{S1} V_2^a - \rho V_a C_{S2} V_1^a - (C_{K1} + C_{R1})u_2 - (C_{K2} + C_{R2})u_1 - \frac{2A_w}{Fr^2} R_3 \sin\varphi \cos\theta = 0 \tag{5.2}$$

$$\rho V_a C_{S1} V_3^a - (C_{K1} + C_{R1})u_3 - \frac{2A_w}{Fr^2} R_3 \cos\varphi \cos\theta = 0 \tag{5.3}$$

$$\rho V_a[C_{s1}(r_2^s V_3^a - r_3^s V_2^a) + C_{s2} r_3^s V_1^a] + (C_{K2} r_3^K + C_{R2} r_3^R)u_1 + (C_{K1} r_3^K + C_{R1} r_3^R)u_2$$

$$- (C_{K1} r_2^K + C_{R1} r_2^R)u_3 - \frac{m}{Fr^2}(\overline{GM} \sin\varphi \cos\theta + r_2^m \cos\varphi \cos\theta)$$

$$- \frac{2A_w R_3}{Fr^2}(r_2^f \cos\varphi \cos\theta - r_3^f \sin\varphi \cos\theta = 0 \qquad (5.4)$$

$$\rho V_a[C_{s1}(r_3^s V_1^a - r_1^s V_3^a) + C_{s2} V_2^a r_3^s] - (C_{K1} r_3^K + C_{R1} r_3^R)u_1 + (C_{K2} r_3^K + C_{R2} r_3^R)u_2$$

$$+ (C_{K1} r_1^K + C_{R1} r_1^R)u_3 + \frac{m}{Fr^2}(-\overline{GM_L} \sin\theta + r_1^m \cos\varphi \cos\theta)$$

$$+ \frac{2A_w R_3}{Fr^2}(r_1^f \cos\varphi \cos\theta + r_3^f \sin\theta) = 0 \qquad (5.5)$$

$$\rho V_a[C_{s1}(r_1^s V_2^a - r_2^s V_1^a) - C_{s2}(r_1^s V_1^a + r_2^s V_2^a)] + [C_{K1} r_2^K + C_{R1} r_2^R$$

$$- (C_{K2} r_1^K + C_{R2} r_1^R)]u_1 - [C_{K1} r_1^K + C_{K2} r_2^K + C_{R1} r_1^R + C_{R2} r_2^R]u_2$$

$$+ \frac{m}{Fr^2}[(\overline{GM_L} - \overline{GM}) \tan\varphi \sin\theta - (r_1^m \sin\varphi \cos\theta + r_2^m \sin\theta)]$$

$$- \frac{2A_w R_3}{Fr^2}(r_1^f \sin\varphi \cos\theta + r_2^f \sin\theta) = 0 \qquad (5.6)$$

Equations (5.1) - (5.6) are a system on nonlinear algebraic equations with tabular coefficients. The independent variables are

u_1, u_2, u_3	Vessel Velocity
φ, θ, ψ	Eulerian Angles
V_T	True Wind Speed
R_3	Sinkage
δ_s	Boom Angle
δ_R	Helm Angle

In addition there are system parameters, e.g., ballast location $\underline{r}_m$, which must be appropriately specified. However, these are external to the solution process.

Froude Number (Fr) and Sailing Angle (γ) are the free parameters of the sailing envelope shown in Figure 3.1. They are related to the independent variables by equations (2.15), (2.17) and (3.1), i.e., in dimensional form

$$\underline{u} = \sqrt{gL}\, Fr\, T(\varphi, \theta, \psi) \begin{Bmatrix} \cos\gamma \\ \sin\gamma \\ 0 \end{Bmatrix} \quad . \tag{5.7}$$

This equation simply states that the steady state velocity lies in the plane of the free surface. This condition together with an appropriately selected boom angle* reduces equations (5.1) - (5.6) to a system of six equations in six unknowns, i.e.,

$$\underline{f}(\underline{x}) = \underline{0} \quad , \tag{5.8}$$

---

*The roles played by the helm angle and boom angle are interchangeable. For example, neutral helm could be assumed, and the solution would provide the required boom angle.

where

$$\underline{x} = \begin{Bmatrix} \varphi \\ \theta \\ \psi \\ \delta_R \\ V_T \\ R_3 \end{Bmatrix} \tag{5.9}$$

The existence and uniqueness of solutions to the Steady State Equations (5.8) can be demonstrated by the technique of contraction mapping (Issacson and Keller 1966). Since the force coefficients are valid only when the vessel is making headway in an apparent wind, solutions near $V_s = 0$ and $V_a = 0$ are omitted. Evaluation of equation (5.8) requires interpolation of the force coefficients. An Aitken iterative method is used. Thus in the neighborhood of a solution, the tabular coefficients are replaced by polynomials.

5.2 Summary of Numerical Methods

The following is a brief sketch of the details of the numerical scheme used to calculate the steady state solutions:

1. Choose values of the free parameters Fr and γ.

2. Make an initial estimate of the solution $\underline{x}^o$ appropriate to the choice of Fr and γ.

3. Scale $\underline{x}^o$ such that

$$y_i^o = x_i^o s_i^x = 1 \quad , \quad \forall\, i \in (1,6) \tag{5.10}$$

4. Estimate the apparent wind angle

$$\beta_a = \alpha_s + \delta_s + \gamma - \psi \tag{5.11}$$

5. Choose

$$\delta_s \ni C_{s2}(\alpha_s^o) \sim \max |C_{s2}| \tag{5.12}$$

6. Check

$$\delta_s > \max \delta_s \Rightarrow \delta_s = \max \delta_s \tag{5.13a}$$

$$\delta_s < \min \delta_s \Rightarrow \delta_s = \min \delta_s \tag{5.13b}$$

7. Select an appropriate sail area S_A from the inventory based on the estimate of β_a (Appendix A.5).

8. Scale the aerodynamic coefficients

$$C_{s2}(\alpha_s) = \hat{C}_{s2}(\alpha_s) \frac{S_A}{\hat{S}_A} \tag{5.14}$$

where $\hat{C}_{s2}(\alpha_s)$ and $\hat{S}_A$ are the test data from Appendix A.4.

9. Select an appropriate ballast location $\underline{r}_m$ and calculate any corrections due to center of gravity shift.

10. Scale equation (5.8) such that

$$g_i(\underline{y}^o) = f_i(\underline{x}^o) s_i^f = 1 \qquad \forall\, i \in (1,6) \tag{5.15}$$

11. Solve the scaled system of equations

$$\underline{g}(\underline{y}) = \underline{0} \tag{5.16}$$

using the algorithm of Powell (1970b).

12. The routine usually finishes at the vth call when

$$\| \underline{g}(\underline{y}^{v}) \|_2^2 < 10^{-6} \tag{5.17}$$

13. If this inequality is not satisfied, replace δ_s with $\delta_s - 5^o$ and repeat the solution process.

14. If luffing occurs, i.e.,

$$\alpha_s^{v} < \min \alpha_s \ , \tag{5.18}$$

a new initial estimate is taken ($\underline{x}^o = \underline{x}^v$), and the process is repeated.

Item 11 is the core element in this scheme. The routine is Newton's Method modified by applying the method of steepest descent to the sum of squares of the residuals, i.e.,

$$\| \underline{g}(\underline{y}^{v}) \|_2^2$$

This routine is well suited for calculating the steady state solutions, since it does not require sharp initial estimates or an explicit representation of the Jacobian. Of course, at each step in the process all the intermediate quantities must be calculated, e.g., $\underline{u}^v$, $\underline{V}_a^v$, α_s^v, and α_κ^v.

The solution typically requires about 30 functional evaluations to achieve the finishing criterion (5.17). This provides at least four accurate digits. Increased accuracy is obtained with additional evaluations, but this seems unwarranted due to the nature of the data. The process may stop without achieving the solution on some rare occasions, e.g., the finite difference estimate of Jacobian is singular or repeated selection of boom angles fails. Experience with these calculations seems to indicate that solutions can be found in these special cases by repeated trials with initial estimates. However, this may require substantial computer costs. Also since sail area and ballast location are determined by a priori estimates, the final solution may not be consistent with these choices, i.e., the solution corresponds to a different point of sail. This can be corrected with new initial estimates.

No attempt has been made to optimize the solutions, e.g., Letcher (1976b). However, the boom angle criteria given in equations (5.12) and (5.13) can be considered as a weak optimization condition. Similar to what occurs in practice, without a rigorous optimization scheme it is possible to obtain unconventional solutions. These are usually caused by inappropriate boom angles. The method has provided solutions with $\varphi > 35^{o}$, but in general this is an upper limit.

5.3 Numerical Solutions

Steady state solutions have been calculated for several data cases similar to those in Chapter IV. The specific objectives here

are (1) to demonstrate the method developed in the previous chapters, (2) to compare the numerical results with observations on full scale sailing vessels, and (3) to calculate the input data required for the Perturbation Equations. The same cautions should be applied to these results as noted in the numerical studies of Chapter IV. Detailed comparisons with the full scale data are given in Appendix B.

Figure 5.1 shows the sailing envelope of discrete solutions calculated for the Base Boat. This plot shows how the point of

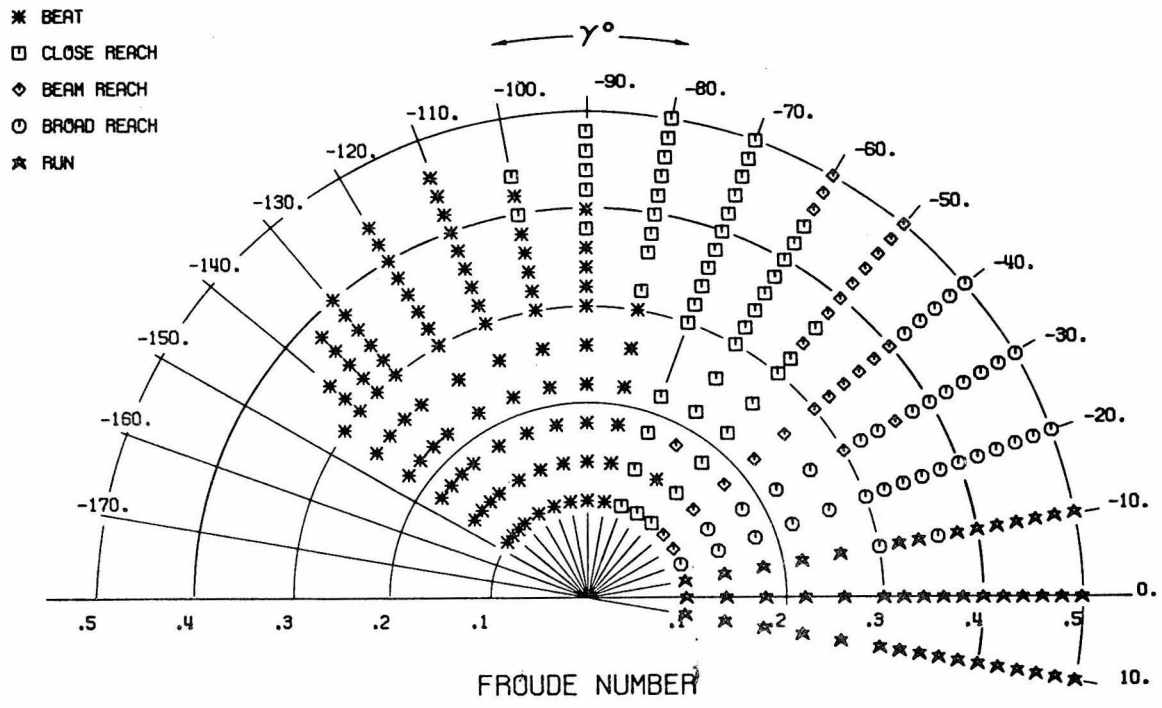


Figure 5.1. Sailing Envelope for Base Boat

sail varies with the free parameters Fr and γ. The solution for $\gamma = -60^{o}$, Fr = .18 is an example of a case where the a priori estimates are inconsistent with the final solution, i.e., the solution crossed the parameter boundaries established in Appendix A.5 for close reaching. This is not a serious problem, since in the physical case, these boundaries are not sharp.

Figure 5.2 summarizes similar data from the full scale observations in Appendix B. The data are not uniformly dense; they are clustered about the common yacht racing conditions:

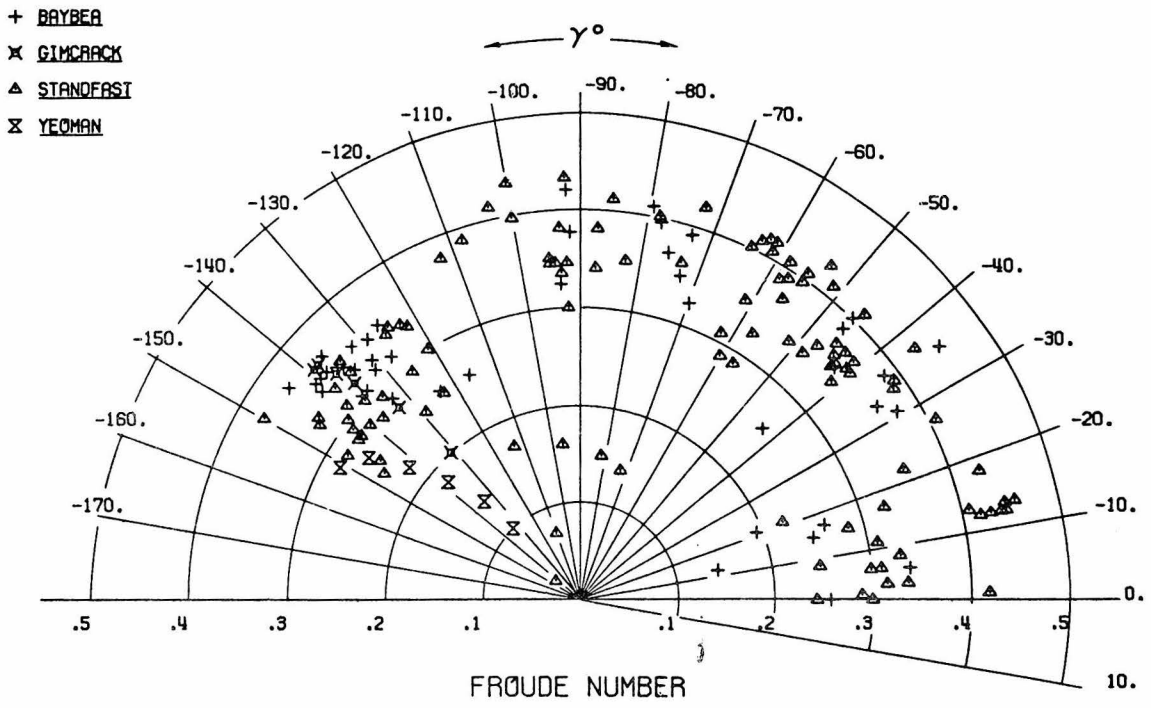


Figure 5.2. Envelope of Full Scale Sailing Observations

close-hauled and high speed reaching. This plot supports the notion of the sailing envelope. The close-hauled solutions found in Figure 5.1 show nearly the same windward boundary as the data in Figure 5.2. This is due to the vessel achieving maximum heel angles at progressively lower speeds as $|\gamma| \rightarrow 180^{o}$. Additionally, Figure 5.1 shows that the method provides solutions throughout nearly all the sailing envelope without resorting to repeated trials of initial estimates.

5.4 Performance

Most analytical and experimental work on sailing vessels has been directed toward determining optimum windward performance, e.g., Letcher (1976). For a given wind speed, the objective is to find the vessel speed and sailing angle which maximize

$$V_{mg} \equiv V_s \cos |\gamma| \tag{5.19}$$

This basic measure of performance can be extended to more general sailing conditions. In this formulation the performance criterion is the minimum true wind speed ($x_5 = V_T$) required to establish any given sailing condition Fr and γ*. Figures 5.3 and 5.4 show plots of the calculated true wind speed vs. sailing angle for the Base Boat with the Finn sail and with the Gottingen foil data. The Gottingen coefficients were scaled such that max C_{s_1} is identical with the model Finn sail.

---

*If a sufficient number of calculations were run, it would be easy to convert this data back to the simple V_{mg} estimates.

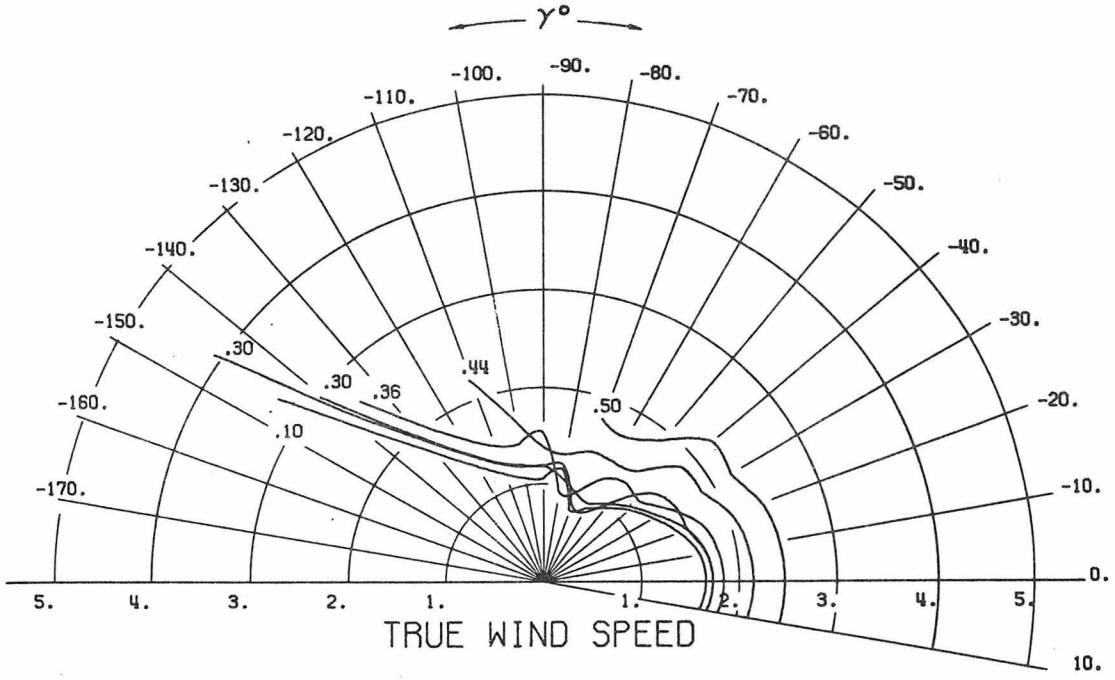


Figure 5.3. Performance Data for Base Boat with Finn Sail

The curves for low to moderate Froude Numbers are all very similar in shape. The performance gains associated with reaching courses are clearly evident. As Froude Number increases there is a general increase in the required nondimensional wind speed. At high speed the curves terminate about $\gamma = -70^{\circ}$ due to very large heel angles. The effectiveness of live ballast on performance is shown in Figure 5.3 for the two curves at Fr = .30. When the ballast is shifted 1 foot off the centerline towards the weather rail, the Base Boat sails 1°-2° closer to the true wind.

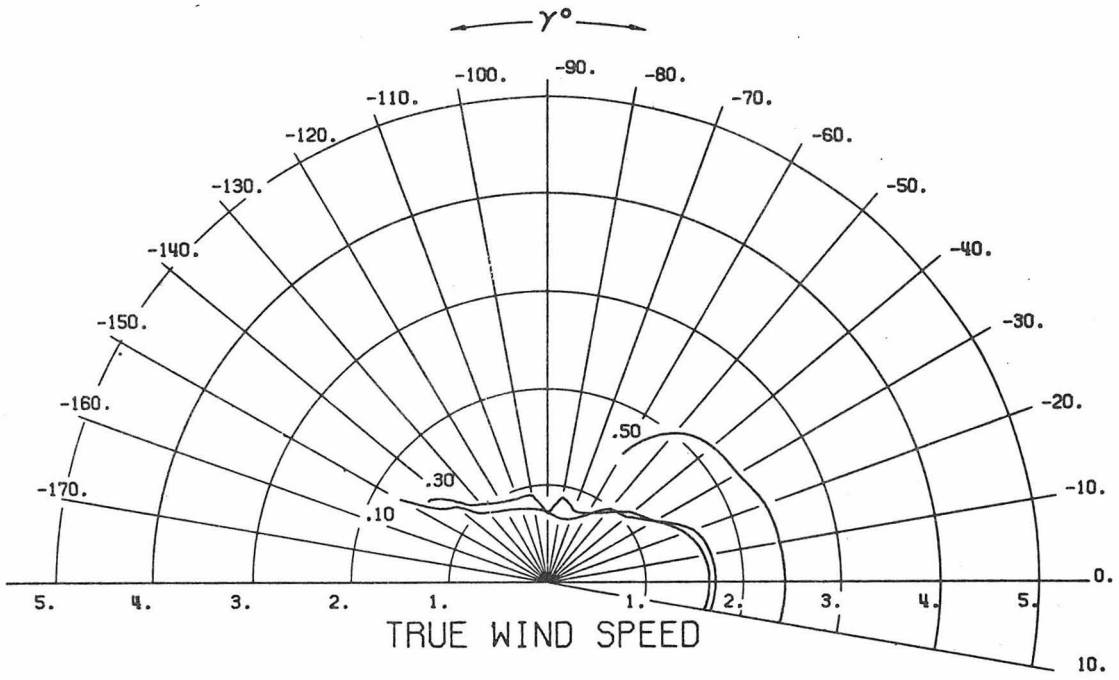


Figure 5.4. Performance Data for Base Boat with Gottingen Foil

Figures 5.5 - 5.7 show results from the same calculations together with full scale data from Appendix B. The performance curves for the Base Boat with the Gottingen Foil appear to be an approximate lower bound for all the data. Excluding the Standfast data, the pair of curves for the Base Boat, differing only in sail coefficients, bracket almost all of the full scale data. Considering the approximations of the model and the difficulties in obtaining

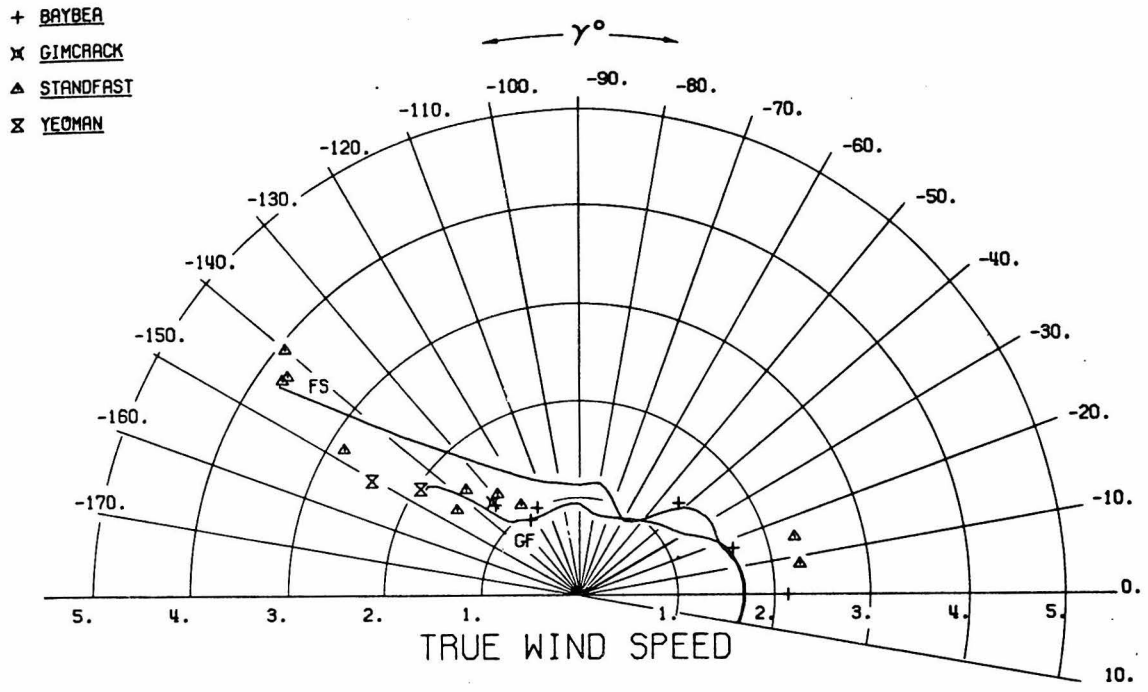


Figure 5.5. Performance Data Fr ~ .26

model and full scale force data, the agreement is remarkable. The Standfast data show very large scatter, but the optimum performance agrees well with the calculations and data from the other vessels.

The trend of the performance curves on windward courses follows the data very well; this is somewhat surprising, since without an optimization scheme lesser agreement was anticipated. The model consistently underestimates the wind speed on running courses. Without doing fine tuned calculations for these vessels it

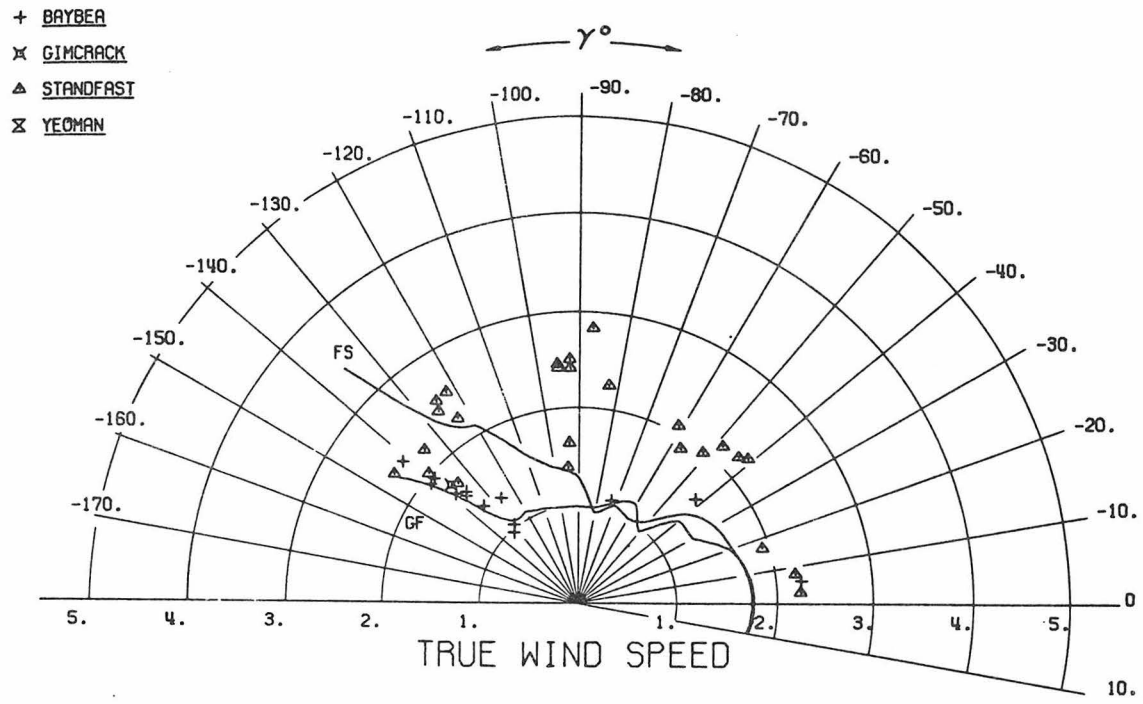


Figure 5.6. Performance Data Fr ~ .34

is not possible to state with any precision why this occurs. However, there are some interesting speculations. On offwind courses racing yachts fly several sails simultaneously, and the decreased performance may be due to sail interaction not accounted for in this analysis. More in keeping with the theme of this study, it is interesting to speculate as to whether this discrepancy is an indication of the vessels not being able to sustain steady high performance conditions.

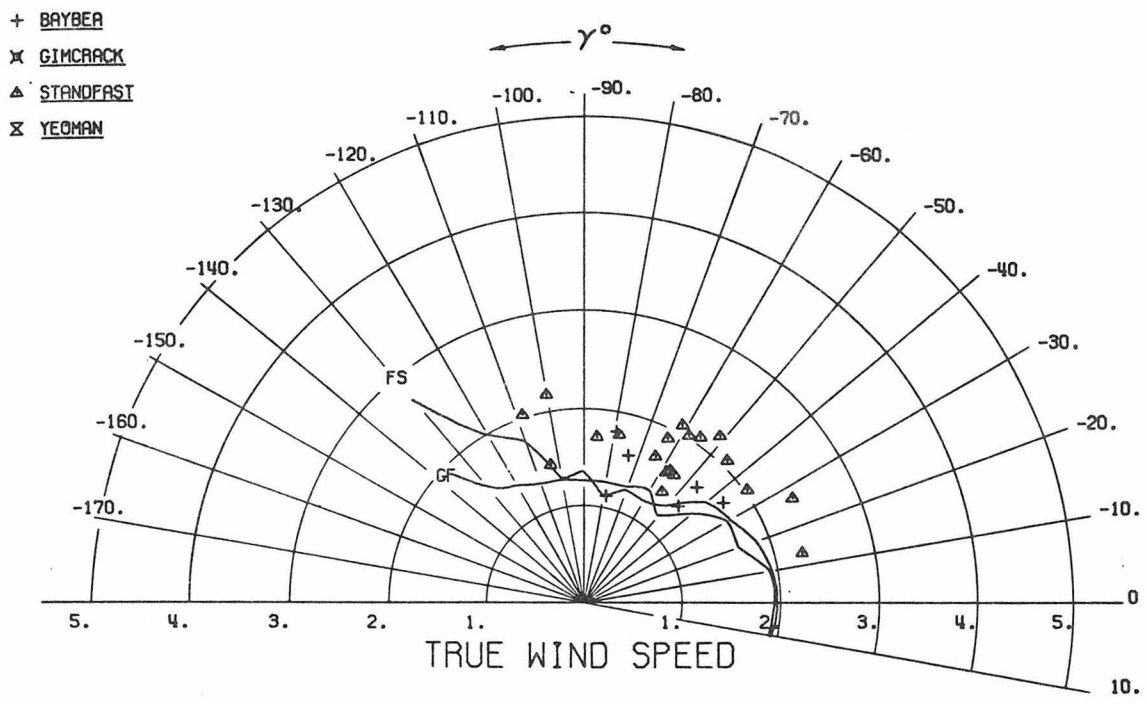


Figure 5.7. Performance Data Fr ~ .40

The curves in Figures 5.5 - 5.7 indicate that the Gottingen foil outperforms the Finn sail on all points of sail. The change in sail coefficients alone accounts for the Base Boat sailing about 10° closer to the wind on a beat. This large difference could be anticipated from Appendix A.4: the Gottingen Foil develops about 20% greater maximum sideforce at $\alpha_s \sim 15°$ compared to the maximum for the Finn sail at $\alpha_s \sim 35°$. Appendix B gives some detailed comparisons between these two cases and the full scale data.

5.5 Attitude and Ballasting

Figure 5.8 shows the heel angle ($x_1 = \varphi$) vs. sailing angle for the Base Boat with the Finn sail at several speeds. The discontinuities in slope of these curves indicate shifts of live ballast in accordance with Appendix A.5. The data indicate that the roll stiffness parameters for the Base Boat ($\overline{GM}$ and $\underline{r}_m$) are adequate to keep the vessel relatively upright for $|\gamma| < 130^\circ$. On close-hauled courses at moderate to high speeds the characteristic large increase of heel angle is evident. Figure 5.9 replots the Fr = .36 curve and a curve for the Heavy Displacement vessel (Fr = .34). Full scale data for this speed range are also plotted. Consistent

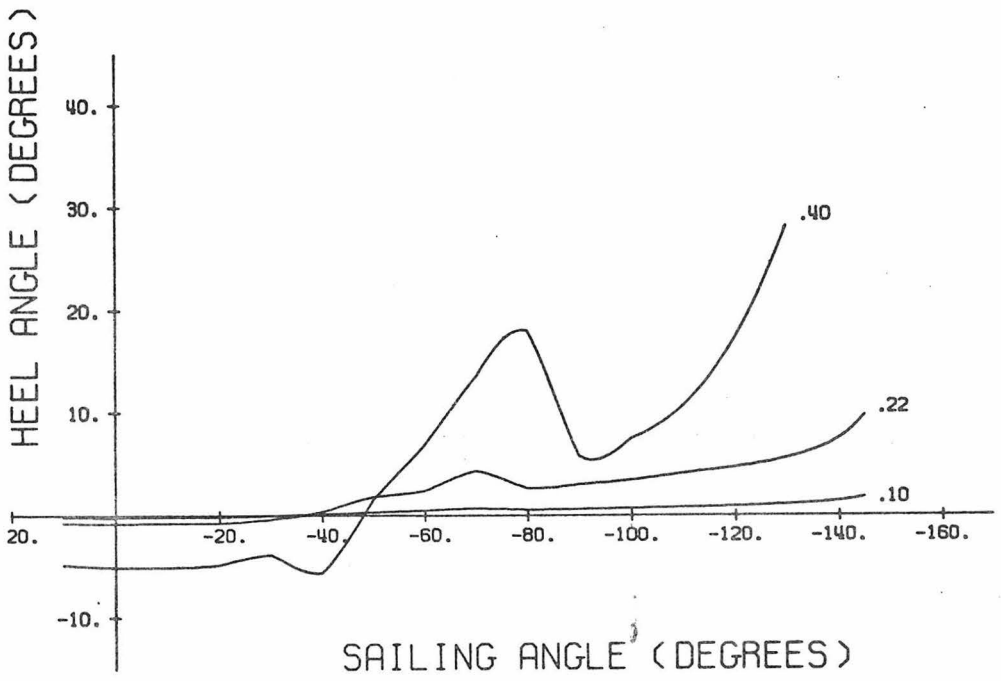


Figure 5.8. Heel Angle for Base Boat with Finn Sail

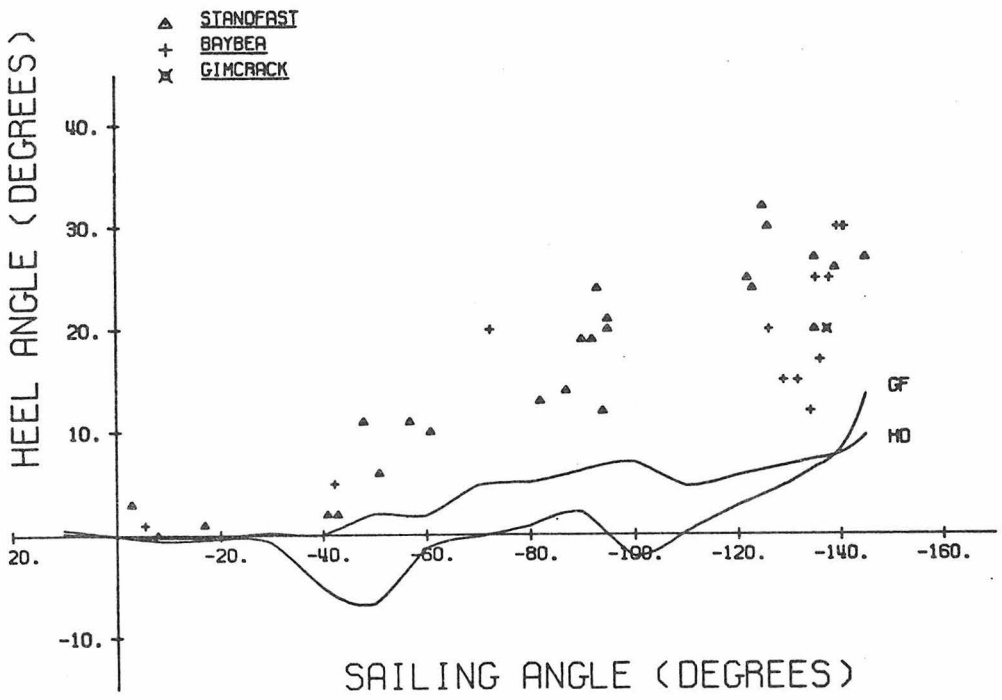


Figure 5.9. Comparison of Heel Angle Data

with the performance curves, the numerical results appear to be a lower bound on the heel angles. There is considerable scatter in the full scale data; however, the trend of the data on windward courses agrees reasonably well with the calculations.

The trim angle ($x_2 = \theta$) and sinkage ($x_6 = R_3$) are small quantities. Figure 5.10 shows a typical plot of trim angle vs. sailing angle near hull speed for the Base Boat with Gottingen foil. Figure 5.11 is a similar plot of the sinkage in dimensional form. As demonstrated in Chapter IV it is possible to achieve trim angles approaching $\pm 10^{o}$ for a vessel with low longitudinal metacentric

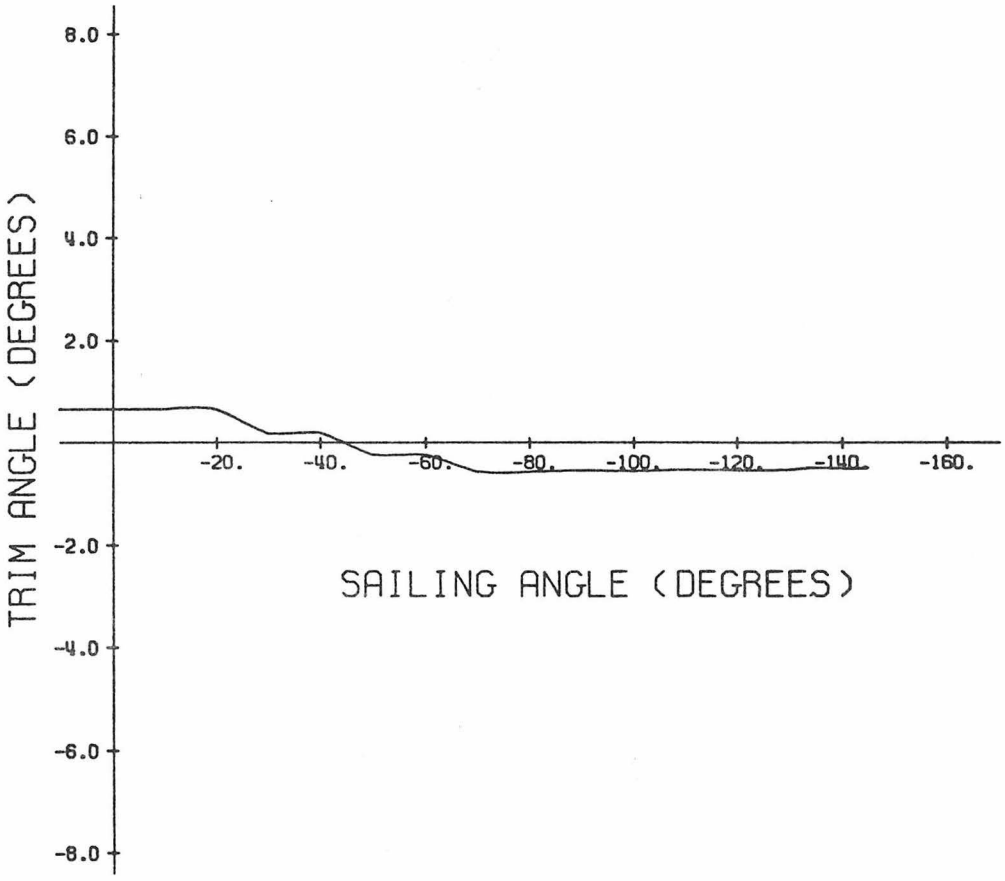


Figure 5.10. Trim Angle for Base Boat with Gottingen Foil (Fr = .36)

height. However, for a relatively stiff vessel such as the Base Boat, the trim angle under most sailing conditions is quite small. Figure 5.11 indicates that less than 20 mils of sinkage are required for a keelboat with 20 foot waterline moving at hull speed. There are special cases, e.g., Downwind Sailing, where there is no sinkage. However, in general the sinkage is of the order shown in Figure 5.11. Dynamic sinkage is much larger. Herreshoff and Newman (1967) report values of about 3 inches during the Antiope tests at similar speeds. These tests also indicate a dynamic trim angle of 0.4^{o}.

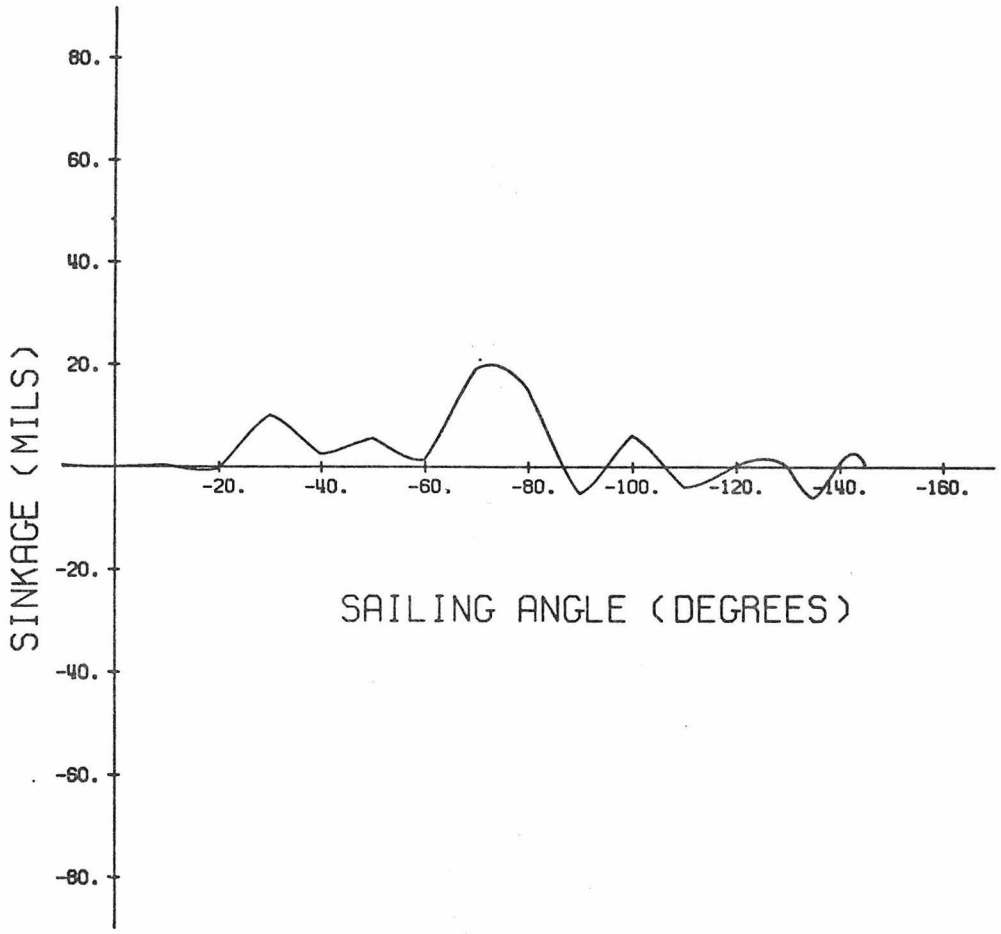


Figure 5.11. Sinkage for Base Boat with Gottingen Foil (Fr = .36)

5.6 Leeway, Helm and Crossflow Angles

The remaining steady state variables are the heading angle ($x_3 = \psi$) and the helm angle ($x_4 = \delta_R$). These are related to the crossflow angles by equations (2.16), (3.14) and (3.64). Figure 5.12 shows the hull-keel crossflow angle for the Base Boat with Gottingen foil. Except for ballast shifts and sail changes, the crossflow angle increases smoothly with sailing angle and speed. The crossflow angle for windward work is in the range of 2°-3.5^o. This is in agreement with the conclusions of Herreshoff and Newman (1967) based on the tank tests of Antiope. This agreement must be

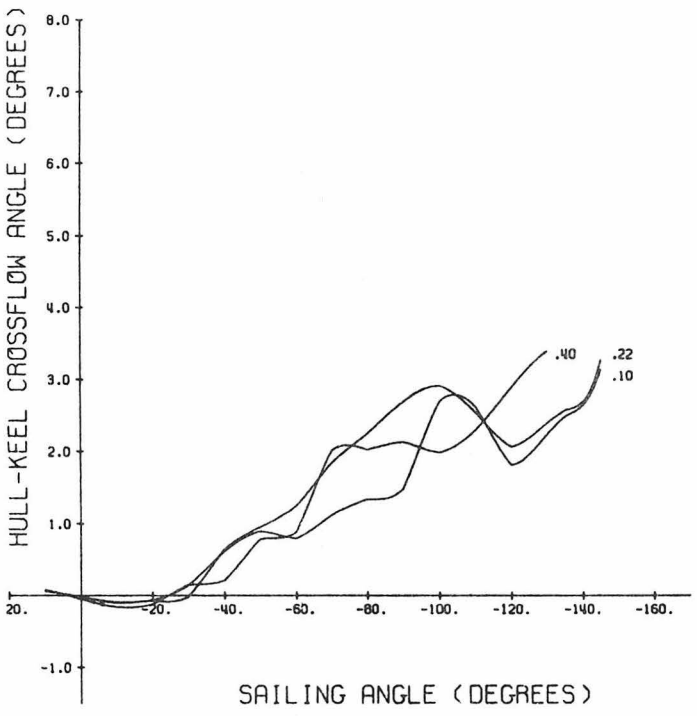


Figure 5.12. Hull-Keel Crossflow Angle for Base Boat with Gottingen Foil

accepted with reservation, since there is a difference in definition of angles of incidence (Letcher 1975). Typical leeway angles, as defined in equation (2.16), are plotted in Figure 5.13 for the Base Boat with Gottingen foil. Leeway angles from Appendix B are also plotted; these were calculated from the full scale observations by the original investigators. The results for the Base Boat are again a reasonable lower bound to the data and are very encouraging.*

The rudder crossflow angle α_R for the Base Boat with Gottingen foil is plotted in Figure 5.14. The calculated rudder crossflow angles shown in Figure 5.14 are quite small. The

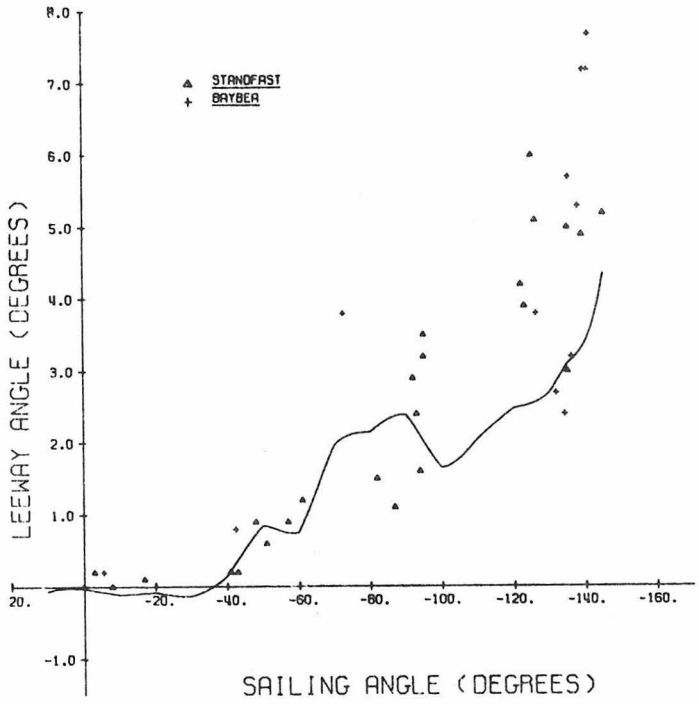


Figure 5.13. Comparison of Calculated Leeway Angles (Fr ~ .34)

---

*Kerwin et al. (1974) discuss the problem of leeway angle calculations:

> "This is a matter which has caused concern for at least the last decade [2], and still appears unresolved. Tank predicted side forces, coupled with full scale static stability and observed heel angles frequently result in predicted leeway angles as high as 8 degrees. There are many who question whether such large angles are actually encountered, and accurate full-scale measurements still appear to be lacking."

The reference is to Herreshoff (1964).

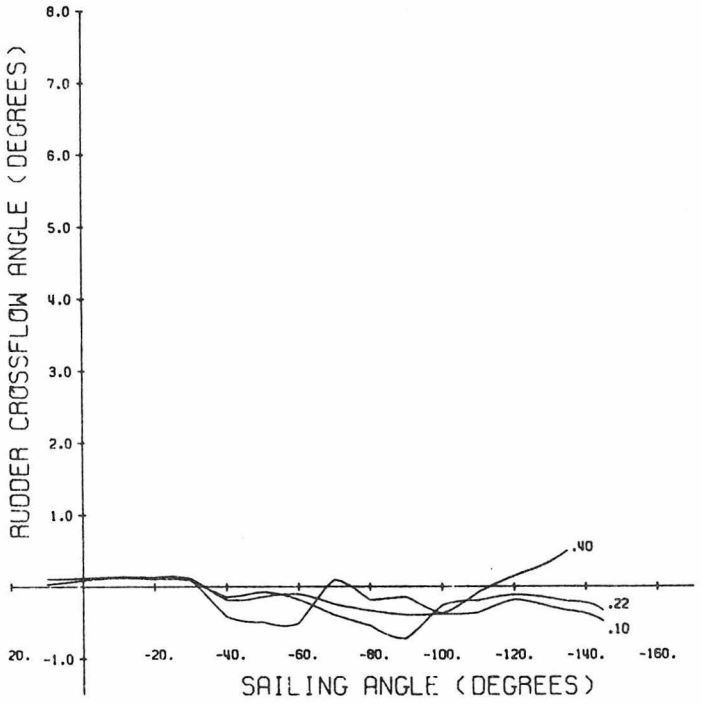


Figure 5.14. Rudder Crossflow Angle for Base Boat with Gottingen Foil

rudder sideforce coefficients used here are developed in Appendix A.3 from the half ton model tests reported by Gerritsma (1968). As speed increases the rudder crossflow angle increases. This is observed in practice and has been previously analyzed (Letcher 1971). Figure 5.15 shows the helm angle ($x_4 = \delta_R$) for this case and the results of a similar calculation using the Valiant coefficients from Appendix A.3. Full scale data from Standfast are also shown. The sign convention is that $\delta_R < 0$ corresponds to weather helm on port tack.

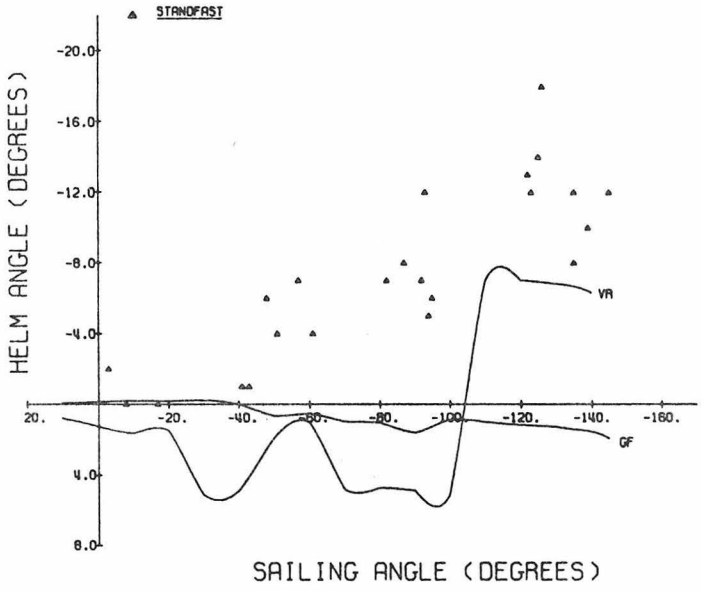


Figure 5.15. Comparison of Helm Angle Data (Fr ~ .34)

The Standfast data indicate that on windward courses about 12° of weather helm was common. Herreshoff and Newman (1967) conclude that 6° of weather helm is a typical upper limit in practice for Antiope. The helm angle, corresponding to the crossflow angles for the Base Boat shown in Figure 5.14, is not only much smaller but of opposite sign. This is attributed to the simplistic model of the rudder assumed in Chapter III. There are data indicating that the effectiveness of the rudder is much reduced due to its location in the wake of the hull and keel (Gerritsma 1968). The data from the Valiant model tests indicate the complexity of this

problem. However, the calculations shown in Figure 5.15 using the Valiant data result in windward helm angles which are more typical of observed angles.

VI. GENERAL SAILING CONDITIONS: SOLUTIONS TO PERTURBATION EQUATIONS

This chapter discusses numerical solutions to the Perturbation Equations using the results of the previous chapter. The data cases presented here are similar to those in Chapters IV and V.

6.1 Perturbation Equations and Numerical Methods

The Perturbation Equations from Chapter II are

$$\frac{d\underline{x}}{dt} = A\underline{x} \ , \qquad \underline{x}(0) = \underline{c} \tag{6.1}$$

where

$$\underline{x} = \begin{Bmatrix} z_1 \\ z_2 \\ z_3 \end{Bmatrix} \text{ perturbations in position}$$
$$\begin{Bmatrix} z_4 \\ z_5 \\ z_6 \end{Bmatrix} \text{ perturbations in attitude}$$
$$\begin{Bmatrix} z_7 \\ z_8 \\ z_9 \end{Bmatrix} \text{ perturbations in translational velocity}$$
$$\begin{Bmatrix} z_{10} \\ z_{11} \\ z_{12} \end{Bmatrix} \text{ perturbations in rotational velocity} \tag{6.2}$$

$$A = \begin{bmatrix} 0 & I \\ -ZM^{-1}K & -ZM^{-1}C \end{bmatrix} \tag{6.3}$$

The perturbation matrix A is composed of stiffness, damping and inertial elements from Chapter III. The non-zero contributions to the elements of these matrices are summarized in Table 6.1.

Calculating numerical solutions to the Perturbation Equations is straightforward. Finite difference estimates of the derivatives of the force coefficients are used. The inertial matrix is inverted via Jordan's Method (Issacson and Keller 1966). The eigenvalues and eigenvectors of the asymmetric perturbation matrix are found using a standard algorithm (Grad and Brebner 1968). The results of these calculations are presented in the same format as Chapter IV.

6.2 Base Boat

The Perturbation Equations were solved for the Base Boat at each of the discrete points indicated on the sailing envelope (Figure 5.1). The results of these calculations are briefly summarized in Figures 6.1 - 6.8*. As before, dimensional data are based on a vessel with L = 20 feet. The printed letters refer to the modes of Section 6.3.

These plots exhibit several general features. For most sailing conditions, there are seven natural modes: three are complex modes and four are purely real modes. In addition, there are two zero eigenvalues which correspond to unrestricted position on the free surface. Most modes show a significant dependence on Froude Number and sailing angle, and it is common to see real

---

*Appendix C presents all the data for this case including a detailed explanation of these plots.

Table 6.1

Summary of Contributions to Perturbation Matrix

Stiffness Matrix		Non-zero Contributions
Buoyancy		
Principal ($\overline{GM}, \overline{GM_L}$)		7
Live Ballast ($\underline{r}_m$)		9
Incremental ($A_w, \underline{r}_f$)		36
Hull-Keel Hydrodynamics		
Resistance ($C_{K1}, \underline{r}_K$)		18
Sideforce ($C_{K2}, \underline{r}_K$)		15
Rudder Sideforce ($C_{R2}, \underline{r}_R$)		15
Aerodynamic		
Resistance ($C_{S1}, \underline{r}_S$)		18
Sideforce ($C_{S2}, \underline{r}_S$)		15
	Subtotal	133
Damping Matrix		
Hull-Keel Hydrodynamics		
Resistance ($C_{K1}, \underline{r}_K$)		36
Sideforce ($C_{K2}, \underline{r}_K$)		30
Wave Generation		2
Rudder Sideforce ($C_{R2}, \underline{r}_R$)		30
Aerodynamic		
Resistance ($C_{S1}, \underline{r}_S$)		36
Sideforce ($C_{S2}, \underline{r}_S$)		30
Linear Terms from $\underline{\Omega} \times \underline{u}$		6
	Subtotal	170
Inertial Matrix		
Mass (m, I_{ij})		12
Hydrodynamic Inertial Matrix (H)		8
	Subtotal	20
Grand Total		323

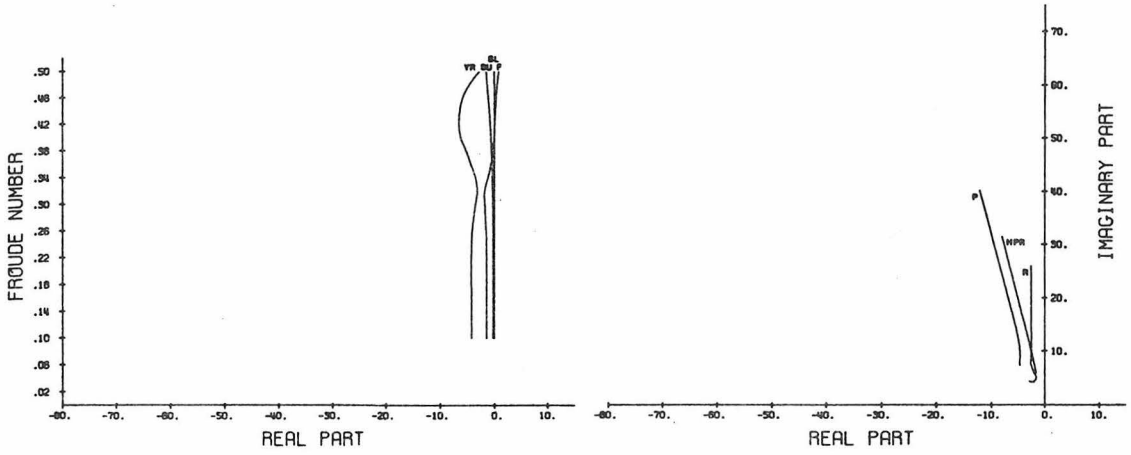


Figure 6.1. Eigenvalues for Base Boat $\gamma = 0^{o}$ (Run)

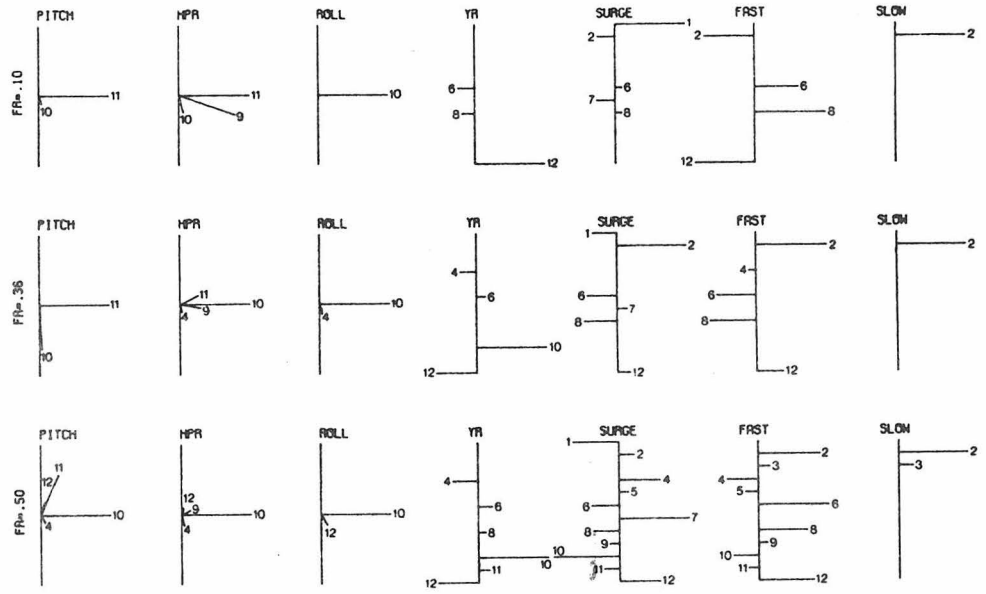


Figure 6.2. Normal Modes for Base Boat $\gamma = 0^{o}$ (Run)

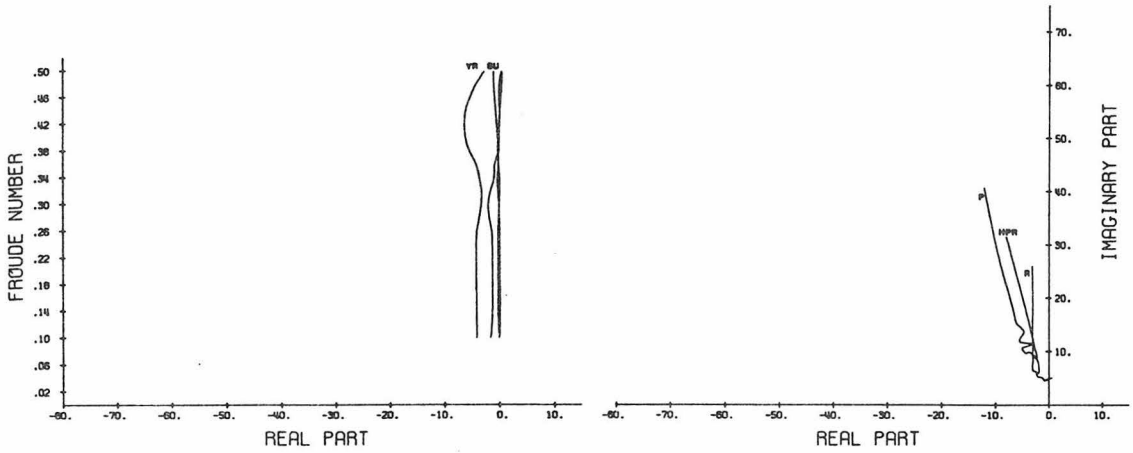


Figure 6.3. Eigenvalues for Base Boat $\gamma = -30^{o}$ (Broad Reach)

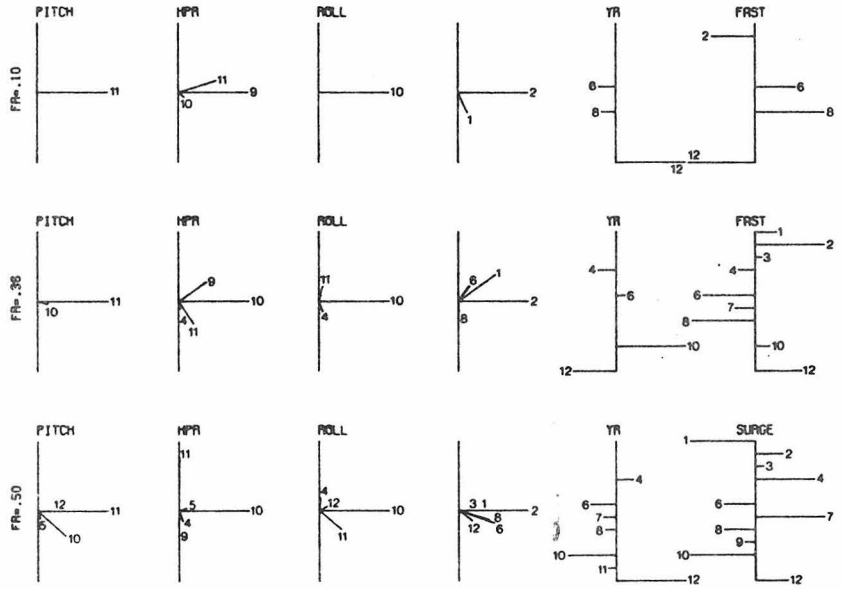


Figure 6.4. Normal Modes for Base Boat $\gamma = -30^{o}$ (Broad Reach)

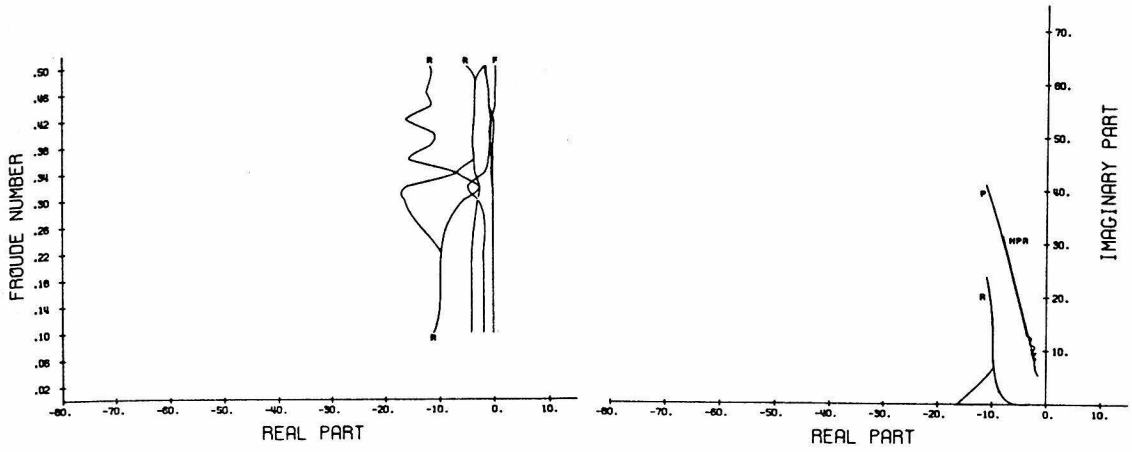


Figure 6.5. Eigenvalues for Base Boat $\gamma = -70^{o}$ (Close Reach)

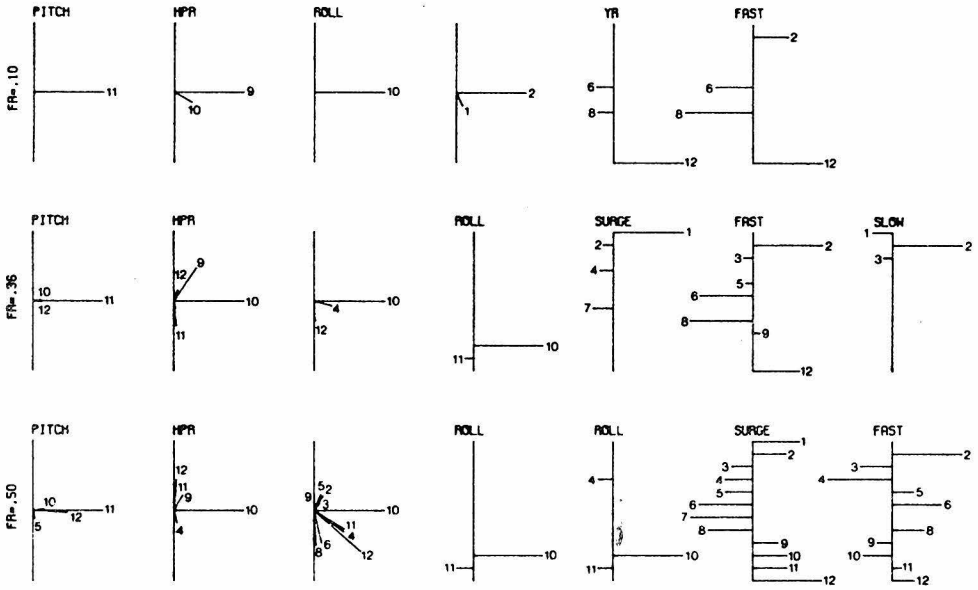


Figure 6.6. Normal Modes for Base Boat $\gamma = -70^{o}$ (Close Reach)

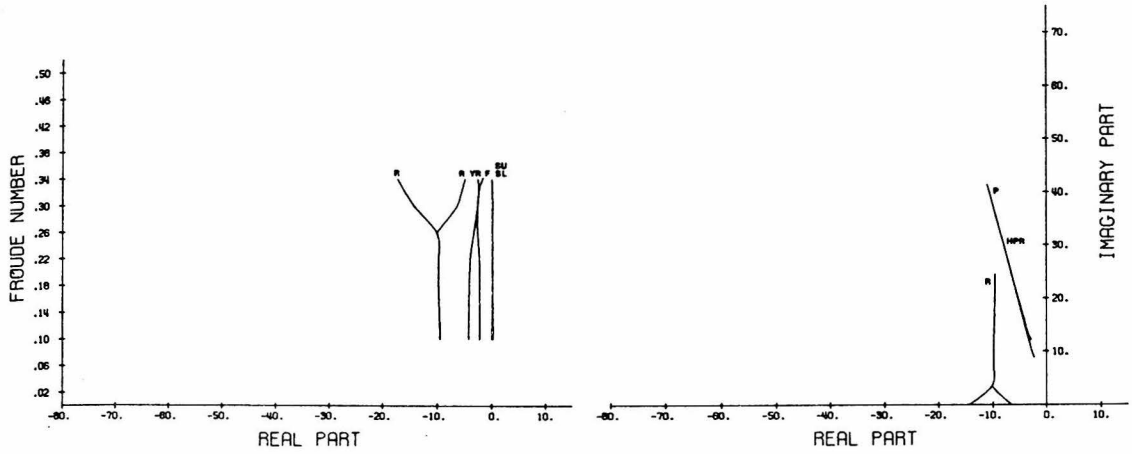


Figure 6.7. Eigenvalues for Base Boat $\gamma = -140^{o}$ (Beat)

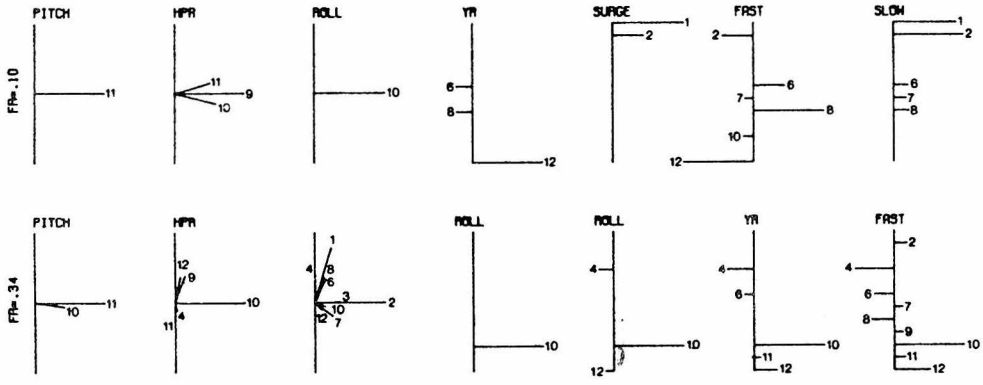


Figure 6.8. Normal Modes for Base Boat $\gamma = -140^{o}$ (Beat)

roots coalesce to form complex modes for certain sailing conditions. This interaction makes physical interpretation difficult; however, Section 6.3 discusses the gross characteristics of these basic modes.

The roll degree of freedom ($x_4 = z_4$) is important in all modes for some sailing conditions. Unlike Downwind Sailing where roll was coupled with sway and yaw only, at high speed the modal coefficients indicate a strong coupling with pitch, heave and surge. There are some cases where all rigid body degrees of freedom are important, e.g., Fr = .34, $\gamma = -140^{o}$.

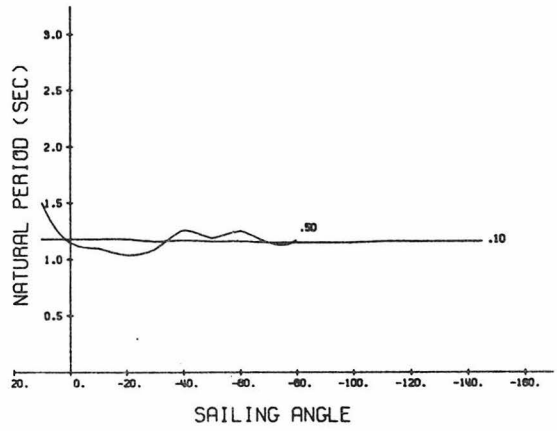
For fixed sailing angle γ, the eigenvalues are relatively constant at low speed. As the vessel approaches hull speed (Fr ~ .4) there is a much stronger variation, and interaction between modes occurs. The eigenvalue plots also show some small scale irregularities due to ballast shifts and sail changes. These occurrences are shown in Figure 5.1.

There are numerous cases in these plots where the real part of at least one eigenvalue is positive. However, many of these have large time constants indicating weak modes.

6.3 Discussion of Normal Modes for Base Boat

Pitch Mode

One complex conjugate pair of eigenvalues corresponds to almost pure pitching oscillations ($x_{11} = \dot{z}_5$). The natural period and damping ratio for this mode are shown in Figure 6.9 as functions of sailing angle.



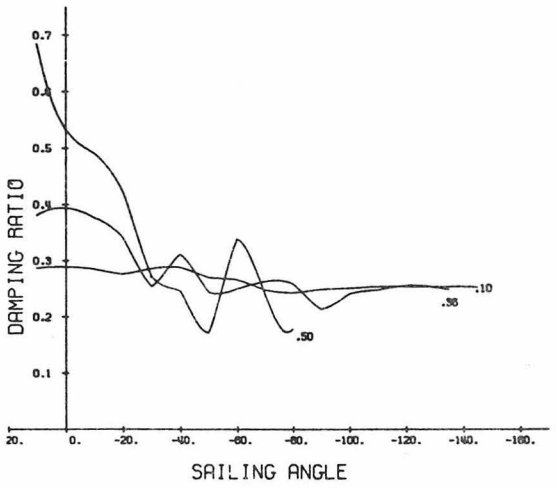


Figure 6.9. Natural Period and Damping Ratio for Pitch Mode

The large increase in damping on offwind courses is due to roll motions. Figures 6.2 and 6.4 indicate that at moderate and high speeds the contribution from roll dominates the mode shape. Yaw motions ($x_{12} = \dot{z}_6$) are also significant in this mode on windward courses.

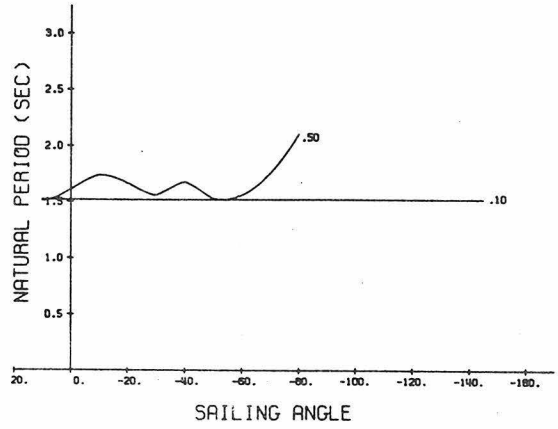
The root locus for the Pitch Mode shifts toward the stability boundary as the sailing angle is increased from leeward to windward courses. Close-hauled, the Pitch Mode appears to coincide with another mode, e.g., Figure 6.7. However, due to differences in Froude Number the eigenvalues are actually well separated. For the Base Boat, the Pitch Mode is stable in all cases.

HPR Mode

The second complex mode is primarily a coupled heave ($x_9 = \dot{z}_3$), pitch and roll oscillation. The HPR Mode is fundamentally a coupled pitch-heave motion, but similar to the Pitch Mode, roll tends to dominate near hull speed. Figure 6.10 shows the natural period and damping for this mode. The root locus for the HPR mode remains nearly stationary in the complex plane with variations in sailing angle. As noted, the Pitch Mode tends toward it on windward courses. The HPR mode is also stable in all cases.

Roll Mode

The remaining complex mode is dominated by roll motions for all sailing conditions with only small influences from yaw and pitch. The eigenvalue plots for this mode show the greatest sensitivity to Froude Number and sailing angle. The root locus shifts toward the



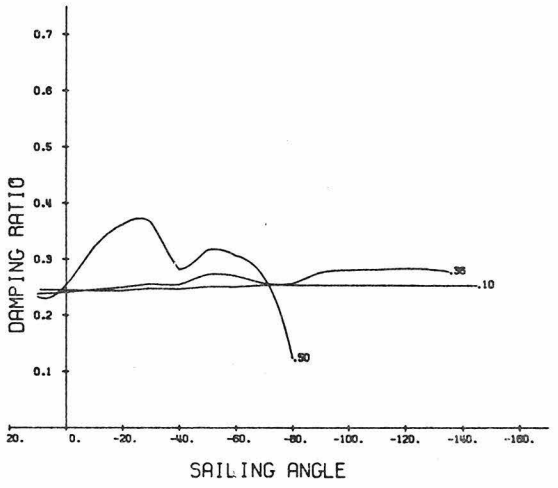


Figure 6.10. Natural Period and Damping Ratio for HPR Mode

stability boundary as the vessel heads up from a dead run to a broad reach; then above $\gamma = -30^{o}$ the root locus moves back towards increasingly negative values. These shifts are sufficient to cause the Roll Mode to become unstable at $\gamma = -30^{o}$, Fr = .50. The characteristics of this mode for these conditions are given in Table 6.2.

Table 6.2. Natural Period and Damping Ratio of Roll Mode ($\gamma = -30^{o}$, Fr = .50)

Natural Period	1.9 sec
Damping Ratio	-.12

This instability is similar to that discussed in Chapter IV for the Base Boat with Gottingen foil.

As the vessel tends toward higher reaching courses, the complex conjugate pair corresponding to the Roll Mode degenerates into two real roots. This first occurs on a beam reach at Fr = .34 and $\gamma = -50^{o}$, and it is a consistent feature of windward courses at moderate speeds and above. The time constants for these real roots are always very short: approximately 0.1 and 0.3 seconds. The shorter root remains real as speed increases, and the modal coefficients indicate predominately roll motions with some pitch. However, the longer root sometimes joins with another real root to form a new complex mode. Figure 6.5 shows this behavior. The new complex mode is dominated by roll, but otherwise it is dissimilar with the Roll Mode. Table 6.3 compares these modes.

Table 6.3. Comparison of Modal Characteristics ($\gamma = -70^{o}$)

	Roll Mode (Fr = .22)	New Mode (Fr = .36)
Natural Period (sec.)	1.9	3.8
Damping Ratio	.81	.97

As indicated in Figure 6.6 this new mode contains substantial yaw motions.

The eigenvalue plots show considerable interaction between the real roots. At low speed it is relatively easy to identify each mode, but at higher speeds the root loci intersect and sometimes form new modes. However, the following is an attempt to categorize their major features.

YR Mode

The YR Mode is relatively simple on offwind courses. It corresponds to coupled yaw, roll and sway motions as in the case of Downwind Sailing. Roll is unimportant at low speed, but at high speeds this mode is also dominated by rolling motions. The mode is always stable, with time constants varying from about 2 seconds at low speed to 0.5 second at high speed. On reaching and windward courses, it is this root that joins with one of the roots of the Roll Mode to form the new, long period roll mode.

Surge Mode

One root is usually dominated by surge motions ($x_7 = \dot{z}_1$). Unlike Downwind Sailing, sway and yaw are significant in this mode,

and at high speeds all the rigid body degrees of freedom are important, e.g., Figure 6.6. The time constant varies from 35 seconds at low speed to about 1 second at high speed. This mode is usually stable, but it may join with another root to form an unstable, long period complex mode. On windward courses the Surge Mode sometimes combines to form a complex weathercock mode such as in Figure 6.8. The surge velocity ($x_7 = \dot{z}_1$) is about 90° out of phase with yaw and sway velocity. The natural period for this oscillation is rather long at about 40 seconds, and the damping ratio is about 0.3.

Fast and Slow Modes

It is difficult to be precise about the remaining two real roots due to their interaction. One root is always close to the stability boundary, and it is positive or negative depending on the specific sailing conditions. The time constant for this Slow Mode is always long varying from about 1000 seconds at low speed up to about 10 seconds at high speed. Sway is the dominant motion.

The Fast Mode is readily identifiable at low speed. It is a stable sway-yaw motion with time constant of about 5.5 seconds. As speed increases the root tends toward the stability boundary, forms a complex mode with another real root, or remains a stable, real root.

On offwind courses at high speed there is usually one unstable real root with a time constant of 1-2 seconds. The modal coefficients indicate a coupled roll-sway-yaw motion. For courses above

a close reach this root remains negative for all speeds. This root is interpreted as the high speed extension of the Fast Mode, since its time constant and modal coefficients are generally similar to the low speed version.

6.4 Base Boat with Gottingen Foil

In order to demonstrate the sensitivity of these calculations to the input data, two additional data cases are discussed. The first case is identical with the previous section except the Finn sail coefficients are replaced with the coefficients from the Gottingen foil. Chapter V indicated the important differences in the steady state solutions for these data. Figures 6.11 - 6.18 summarize the solutions to the Perturbation Equations.

The eigenvalues and normal modes show some significant changes with the new aerodynamic coefficients. On offwind courses the root locus of the Roll Mode is shifted toward the stability boundary, and for ($\gamma = 0^{o}$, $.40 \leq Fr \leq .48$) the mode is unstable. This parallels the results for Downwind Sailing. At high speed both the Slow and Fast Modes are unstable with time constants of -5.6 seconds and -1.9 seconds. These are windward broaches, whereas with the Finn sail there was only one positive root corresponding to a leeward broach. The Pitch Mode for $\gamma = 0^{o}$ shows no influence of roll, but when broad reaching at high speed, both the Pitch and HPR Modes display significant roll motions.

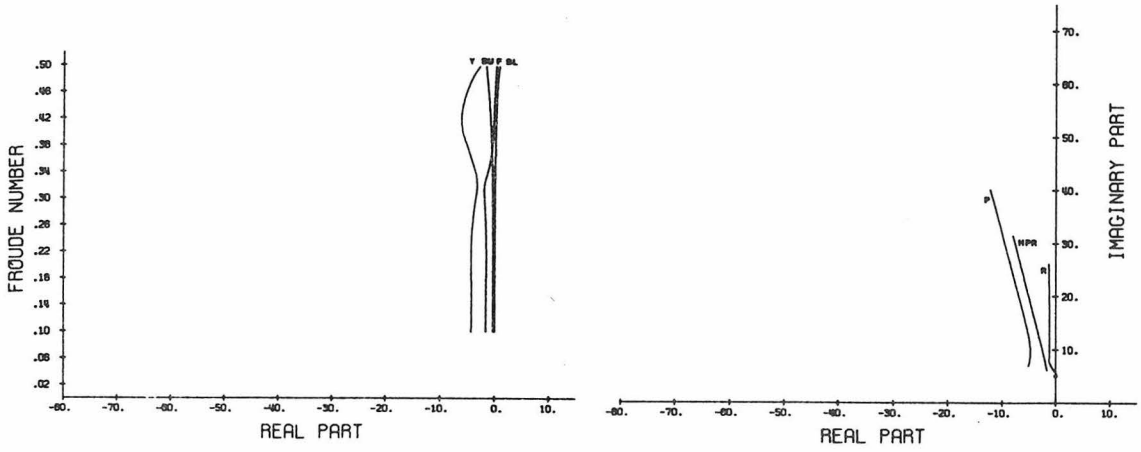


Figure 6.11. Eigenvalues for Base Boat with Gottingen Foil $\gamma = 0^{o}$ (Run)

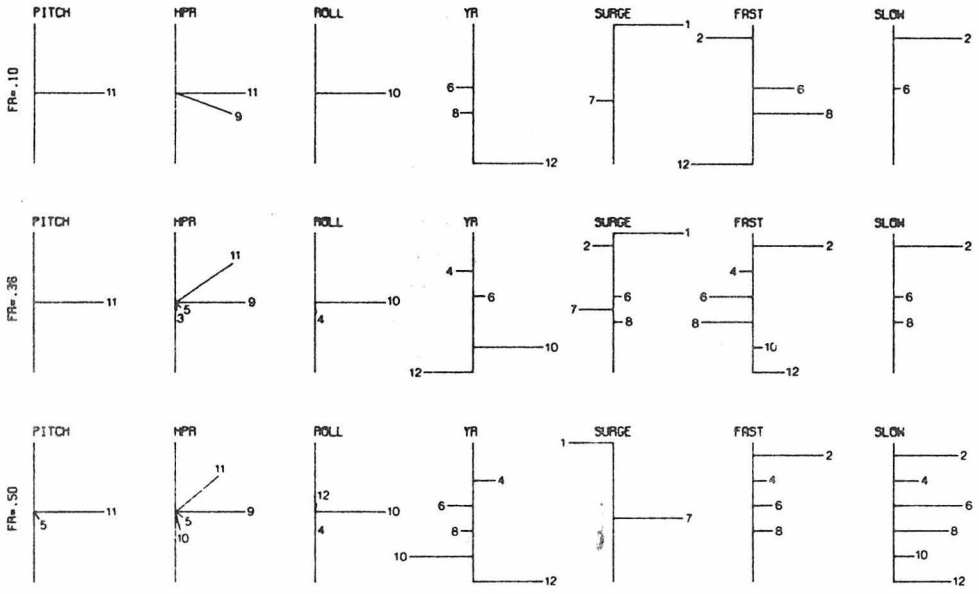


Figure 6.12. Normal Modes for Base Boat with Gottingen Foil $\gamma = 0^{o}$ (Run)

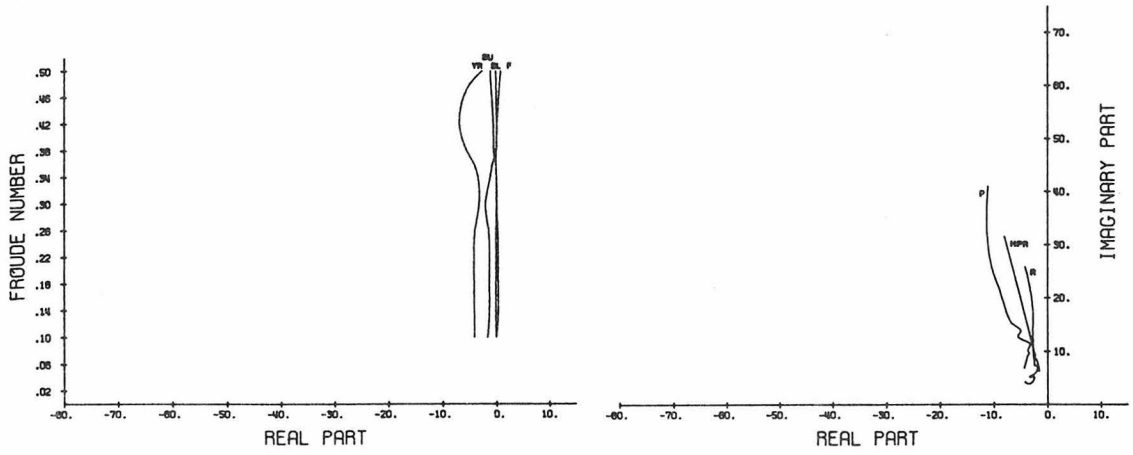


Figure 6.13. Eigenvalues for Base Boat with Gottingen Foil $\gamma = -30^{o}$ (Broad Reach)

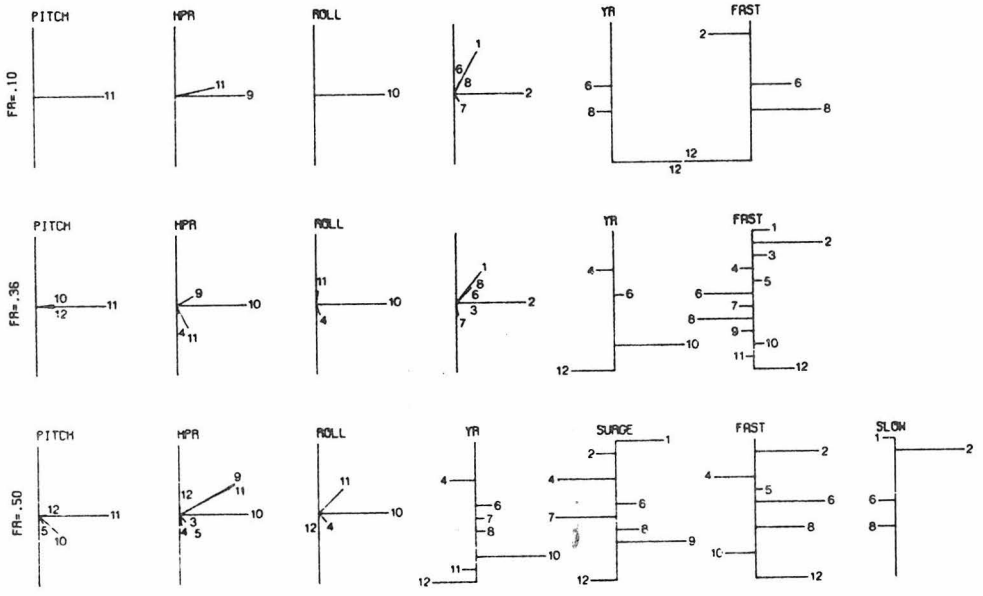


Figure 6.14. Normal Modes for Base Boat with Gottingen Foil $\gamma = -30^{o}$ (Broad Reach)

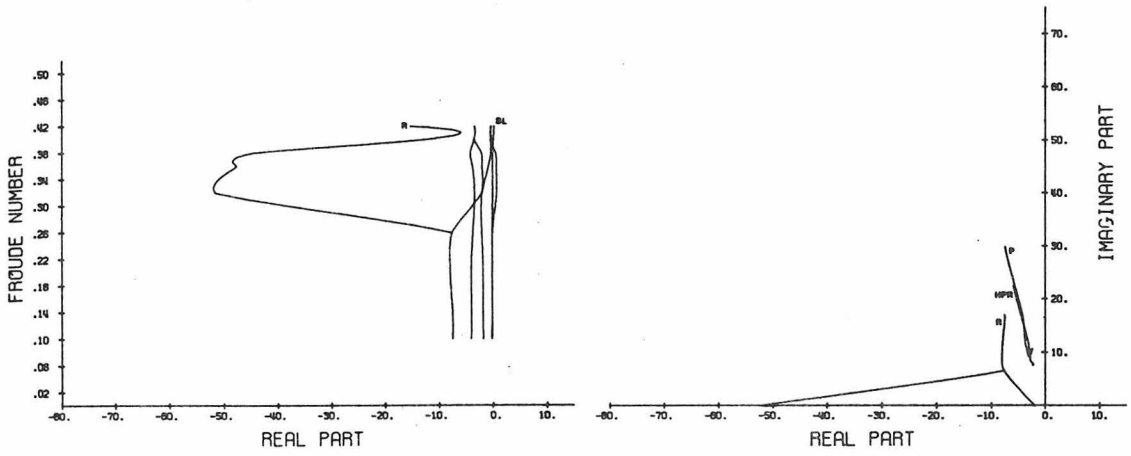


Figure 6.15. Eigenvalues for Base Boat with Gottingen Foil $\gamma = -70^{o}$ (Close Reach)

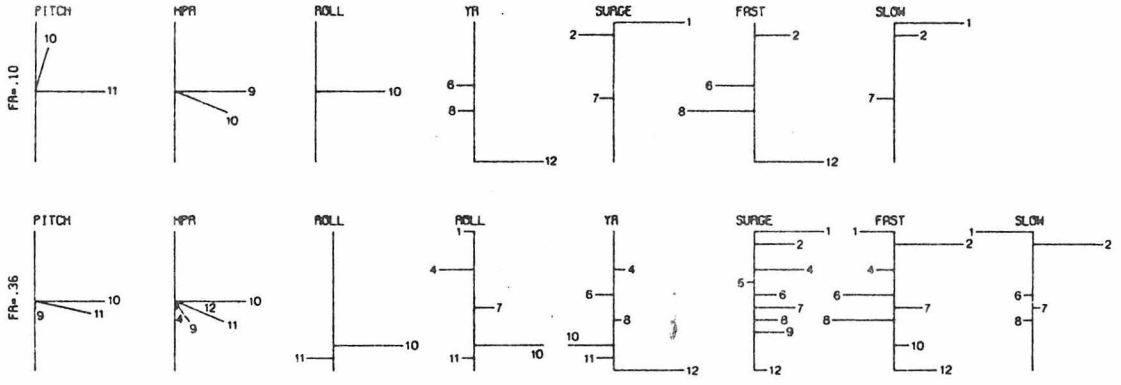


Figure 6.16. Normal Modes for Base Boat with Gottingen Foil $\gamma = -70^{o}$ (Close Reach)

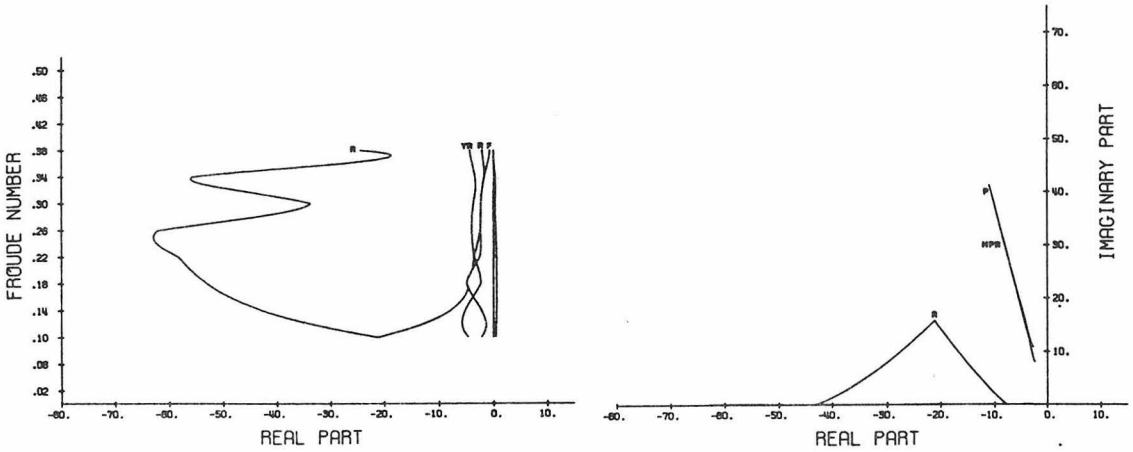


Figure 6.17. Eigenvalues for Base Boat with Gottingen Foil $\gamma = -140^{o}$ (Beat)

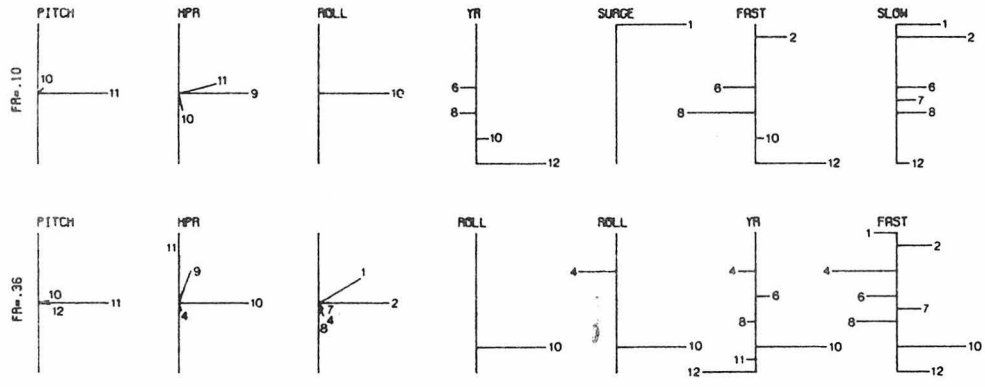


Figure 6.18. Normal Modes for Base Boat with Gottingen Foil $\gamma = -140^{o}$ (Beat)

On reaching courses the root locus for the Roll Mode again shifts away from the stability boundary. The critical Froude Number, where the mode degenerates into real modes, is higher (Fr ~ .3). The time constant for the short root of the Roll Mode is much smaller. On a close reach there is a relatively large unstable root at moderate speeds. The time constant is about -3.7 seconds, and the mode involves all motions but heave. At high speed there is a related long period roll mode with T^N = 12.2 seconds and ζ = -.69. This mode is rather unusual due to the large surge motions.

Close-hauled the Roll Mode is complex only at the lowest speed, and one of the resulting time constants is much shorter. This is shown in Table 6.4.

Table 6.4. Comparison of Roll Mode Time Constants for (γ = -140°, Fr = .34)

	Finn Sail	Gottingen Foil
T_1 (sec.)	.13	.04
T_2 (sec.)	.46	.68

Close-hauled at low speeds the Gottingen foil produces an unstable real root with time constants varying from -36 seconds to -19 seconds. The modal coefficients resemble the Slow Mode except surge motions are important.

6.5 Heavy Displacement

Solutions to the Steady State and Perturbation Equations were calculated for a keelboat with DLR ~ 360. Unlike the Downwind case, the Gottingen foil coefficients were used. Figures 6.19 - 6.26 summarize the eigenvalues and normal modes.

The modes for the heavy displacement vessel are much easier to identify, since as with Downwind Sailing, the variation of the eigenvalues with Froude Number is attenuated. For this case the live ballast was not shifted from the centerline, since reasonable heel angles are achieved without it (Figure 5.9). This eliminates some of the irregularities of the previous cases.

Offwind the HPR mode is almost a pure heaving oscillation, and the modes appear to be very nearly decoupled into lateral and longitudinal groups. However, on broad reaching courses the more general situation is evident. The Roll Mode degenerates at a very low speed on close reaches, and a very short time constant results. An unusual complex mode occurs on this point of sail at high speed when the Slow and Fast roots coalesce. All motions are significant except pitch; the natural period is 13 seconds and the damping ratio is -.4. Close-hauled, the long period roll mode exists over a large speed range, and the remaining Roll Mode time constant is very short.

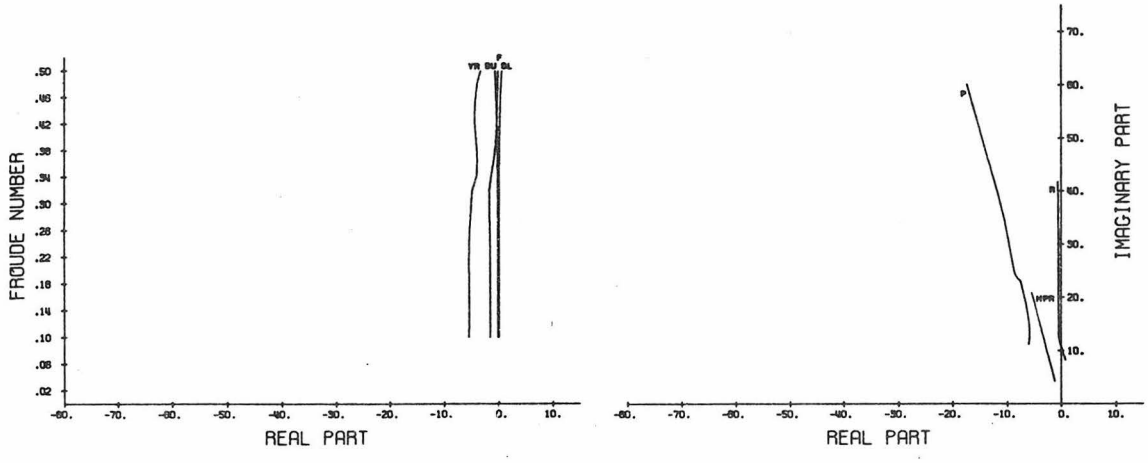


Figure 6.19. Eigenvalues for Heavy Displacement $\gamma = 0^{o}$ (Run)

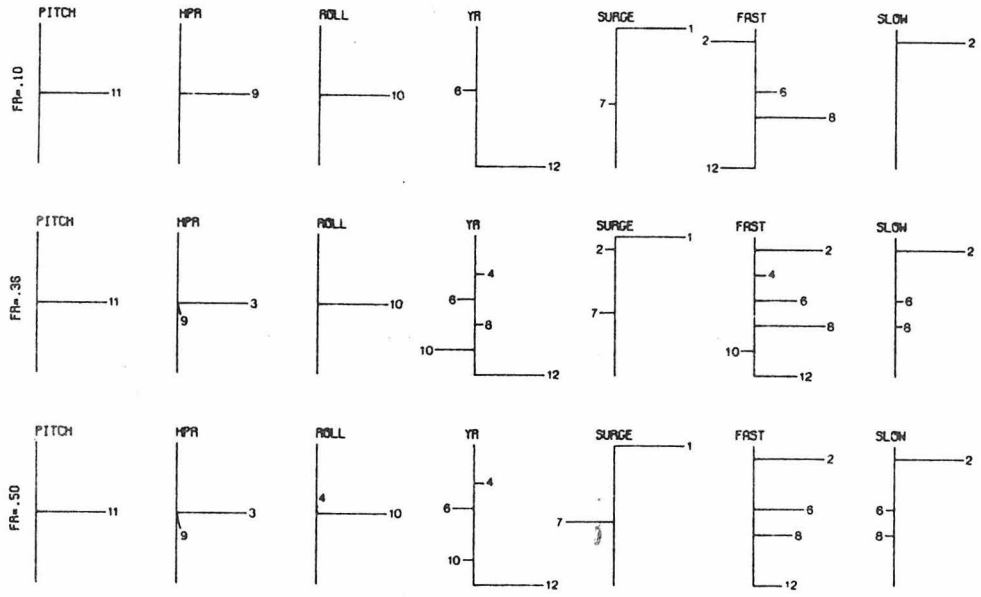


Figure 6.20. Normal Modes for Heavy Displacement $\gamma = 0^{o}$ (Run)

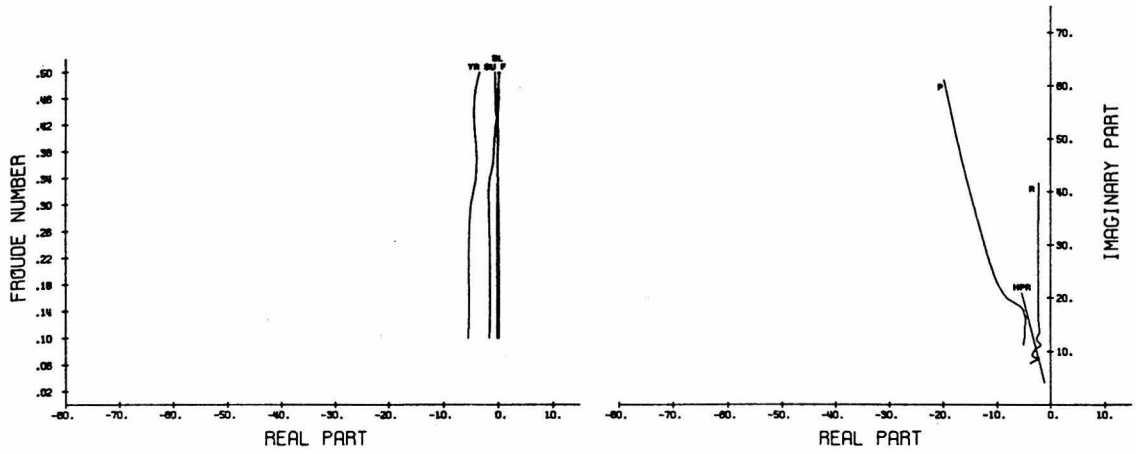


Figure 6.21. Eigenvalues for Heavy Displacement $\gamma = -30^{o}$ (Broad Reach)

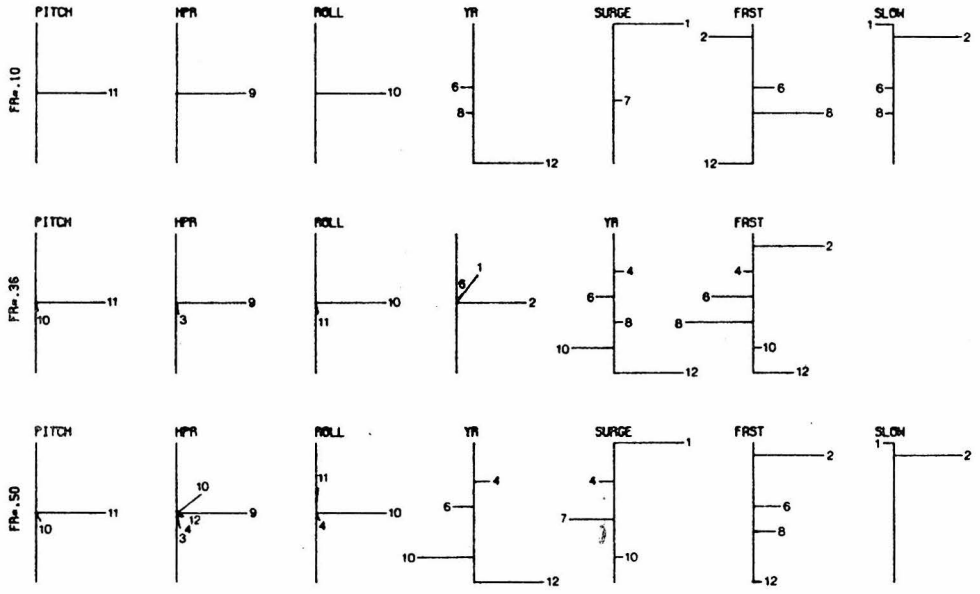


Figure 6.22. Normal Modes for Heavy Displacement $\gamma = -30^{o}$ (Broad Reach)

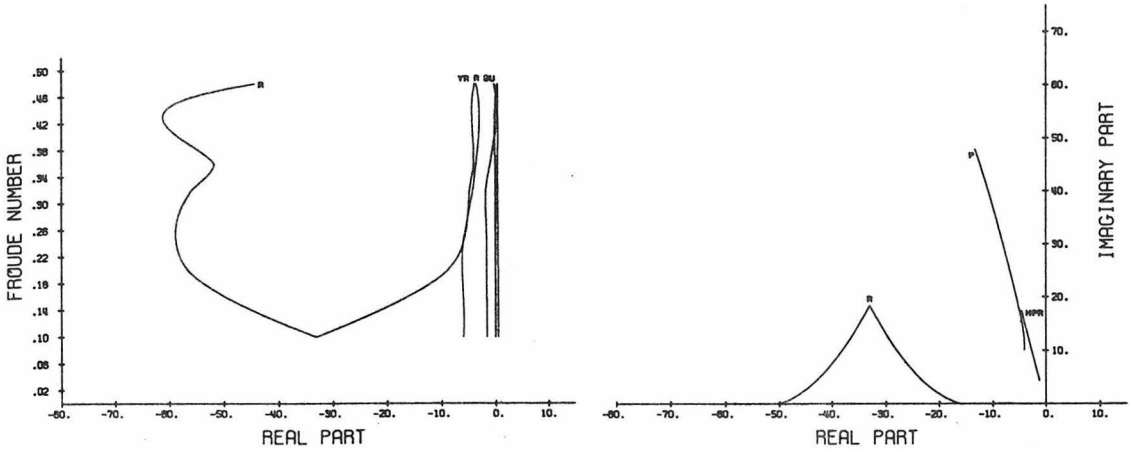


Figure 6.23. Eigenvalues for Heavy Displacement
$\gamma = -70^{o}$ (Close Reach)

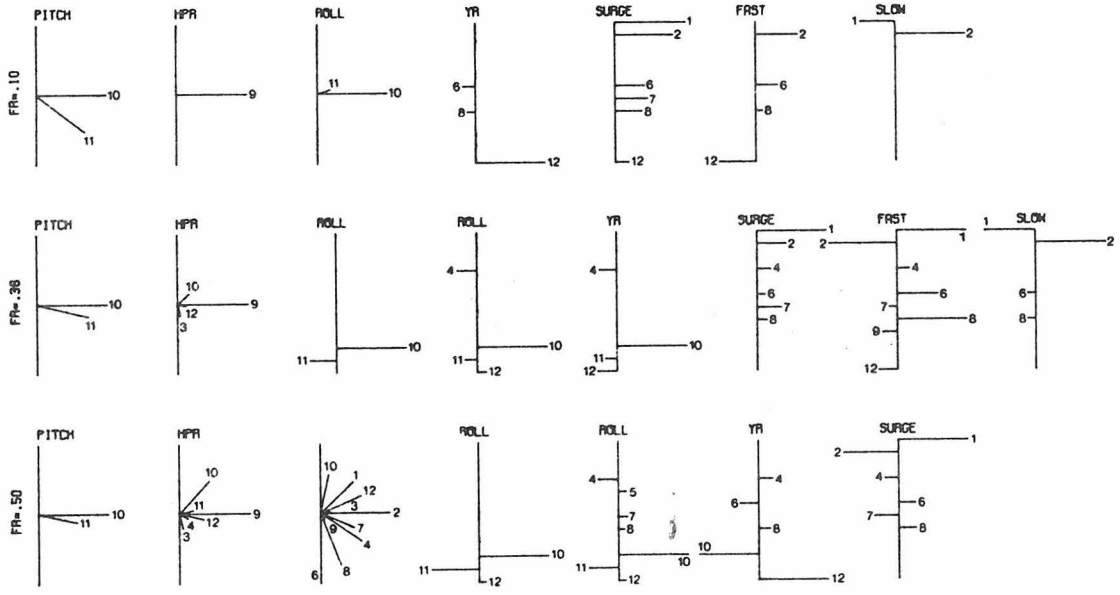


Figure 6.24. Normal Modes for Heavy Displacement
$\gamma = -70^{o}$ (Close Reach)

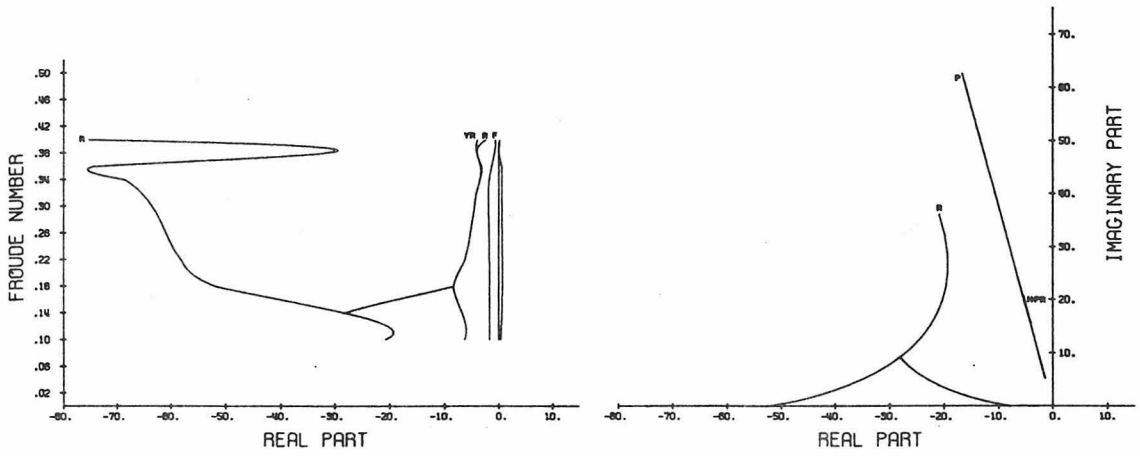


Figure 6.25. Eigenvalues for Heavy Displacement
$\gamma = -140^{o}$ (Beat)

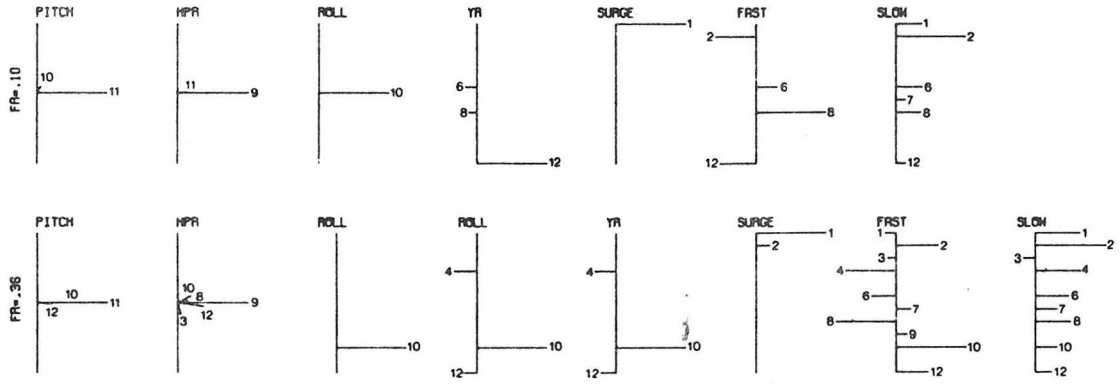


Figure 6.26. Normal Modes for Heavy Displacement
$\gamma = -140^{o}$ (Beat)

VII. SUMMARY AND CONCLUSIONS

7.1 General

The dynamic model developed in Chapters II and III has produced encouraging results. The scheme has proved to be relatively efficient and shows good correlation with the limited full scale data. The simplified model of the fluid forces predicts quite reasonable boom and leeway angles for the various points of sail; however, the extremely small rudder angles appear to be a result of oversimplification. Due to the large number of parameters required to describe the system, the results are rather complicated.

The model treats Froude Number and sailing angle as free parameters, and solutions were found throughout the domain appropriate for non-surfing keelboats. The steady state solutions show the usual variation with the sailing conditions, but the perturbational solutions also display a strong dependence of these quantities. Well below hull speed the dynamic characteristics show only small variation with Fr and Υ. But near and above hull speed there are wide variations in the modal characteristics. The existence and nature of these variations needs experimental verification.

The calculations show that the roll degree of freedom (z_4) plays a fundamental role in all modes under some sailing conditions. This implies that the vessel's roll-stiffness parameters ($\overline{GM}$ and r_2^m) are strong determinants of the dynamic behavior. These results support an extension to the dynamic case of an earlier conclusion of Letcher (1971), i.e., the behavior of sailing vessels may be largely

determined by gross physical characteristics rather than the details of the hull and fluid flows. However, the results with Valiant's rudder seem to indicate that if the flows break down, the dynamic behavior may be radically different.

The limited data used in the calculations provide only a partial answer to the question of Liapunov asymptotic stability. These data show that under nearly all sailing conditions there exists at least one eigenvalue with positive real part. However, the time constants of the Slow Mode are sufficiently long that it is doubtful whether these significantly effect course-keeping ability. On offwind courses at high speed the model predicts unstable exponential and oscillatory modes which seem to be rapid enough to cause steering difficulties. Determining the level at which unstable roots can no longer be adequately handled by conventional steering systems is a second topic for experimental work.

No definitive statements can be made on which factors essentially govern the dynamic characteristics until fine tuned analyses are conducted on specific sailing vessels. The calculations of Chapters IV and VI suggest that several factors are important. The roll-stiffness parameters are critical, since very tender vessels appear to amplify local dependence on Froude Number. Aerodynamic characteristics strongly effect dynamic behavior, especially in regions where the gradient of the sideforce coefficient is negative. Somewhat surprisingly, rudder characteristics also appear to be a prime determinant of helm-fixed behavior. For vessels tending

toward the low end of the nondimensional mass spectrum (i.e., DLR), the inertial properties must also be included. As full scale tank and towing data become available it will be possible to do these studies and check for any idiosyncrasies of the Antiope data.

7.2 Steady State Equations and Solutions

The Steady State Equations were formulated primarily as an adjunct to the Perturbation Equations. Without employing fine tuned data or optimization schemes, good agreement was obtained describing gross performance and attitude. The calculated steady state variables are approximate lower bounds to the values typically reported. In the case of true wind speed, the lower bound represents maximum performance. The calculated solutions show a strong dependence on the input parameters, especially sail characteristics. It is anticipated that new hull-keel data may show significant differences from the high performance characteristics of Antiope.

These solutions show several encouraging features. Windward leeway angles agree very well with those expected of Antiope. Similarly, the location of live ballast can be exploited to obtain performance gains. Calculated rudder angles are much smaller than those common in practice, but close-hauled solutions do show increasing weather helm with increasing boat speed.

7.3 Perturbation Equations and Solutions

In contrast to the small differences reported by Milgram (1972), the model developed here shows both large scale and local variations

in the dynamic characteristics. In general the perturbational motions of a sailing vessel are represented by three complex modes, four purely real modes and two zero eigenvalues. However, depending on the sailing conditions and input parameters, other modes may be formed which display a widely different mix of modal elements. The Roll Mode is most interesting due to its strong sensitivity to Fr and γ. The predicted offwind instability correlates well with the observations and wind tunnel experiments reported by Marchaj (1971). The entire root locus of this mode shifts in the complex plane with γ, and on courses above a beam reach ($|\gamma| \geq 50^{o}$) the complex mode degenerates into two real modes.

The Pitch and HPR Modes are always stable. Depending on sailing conditions and vessel characteristics, these modes may closely resemble conventional ship behavior. Both modes are strongly dependent on free surface wave generation.

The YR Mode is always stable and relatively simple. The Surge Mode shows strong coupling with sway and yaw, and it is weakly unstable under some conditions. The Fast and Slow Modes display very complicated behavior. One eigenvalue is usually very close to the stability boundary and represents a weak mode. On offwind courses at high speed the second eigenvalue appears to produce a significant instability.

Chapter IV presents a simplified model for Downwind Sailing. The principal advantages of this model are that the Steady State Equations are reduced to simple form and the Perturbation Equations

decouple into longitudinal and lateral groups. The resulting solutions are in reasonable agreement with the full equations for $\gamma = 0^{o}$, but the simplified model can not account for the strong influence of roll motions in all modes. The full model also shows that depending on sail characteristics, the Roll Mode instability may not occur directly downwind but on reaching courses as high as $|\gamma| = 30^{o}$. Of course, since most crews avoid sailing directly before the wind for various reasons, this model is of little practical importance.

REFERENCES

Abkowitz, Martin A., 1969, Stability and motion control of ocean vehicles, Cambridge, The MIT Press.

Baker, Robert M. L., Jr., and Douglas, James S., 1977, Four-dimensional simulation of a hydrofoil craft, Proc. Eighth AIAA Symposium on Aer/Hydronautics of Sailing, vol. 23, Stanford University, pp. 100-118.

Blagoveshchensky, S. N., 1962, Theory of ship motions, 2 vols., Translated by Theodor and Leonilla Strelkoff, New York, Dover Publications.

Bradfield, W. S., 1968, Predicted and measured performance of a day-sailing catamaran, University of Southampton, SUYR Report No. 25.

Bradfield, W. S., and Griswold, Lee M., 1977, The evaluation of sailing vehicle rig polars from two-dimensional wind tunnel data, Proc. Eighth AIAA Symposium on Aer/Hydronautics of Sailing, vol. 23, Stanford University, pp. 78-88.

Bryan, G. H., and Williams, W. E., 1904, The longitudinal stability of aerial gliders, Proc. Roy. Soc., vol. 73, pp. 100-16.

Buchan, A. L., and Flewitt, J. R., 1968, The behaviour and stability of wind operated steering systems for sailing yachts, University of Southampton, SUYR Report No. 27.

Chapman, R. B., 1976, Free-surface effects for yawed surface-piercing plates, J. Ship Research, vol. 20, no. 3, pp. 125-36.

Clauser, Milton U., 1975, The tow testing of full scale yachts, Proc. Sixth AIAA Symposium on Aer/Hydronautics of Sailing, vol. 15, North Hollywood, Western Periodicals Co., pp. 70-7.

Coddington, Earl A., and Levinson, Norman, 1955, Theory of ordinary differential equations, New York, McGraw-Hill.

Critzos, Chris C., Heyson, Harry H., and Boswinkle, Robert W., Jr., 1955, Aerodynamic characteristics of NACA 0012 airfoil section at angles of attack from 0° to 180°, NACA, TN3361.

Curtiss, H. C., Jr., 1970, On the stability and control of sailing yachts, Proc. Second AIAA Symposium on Aer/Hydronautics of Sailing, vol. 9, Los Angeles, pp. 21-32.

Davidson, K. S. M., 1936, Some experimental studies of the sailing yacht, Trans. SNAME, vol. 44, pp. 288-334.

Davidson, K. S. M., 1944, On the turning and steering of ships, SNAME, Preprint No. 8.

Davidson, K. S. M., 1948, A note on steering of ships in following seas, Proc. Seventh Int. Congress App. Mech., vol. 2, London.

Davidson, K. S. M., 1956, The mechanics of sailing ships and yachts, Surveys in Mechanics, ed. by G. K. Batchelor and H. Bondi, Cambridge University Press, pp. 431-74.

Dayman, Bain, Jr., 1953, Experimental aerodynamics of a two-dimensional sail, Aeronautical Engineer Thesis, Pasadena, California Institute of Technology.

Den Hartog, J. P., 1956, Mechanical vibrations, New York, McGraw-Hill.

Eda, Haruzo, and Crane, C. Lincoln, 1965, Steering characteristics of ships in calm water and waves, Trans. SNAME, vol. 73.

Eda, Haruzo, 1968, Low-speed controllability of ships in wind, J. Ship Research, vol. 12, no. 3.

Eda, Haruzo, 1971, Directional stability and control of ships in restricted channels, Trans. SNAME, vol. 79, pp. 71-116.

Eda, Haruzo, 1972, Directional stability and control of ships in waves, J. Ship Research, vol. 16, no. 3.

Etkin, Bernard, 1972, Dynamics of atmospheric flight, New York, John Wiley and Sons.

Froude, W., 1861, On the rolling of ships, Trans. INA, pp. 180-229.

Gerritsma, J., 1968, Course keeping qualities and motions in waves of a sailing yacht, Laboratorium voor Scheepbouwkunde, Technische Hogeschool Delft, Report No. 200.

Gerritsma, J., and Moeyes, G., 1973, The seakeeping performance and steering properties of sailing yachts, Report No. 366, Preprint to Third HISWA Symposium of Yachts, Amsterdam.

Gerritsma, J., Kerwin, J. E., and Moeyes, G., 1975, Determination of sail forces based on full scale measurements and model tests, MIT Ocean Engineering, Report No. 75-15.

Grad, J., and Brebner, M. A., 1968, Algorithm 343: eigenvalues and eigenvectors of a real general matrix, Comm. ACM, vol. 11, no. 12, pp. 820-26.

Hammitt, A. G., 1975, Technical yacht design, London, Adlard Coles.

Herreshoff, H. C., 1964, Hydrodynamics and aerodynamics of the sailing yacht, Trans. SNAME, vol. 72, pp. 445-492.

Herreshoff, H. C., and Newman, J. N., 1967, Full scale tank tests of the 5.5 meter yacht Antiope, SNAME Tech. and Res. Bulletin No. 1-28.

Hoerner, Sighard F., 1975, Fluid-dynamic lift, Brick Town, New Jersey, Hoerner Fluid Dynamics.

Issacson, Eugene, and Keller, Herbert Bishop, 1966, Analysis of numerical methods, New York, John Wiley and Sons.

Kerwin, J. E., Oppenheim, B. W., and Mays, J. H., 1974, A procedure for sailing performance analysis based on full scale log entries and towing tank data, MIT Ocean Engineering, Report No. 74-17.

Kerwin, J. E., 1975, A velocity prediction program for ocean racing yachts, MIT OCean Engineering, Report No. 75-17.

Kirkman, Karl L., and Pedrick, David R., 1974, Scale effects in sailing yacht hydrodynamic testing, SNAME Advance Copy, No. 1.

Letcher, J. S., Jr., 1965, Balance of helm and static directional stability of yachts sailing close-hauled, J. Roy. Aero. Soc., vol. 69, pp. 241-248.

Letcher, J. S., Jr., 1971, Steering qualities off the wind, Proc. Third AIAA Symposium on Aer/Hydronautics of Sailing, vol. 10, Los Angeles, pp. 108-113.

Letcher, J. S., Jr., 1974, Self-steering for sailing craft, Camden, Maine, International Marine Publishing Company.

Letcher, J. S., Jr., 1975, Sailing hull hydrodynamics, with reanalysis of the Antiope Data, Trans. SNAME, vol. 83, pp. 22-40.

Letcher, J. S., Jr., 1976a, Performance and stability of wind-referenced autopilots for sailing vessels, Marine Technology, vol. 13, no. 3, pp. 301-308.

Letcher, J. S., Jr., 1976b, Optimum windward performance of sailing craft, J. Hydronautics, vol. 10, no. 4, pp. 140-4.

Roskam, J., 1971a, Flight dynamics of rigid and elastic airplanes, Lawrence, Kansas, By the Author.

Roskam, J., 1971b, Methods for estimating stability and control derivatives of conventional subsonic airplanes, Lawrence, Kansas, By the Author.

Rydill, L. J., 1959, A linear theory for the steered motion of ships in waves, Trans. INA, pp. 81-112.

Spens, P. G., De Saix, P., and Brown, P. W., 1967, Some further experimental studies of the sailing yacht, Trans. SNAME, vol. 75, pp. 79-103.

Stoker, J. J., 1957, Water waves, New York, Interscience Publishers.

Tanner, T., et al., 1960, The pitching of sailing ships close-hauled in a head sea, University of Southampton, SUYR Report No. 2.

Titlow, Joseph D., 1977, A dynamic model for downwind sailing, Proc. Eighth AIAA Symposium on Aer/Hydronautics of Sailing, vol. 23, Stanford University, pp. 6-27.

Vugts, J. H., 1968, The hydrodynamic coefficients for swaying, heaving and rolling cylinders in a free surface, Laboratorium voor Scheepsbouwkunde, Technische Hogeschool Delft, Report No. 194.

Wood, David V. V., and Thompson, Kenneth W., 1974, Tall ships and sailormen: Operation Sail 1972, U.S. Naval Institute Proc., pp. 41-54.

Woodward, John B., et al., 1975, Feasibility of sailing ships for the American Merchant Marine, University of Michigan, Naval Arch. and Marine Eng., Report No. 168.

Wu, Th. Y., and Newman, J. N., 1972, Unsteady flow around a slender fish-like body, J. Mech. Eng. Science, vol. 14, no. 7, pp. 43-52.

APPENDIX A

SAILING VESSEL DATA

A.1 Antiope Data

Much of this study is based on the unique full scale towing tests of the 5.5 meter Antiope with L = 24.3 ft (7.41 m). Herreshoff and Newman (1967) conducted these tests primarily as a basis for studying scale effects (Kirkman and Pedrick 1974). Table A.1 indicates the values of the test variables.

Table A.1. Antiope Test Variables

Froude Number	.12, .18, .24, .30, .36, .39
Reynolds Number (E+06)	7.6, 11., 15., 19., 23., 25.
Heel	~0°, ~10°, ~20°
Angle of Incidence	~0°, ~3°, ~6.5°
Helm Angle	0°, 1.6°, 3°, 6°
Number of Data	219

Letcher (1975) reanalyzed these data with the objective of comparing them with theoretical estimates of the hydrodynamic lift force. The interpretations and corrections developed by Letcher were adopted here for the reduction of the test data to forces in the body frame.

The hydrodynamic resistance and sideforce coefficients for the Antiope data are related to the $\underline{e}_1$ and $\underline{e}_2$ components of force by

$$\begin{Bmatrix} C_{K1}(Fr, \alpha_K) \\ C_{K2}(Fr, \alpha_K) \end{Bmatrix} = - \frac{1}{\frac{\rho_w}{2} V_s^2 L^2} \frac{1}{(\cos^2\psi + \cos^2\varphi \sin^2\psi)} \begin{bmatrix} \cos\psi & -\cos\varphi\sin\psi \\ \cos\varphi\sin\psi & \cos\psi \end{bmatrix} \begin{Bmatrix} f_1 \\ f_2 \end{Bmatrix} \tag{A.1}$$

where

$$\tan \alpha_K = -\cos\varphi \tan\psi \tag{A.2}$$

$$\psi = -\alpha' \tag{A.3}$$

Equation (A.3) relates the Eulerian angle ψ to the test angle of incidence (Letcher 1975). These tests show significant forces in the $\underline{e}_3$ direction, probably due to dynamic sinkage, and equation (A.1) substantially underestimates these forces.

In order to calculate solutions throughout the sailing envelope, it is necessary to interpolate and extrapolate these data for the ranges

$$.1 \leq Fr \leq .5 \tag{A.4}$$

$$-7.^\circ \leq \alpha_K \leq 7.^\circ \tag{A.5}$$

The following scheme is used:

(1) Delete runs with $\delta_R \neq 0$

(2) Delete runs 1382-1385

(3) Assume port-starboard symmetry

$$C_{K1}(Fr, -\alpha_K) \equiv C_{K1}(Fr, \alpha_K) \tag{A.6}$$

$$C_{K2}(Fr, -\alpha_K) \equiv -C_{K2}(Fr, \alpha_K) \tag{A.7}$$

$$C_{K2}(Fr,0) \equiv 0 \qquad (A.8)$$

(4) Use a least-squares biquartic polynomial to fit the resistance data

(5) Use a least-squares biquadratic polynomial to fit the sideforce data

Figures A.1 - A.3 show the results of these calculations.

Letcher (1975) includes the results of some hydrostatic calculations for Antiope. Figure A.4 shows a plot of the righting moment of equation (3.46) compared with the test values of Herreshoff and Newman. For these calculations

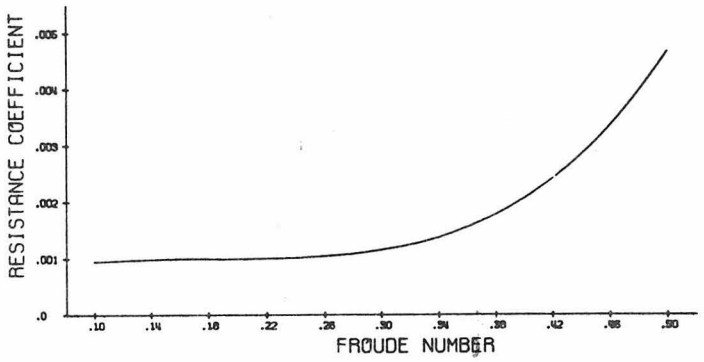


Figure A.1. Antiope Resistance Coefficient for Upright Conditions

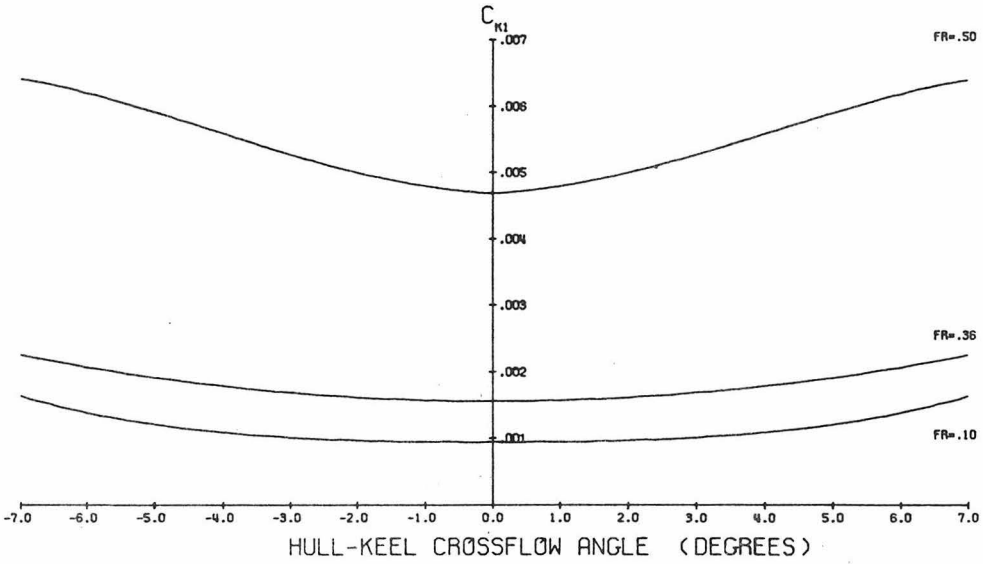


Figure A.2. Antiope Resistance Coefficient $C_{K1}(Fr, \alpha_K)$

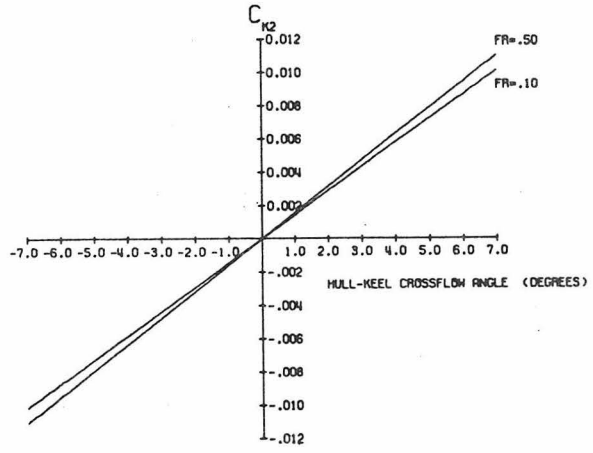


Figure A.3. Antiope Sideforce Coefficient $C_{K2}(Fr, \alpha_K)$

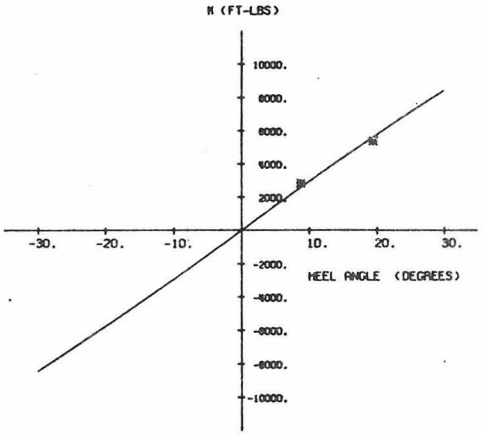


Figure A.4. Antiope Righting Moment

$$\left.\begin{aligned} mg &= 5650 \text{ lbs} = 2563 \text{ kgf} \\ \overline{GM} &= 2.98 \text{ ft} = 0.91 \text{ m} \\ \underline{r}_m &= \underline{0} \end{aligned}\right\} \qquad \text{A.9}$$

A.2 Hydrodynamic Inertial and Damping Coefficients

Several elements of the hydrodynamic inertial matrix H have been calculated or experimentally determined for sailing yachts. Gerritsma (1968) presents results of planar motion tests on a half ton model. Figures A.5 - A.8 show these data in nondimensional form. Froude Number dependence is clearly evident. These plots show the extrapolations and interpolations used in the numerical calculations.

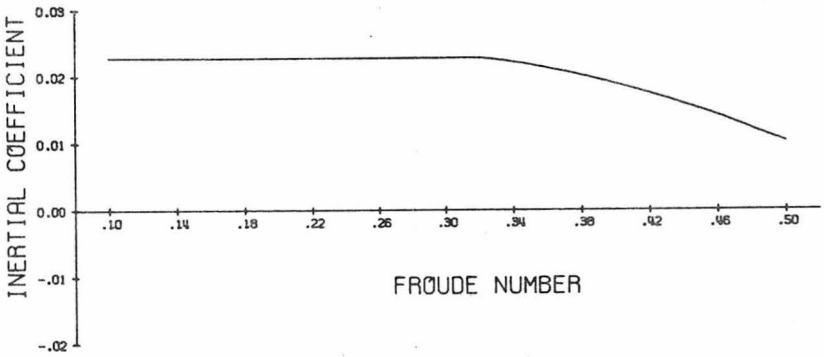


Figure A.5. Hydrodynamic Inertial Coefficient $h_{22}(Fr)$

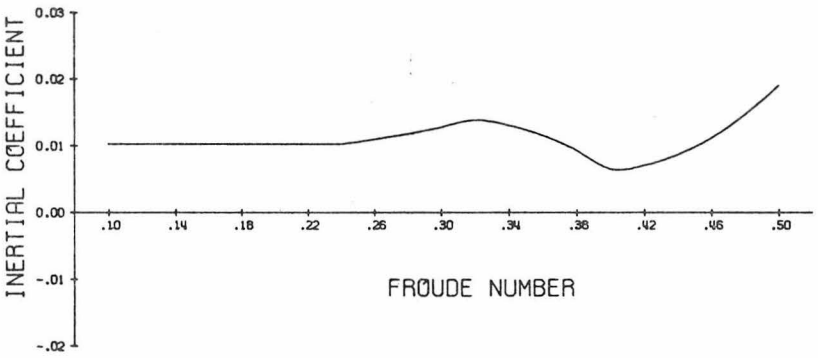


Figure A.6. Hydrodynamic Inertial Coefficient $h_{26}(Fr)$

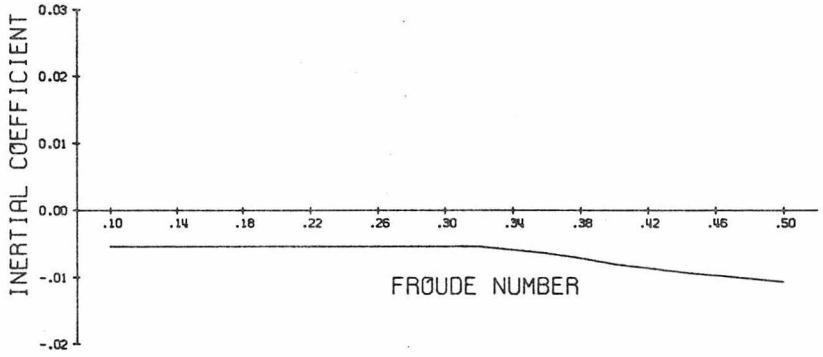


Figure A.7. Hydrodynamic Inertial Coefficient $h_{62}(Fr)$

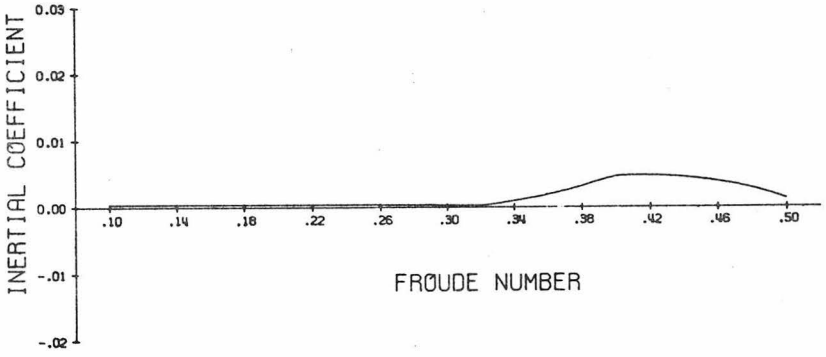


Figure A.8. Hydrodynamic Inertial Coefficient $h_{66}(Fr)$

To fill out the diagonal terms of H, the following rough estimates were used:

$$\left.\begin{aligned} h_{11} &= m \\ h_{33} &= 1.8m \\ h_{44} &= 0.2I_{11} \\ h_{55} &= 0.7I_{22} \end{aligned}\right\} \qquad (A.10)$$

Vugts (1968) gives the results of forced oscillation tests on cylinders in a free surface without forward speed. These tests show that some elements of H and the wave damping coefficients have a strong dependence on oscillation frequency. These data were used to provide the estimates of h_{44} and $\frac{\partial f_3^w}{\partial \dot{z}_3}$. It was assumed that $\frac{\partial f_5^w}{\partial \dot{z}_5}$ was of similar magnitude.

A.3 Rudder Data

Gerritsma (1968) gives the results of rudder sideforce and moment measurements from tests of a 1/5 scale, half ton yacht. The Froude Number for these tests was $.24 \leq Fr \leq .49$, and the Reynolds Number based on waterline length was ~1E+06. Gerritsma notes that due to scale effects these data may not be reliable. Assuming that the tests were made in the upright attitude with no leeway, i.e.,

$$\varphi = \theta = \psi = 0 \quad , \qquad (A.11)$$

the sideforce coefficient is identical with the conventional lift coefficient, and $\alpha_R = \delta_R$. Correcting the method of nondimensionalization, the sideforce coefficient is

$$C_{R2} = \left(\frac{L_S}{L}\right)^2 C_L \quad , \tag{A.12}$$

where for the half ton model

L_S = 2.62 ft = 0.80 m (distance between quarter chords)

L = 4.59 ft = 1.40 m

Figure A.9 shows the sideforce coefficients based on the half ton model. The calculations in Chapters IV, V and VI used a bicubic polynomial to interpolate these data. At low speeds, i.e., Fr $\leq$ .24, the sideforce was assumed to be constant.

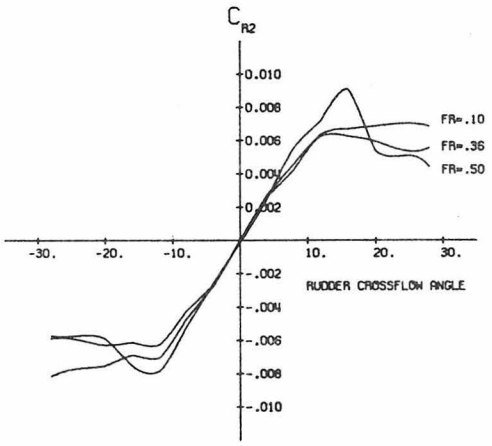


Figure A.9. Rudder Sideforce Data from Half Ton Model $C_{R2}(Fr, \alpha_R)$

Gerritsma and Moeyes (1973) present turning moment data from tests of the two 12-meter yachts Columbia and Valiant. These data were used in the calculations by assuming

$$C_{R2} = \frac{M_3}{\left(\frac{\rho_w g}{2}\right) Fr^2 L^4 r_1^R} \qquad (A.13)$$

with

$$Fr = .2$$

$$L = 45.5 \text{ ft} = 13.9 \text{ m}$$

$$r_1^R = .25$$

These data are replotted in Figure A.10. A cubic polynomial was used to interpolate the data for various α_R, and the coefficients

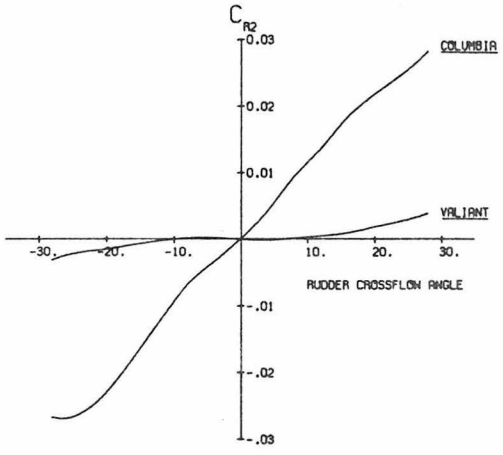


Figure A.10. Rudder Sideforce Data from Valiant and Columbia Models $C_{R2}(\alpha_R)$

were taken to be independent of Froude Number. Gerritsma and Moeyes discuss the unusual behavior of Valiant:

> The turning moment on the "Valiant" however, is not only much smaller but is also strongly non-linear,.... Due to flow separation at the blunt afterbody, the small rudder acts fully in the wake of the ship. At small rudder angles almost no turning moment is produced. Even a turning moment in the wrong direction has been observed, both in the towing tank and in practice. The width of the loop is about 25 degrees. If the helmsman of "Valiant" gives a rudder angle smaller than about 10 degrees, the ship could turn towards the opposite direction than it is supposed to do. During standard yacht performance tests in Delft, the same flow separation phenomena have been observed on several modern ocean racers with very full after-bodies.

A.4 Sail Data

Experimental data on soft sails are scarce, especially for offwind conditions. Some wind tunnel data have been collected, e.g., Dayman (1953), but much of this has not received the appropriate corrections (Milgram 1972). Marchaj (1973) presents corrected data for a 1/5 scale, Finn sail. The tests included mast and boom, and the Reynolds Number was approximately 2E+05. Since the tests were made only in the upright condition, i.e.,

$$\varphi = \theta = 0 \ , \tag{A.14}$$

the force coefficients C_{S1} and C_{S2} are taken to be identical with the conventional lift and drag coefficients except for nondimensionalization. Thus

$$C_{S2} = S_A' C_L \tag{A.15}$$

where for the Finn

$$S_A' = \frac{S_A}{L^2} = .60 \qquad \text{(A. 16)}$$

Figures A. 11 and A. 12 show the resistance and sideforce coefficients for the Finn sail. Also plotted are the coefficients for the rigid Gottingen foil, whose camber distribution is typical of working sails (Marchaj 1964). These latter coefficients have been scaled such that the maximum resistance is identical with the Finn sail.

The sideforce coefficients for these two data sets are quite different. The soft Finn sail has a rounded peak occurring at about 35°, while the rigid foil has a sharp peak near 15°. At large angles of incidence both the resistance and sideforce curves for the Finn

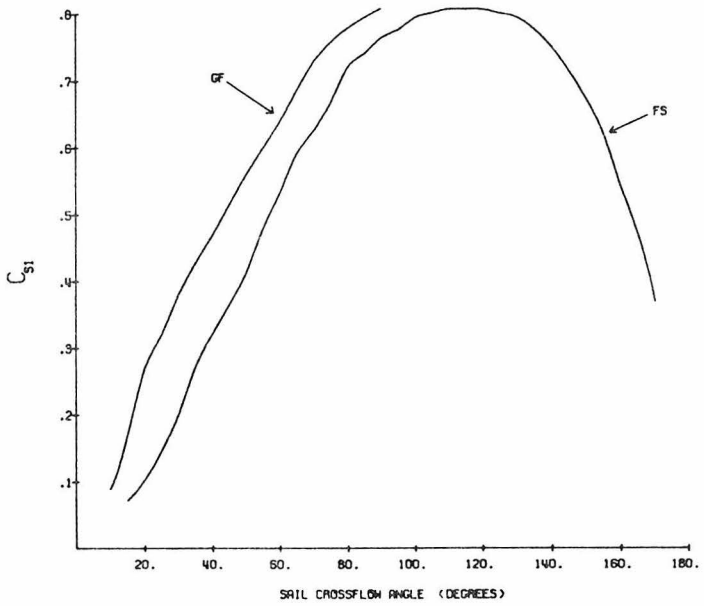


Figure A. 11. Aerodynamic Resistance Coefficients $C_{S1}(\alpha_S)$

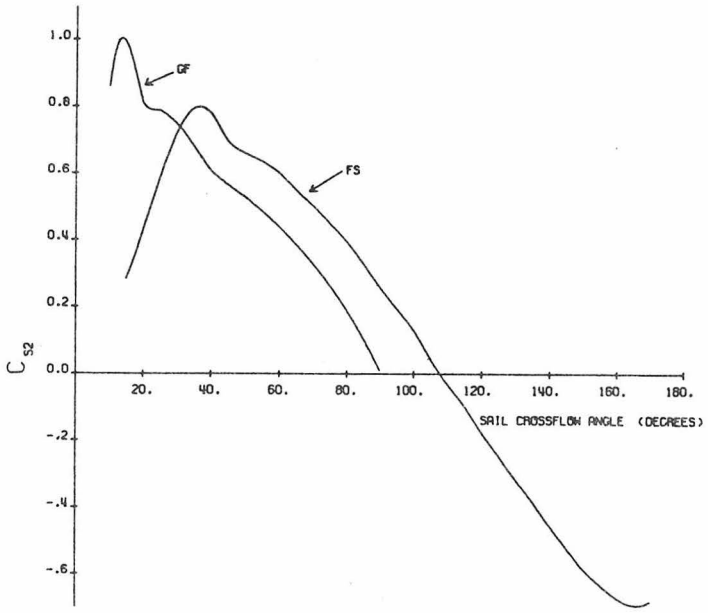


Figure A.12. Aerodynamic Sideforce Coefficients $C_{S2}(\alpha_S)$

sail are offset about 15°. The data for the Gottingen foil are similar to the NACA 0012 airfoil section (Critzos et al., 1955). Unfortunately, the airfoil data show hysteretic effects in regions of steep negative slopes. Tests should be made to determine if modern sails exhibit such characteristics, since this may have a strong effect on vessel dynamics.

A.5 Vessel Geometry

This appendix contains a summary of the geometric data used in the numerical calculations of Chapters IV, V and VI. The data presented here are not specific to any one vessel. They are intended to be typical of the class of light displacement keelboats.

Table A.2. Vessel Geometry

	Non-Dim.	Metric	English
1. Waterline Length	1.00	6.10 m	20.0 ft
2. Displacement (m′)			
a. Base Boat (DLR* ~ 150)			
Bare	2.97E-03	998. kgf	2200. lbf
Live Ballast	7.93E-03	272. kgf	600. lbf
Total	1.09E-02	1270. kgf	2800. lbf
b. Heavy Displacement (DLR ~ 360)			
Bare	2.30E-02	2631. kgf	5800. lbf
Live Ballast	2.64E-03	272. kgf	600. lbf
Total	2.56E-02	2903. kgf	6400. lbf
c. Ultra Light Displacement (DLR ~ 70)			
Bare	2.81E-03	318. kgf	700. lbf
Live Ballast	2.40E-03	272. kgf	600. lbf
Total	5.21E-03	590. kgf	1300. lbf

*$\text{DLR} = \frac{(\text{Displacement})}{(.01L)^3}$, Displacement in long tons, L in feet.

Table A.2. (Continued)

	Non-Dim.	Metric	English
3. Location of Center of Gravity (Bare)			
a. Distance aft of LWL-Stem intersection ($\underline{e}_1$):	.515	3.14 m	10.3 ft
b. Distance below LWL ($\underline{e}_3$):	.070	.43 m	1.4 ft
4. Coordinates of Live Ballast in $\mathfrak{F}_B$			
a. $\underline{e}_3$: All Sailing Conditions (Fr, $\forall$)	-.10	-.61 m	-2.0 ft
b. Running ($\beta_a \geq 160^\circ$)			
All speeds Fr $\in$ (.10,.50)			
$\underline{e}_1$:	-.15	-.91 m	-3.0 ft
$\underline{e}_2$:	.00	0.0 m	0.0 ft
c. Broad Reaching ($110^\circ \leq \beta_a < 160^\circ$)			
All speeds Fr $\in$ (.10,.50)			
$\underline{e}_1$:	-.15	-.91 m	-3.0 ft
$\underline{e}_2$:	.00	0.0 m	0.0 ft
d. Beam Reaching ($70^\circ \leq \beta_a < 110^\circ$)			
i. Low Speed Fr $\in$ (.10,.28)			
$\underline{e}_1$:	-.10	-.61 m	-2.0 ft
$\underline{e}_2$:	.00	0.0 m	0.0 ft

Table A.2. (Continued)

	Non-Dim.	Metric	English
ii. Moderate Speed Fr $\in$ (.30,.34)			
$\underline{e}_1$:	-.10	-.61 m	-2.0 ft
$\underline{e}_2$:	.00	0.0 m	0.0 ft
iii. High Speed Fr $\in$ (.36,.50)			
$\underline{e}_1$:	-.10	-.61 m	-2.0 ft
$\underline{e}_2$:	-.05	-.30 m	-1.0 ft
e. Close Reaching ($50^{\circ} \leq \beta_a < 70^{\circ}$)			
i. Low Speed Fr $\in$ (.10,.28)			
$\underline{e}_1$:	-.15	-.30 m	-1.0 ft
$\underline{e}_2$:	.00	0.0 m	0.0 ft
ii. Moderate Speed Fr $\in$ (.30,.24)			
$\underline{e}_1$:	-.15	-.30 m	-1.0 ft
$\underline{e}_2$:	.00	0.0 m	0.0 ft
iii. High Speed Fr $\in$ (.36,.50)			
$\underline{e}_1$:	-.05	-.30 m	-1.0 ft
$\underline{e}_2$:	.00	0.0 m	0.0 ft

Table A.2. (Continued)

	Non-Dim.	Metric	English
f. Beating ($\beta_a < 50^o$)			
i. Low Speed Fr $\in$ (.10,.28)			
$\underline{e}_1$:	.00	0.0 m	0.0 ft
$\underline{e}_2$:	.00	0.0 m	0.0 ft
ii. Moderate Speed Fr $\in$ (.30,.34)			
$\underline{e}_1$:	.00	0.0 m	0.0 ft
$\underline{e}_2$:	-.05	-.30 m	-1.0 ft
iii. High Speed Fr $\in$ (.36,.50)			
$\underline{e}_1$:	.00	0.0 m	0.0 ft
$\underline{e}_2$:	-.15	-.91 m	-3.0 ft
5. Moments and Products of Inertia			
I_{11}	1.22E-04	54. kgf-m-sec^2	390. slug-ft^2
I_{22}	4.71E-04	207. kgf-m-sec^2	1500. slug-ft^2
I_{33}	4.08E-04	180. kgf-m-sec^2	1300. slug-ft^2
I_{13}	-4.08E-05	-18. kgf-m-sec^2	-130. slug-ft^2
6. Metacentric Heights			
Transverse ($\overline{GM}$)	.125	.76 m	2.5 ft
Longitudinal ($\overline{GM_L}$)	1.400	8.53 m	28.0 ft

Table A.2. (Continued)

	Non-Dim.	Metric	English
7. Hull-Keel Geometry			
Projected Lateral Area	8.12E-02	3.02 m^2	32.5 ft^2
Aspect Ratio (Geometric)	1.2		
Draft	.212	1.28 m	4.2 ft
Wetted Area	.25	9.29 m^2	100. ft^2
Force Center ($\underline{r}_K$)			
$\underline{e}_1$:	.10	.61 m	2.0 ft
$\underline{e}_2$:	.00	.00 m	0.0 ft
$\underline{e}_3$:	.075	.46 m	1.5 ft
Waterplane Area	.162	6.04 m^2	65. ft^2
Center of Flotation ($\underline{r}_f$)			
$\underline{e}_1$:	-.01	-.06 m	-0.2 ft
$\underline{e}_2$:	.00	.00 m	0.0 ft
$\underline{e}_3$:	-.07	-.43 m	-1.4 ft
8. Rudder Geometry			
Projected Lateral Area	1.05E-02	.39 m^2	4.2 ft^2
Aspect Ratio (Geometric)	1.70		

Table A.2. (Continued)

	Non-Dim.	Metric	English
Force Center ($\underline{r}_R$)			
$\underline{e}_1$:	-4.35E-01	-2.65 m	-8.7 ft
$\underline{e}_2$:	.00	.00 m	0.0 ft
$\underline{e}_3$:	1.25E-02	.08 m	0.25 ft
9. Sail Inventory			
a. Running ($\beta_a \geq 160^\circ$)			
Sail Area	1.5	55.7 m^2	600. ft^2
Force Center ($\underline{r}_s$)			
$\underline{e}_1$:	.36	2.19 m	7.2 ft
$\underline{e}_2$:	.015	.09 m	0.3 ft
$\underline{e}_3$:	-.80	-4.88 m	-16.0 ft
b. Broad Reaching ($110^\circ \leq \beta_a < 160^\circ$)			
Sail Area	1.5	55.7 m^2	600. ft^2
Force Center ($\underline{r}_s$)			
$\underline{e}_1$:	.36	2.19 m	7.2 ft
$\underline{e}_2$:	.015	.09 m	0.3 ft
$\underline{e}_3$:	-.80	-4.88 m	-16.0 ft

Table A.2. (Concluded)

	Non-Dim.	Metric	English
c. Beam Reaching ($70^\circ \leq \beta_a < 110^\circ$)			
Sail Area	1.5	55.7 m^2	600. ft^2
Force Center ($\underline{r}_s$)			
$\underline{e}_1$:	.36	2.19 m	7.2 ft
$\underline{e}_2$:	.10	.61 m	2.0 ft
$\underline{e}_3$:	-.80	-4.99 m	-16.0 ft
d. Close Reaching ($50^\circ \leq \beta_a < 70^\circ$)			
Sail Area	1.3	48.3 m^2	520. ft^2
Force Center ($\underline{r}_s$)			
$\underline{e}_1$:	.25	1.52 m	5.0 ft
$\underline{e}_2$:	.10	.61 m	2.0 ft
$\underline{e}_3$:	-.80	-4.88 m	-16.0 ft
e. Beating ($\beta_a < 50^\circ$)			
Sail Area	.575	21.4 m^2	230. ft^2
Force Center ($\underline{r}_s$)			
$\underline{e}_1$:	.165	1.01 m	3.3 ft
$\underline{e}_2$:	.075	.46 m	1.5 ft
$\underline{e}_3$:	-.655	3.99 m	-13.1 ft

APPENDIX B

RESULTS OF STEADY STATE SAILING OBSERVATIONS

This appendix summarizes the full scale sailing observations, which were used in Chapter V, and presents some additional detailed comparisons with numerical solutions. There is a scarcity of published full scale data on sailing vessels. Much of this is due to the difficulty and expense of accurately measuring the motions of a vessel in the marine environment. However, the recent work summarized here should at least provide a "gross characterization of sailing performance" (Kerwin et al., 1974). This is consistent with the level of sophistication of the numerical results reported in Chapter V.

It is difficult to establish and maintain steady state conditions in the marine environment. Experimental quantities, e.g., V_T, usually show some random fluctuations. The vessel complicates this situation with its dynamic response. The data reported here result from various time averaging schemes.* In addition many of these measurements were taken in waves of significant height.

Table B.1 lists the gross parameters of the four vessels studied here; details are available in the references.

---

*In keeping with the topic of this study, the scheme of Kerwin et al., (1974) should be noted: "Navigators were requested to make frequent entries describing all stable sailing conditions encountered...."

Table B.1. Comparative Vessel Data

	BAYBEA	GIMCRACK	STANDFAST	YEOMAN
Type	Offshore	~6 meter	Offshore	5.5 meter
Length (L = LWL):				
m	11.5	7.25	10.0	7.72
ft	37.6	23.8	32.9	25.3
Displacement:				
m'	1.52E-02	1.52E-02	2.42E-02	
DLR	220	220	350	
kg_f	11,720.	2,976.	12,498.	
lbs	25,837.	6,560.	27,553	
Reference:	Kerwin et al. (1974)	Davidson (1936) and Marchaj (1964)	Gerritsma et al. (1975)	Marchaj (1964)

The table indicates a substantial difference in the nondimensional mass for Standfast, and there are other nondimensional parameters not listed which show significant differences, e.g., S_A'. The difference in these nondimensional parameters and the sailing abilities of the crew, i.e., steering and sail trim, have a very strong influence on the individual data points. Much of the scatter in the data is attributed to these factors.

Tables B.2 - B.6 are detailed comparisons between the numerical solutions and the full scale data for various points of sail. The leeway angles for Baybea and Standfast were not

measured but are the result of calculations based on a steady state analysis of sailing vessels (Kerwin 1975). There is a slight difference in heel angles, since this study uses the Eulerian angle definition. Table B.7 is a comparison with the optimum windward solutions calculated by Letcher (1976b) using the same Antiope data.

Table B.2. Comparative Data - Running

	Baybea	Standfast	Base Boat Finn Sail	Baybea	Standfast	Base Boat Finn Sail
Froude Number (Fr)	.26	.24	.26	.34	.34	.34
Sailing Angle ($\lvert\gamma\rvert^{o}$)	0.0	0.	0.0	5.6	3.	0.0
True Wind Speed (V_T)	2.13	2.06	1.69	2.27	2.26	1.79
Heel Angle (φ^{o})	0.0	1.	-1.1	1.0	3.	-2.5
Helm Angle (δ_R^{o})	——	-2.	-0.4	——	-2.	-0.5
Leeway Angle (λ^{o})	0.0	0.0	0.3	0.2	0.2	0.4
Apparent Wind Angle (β_a^{o})	180.0	180.	180.	170.0	175.	180.0
Apparent Wind Speed (V_a)	1.13	1.09	0.69	1.29	1.26	0.79

Table B.3. Comparative Data - Broad Reaching

	Baybea	Standfast		Base Boat: Gott. Foil	Base Boat: Finn Sail	Base Boat: Heavy Disp.
Froude Number (Fr)	.38	.41	.39	.40	.40	.38
Sailing Angle ($\|\gamma\|^{o}$)	30.8	27.	35.	30.	30.	30.
True Wind Speed (V_T)	1.74	2.38	2.03	1.68	1.72	1.57
Heel Angle (φ^{o})	3.0	2.0	6.	1.8	1.9	0.4
Helm Angle ($\delta_R{}^{o}$)	—	-1.	-5.	0.0	-0.9	-0.5
Leeway Angle (λ^{o})	0.4	0.3	0.0	-0.1	-0.6	0.0
Apparent Wind Angle ($\beta_a{}^{o}$)	119.3	137.	119.	118.5	119.6	114.7
Apparent Wind Speed (V_a)	1.03	1.56	1.33	0.96	0.99	0.87

Table B.4. Comparative Data - Beam Reaching

	Baybea		Standfast		Base Boat: Gott. Foil	Base Boat: Finn Sail	Base Boat: Heavy Disp.	Base Boat: Valiant Rud.
Froude Number (Fr)	.39	.40	.40	.41	.40	.40	.40	.40
Sailing Angle ($\|\gamma\|^{\circ}$)	45.9	45.9	55.	51.	50.	50.	50.	50.
True Wind Speed (V_T)	1.39	1.66	1.40	2.21	1.18	1.31	1.34	1.62
Heel Angle (φ°)	10.0	14.0	18.	7.	-5.8	1.0	1.5	3.6
Helm Angle ($\delta_R{}^{\circ}$)	—	—	-8.	-4.	0.8 (Lee)	0.3 (Lee)	-0.3	0.2 (Lee)
Leeway Angle (λ°)	1.3	1.6	1.0	0.4	0.8	0.7	0.2	1.5
Apparent Wind Angle ($\beta_a{}^{\circ}$)	88.2	97.5	80.	103.	75.1	81.1	82.2	92.0
Apparent Wind Speed (V_a)	1.00	1.20	1.16	1.76	0.94	1.02	1.03	1.24
Notes:								(Close Reach)

Table B.5. Comparative Data - Close Reaching

	Base Boat					
	Baybea	Standfast	Gott. Foil	Finn Sail	Heavy Disp.	Valiant Rud.
Froude Number (Fr)	.38	.38	.38	.38	.38	.38
Sailing Angle ($\|\gamma\|^{o}$)	91.4	93.	90.	90.	90.	90.
True Wind Speed (V_T)	1.14	2.18	1.12	1.17	2.21	2.20
Heel Angle (φ^{o})	10.0	22.	3.0	5.2	9.8	7.3
Helm Angle (δ_R^{o})	—	-10.	0.9 (Lee)	1.0 (Lee)	1.2 (Lee)	-0.2
Leeway Angle (λ^{o})	1.4	2.5	1.7	1.9	3.3	3.4
Apparent Wind Angle (β_a^{o})	48.1	63.	48.3	49.3	65.3	65.4
Apparent Wind Speed (V_a)	1.54	2.45	1.50	1.54	2.43	2.42
Notes:					(Beat)	(Beat)

Table B.6. Comparative Data - Beating

	Baybea	Gimcrack	Standfast (a)	Standfast (b)	Base Boat Gott. Foil	Base Boat Finn Sail	Base Boat Heavy Disp.	Base Boat Valiant Rud.
Froude Number (Fr)	.34	.34	.33	.35	.34	.34	.34	.34
Sailing Angle ($\|\gamma\|^{o}$)	140.9	137.5	139.	135.	140.	140.	140.	140.
True Wind Speed (V_T)	2.30	1.77	2.02	1.73	1.79	3.39	1.93	1.53
Heel Angle (φ^{o})	30.	20.	26.	20.	8.3	19.9	7.86	22.8
Helm Angle (δ_R^{o})	——	——	-10.	-8.	1.6	1.7	1.6	-6.3
Leeway Angle (λ^{o})	7.7	3.0	4.9	3.0	3.3	4.5	3.4	3.9
Apparent Wind Angle (β_a^{o})	27.5	27.6	27.	29.	25.7	29.9	26.4	23.0
Apparent Wind Speed (V_a)	3.14	2.56	2.86	2.52	2.63	4.21	2.77	2.38
Notes:		(λ estimated)			(Lee helm)	(Lee helm)	(Lee helm)	

Table B.7. Comparison with Optimum Windward Solutions

	Base Boat Gottingen Foil			Base Boat Finn Sail			Letcher (1976b)	
Froude Number (Fr)	.14	.18	.22	.14	.18	.22	<.24	
Sailing Angle (γ^{o})	130.	130.	130.	130.	130.	130.	130.8	132.3
True Wind Speed (V_T)	0.96	0.96	0.97	1.78	1.80	1.81	1.07	1.12
Heel Angle (φ^{o})	2.4	3.9	5.9	2.2	3.7	5.6		
Leeway Angle (λ^{o})	2.4	2.4	2.4	2.3	2.3	2.3		
Apparent Wind Angle (β_a^{o})	24.4	24.5	24.5	32.5	32.5	32.5		
Apparent Wind Speed (V_a)	1.77	1.78	1.79	2.54	2.56	2.56	1.88	1.94

APPENDIX C

EIGENVALUE PLOTS FOR BASE BOAT

This appendix contains a full set of eigenvalue plots for the Base Boat as indicated in Figure 5.1. The data in Figures 6.1, 6.3, 6.5 and 6.7 are reproduced here.

The calculated eigenvalues for fixed sailing angle are plotted in the form of root locus diagrams where Froude Number is the running variable. This is the lower plot in each case, and it shows one branch of the complex conjugate pairs of eigenvalues. For all plots the upper tail [max. $\Im m(\lambda_j)$] corresponds to low speed (Fr = .10), and speed increases moving down the curves.

Since the purely real eigenvalues show considerable variation with Fr, they are shown separately in the upper plot. In cases where the Roll Mode degenerates into two real modes, the solution is shown on both of these plots. Similarly, where real roots coalesce to form new complex modes, the upper plot shows the two traces combining into one.

The normal modes (e.g., Figure 6.2) are described by the modal elements at three speeds (Fr = .10, .36 and .50). The coefficients of the complex modes are plotted in polar form via the phase angle ν_{kj}. Real coefficients are plotted in a linear fashion to indicate polarity. The integers correspond to the modal element index k. Only modal coefficients with $b_{kj} \geq .10$ are plotted.

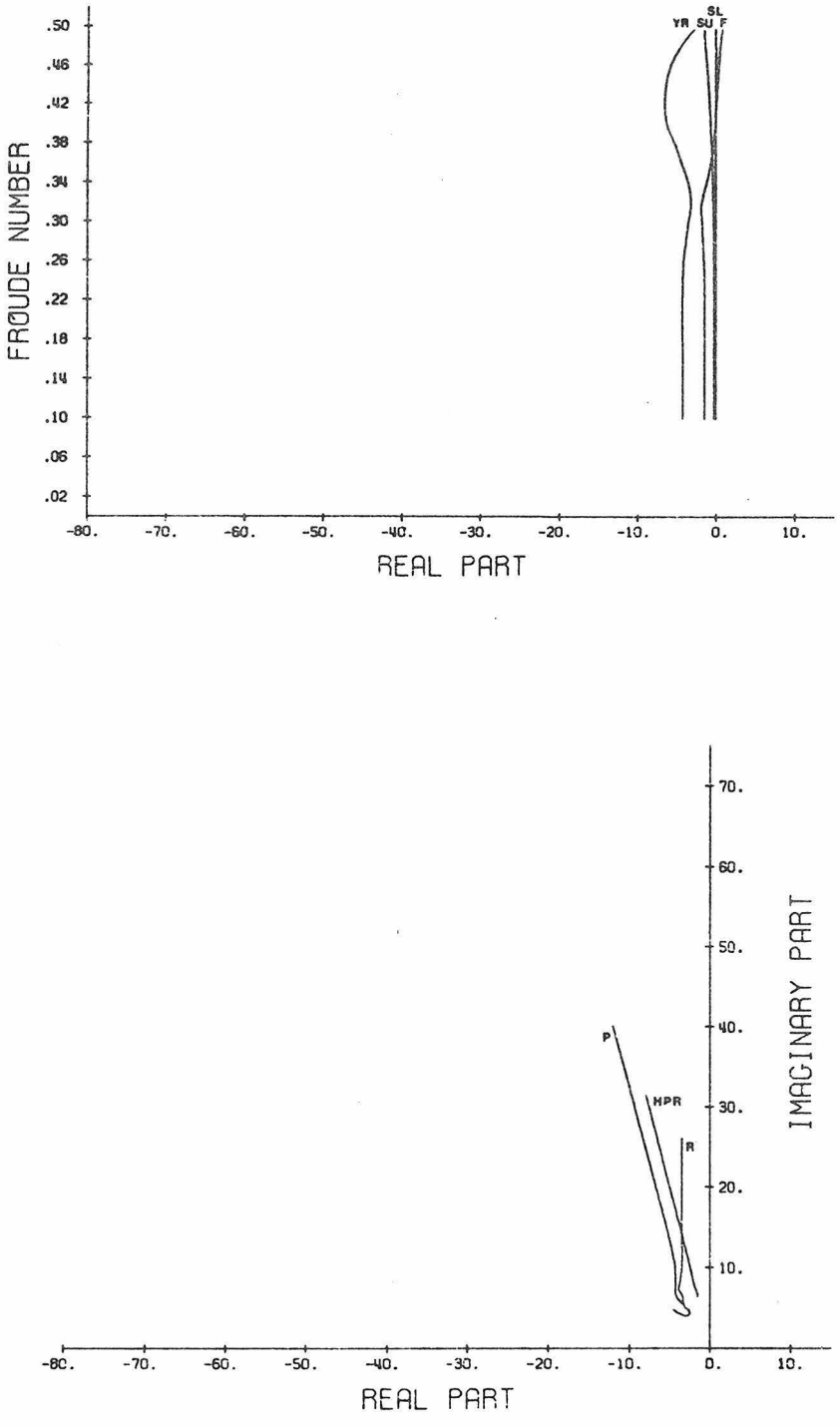
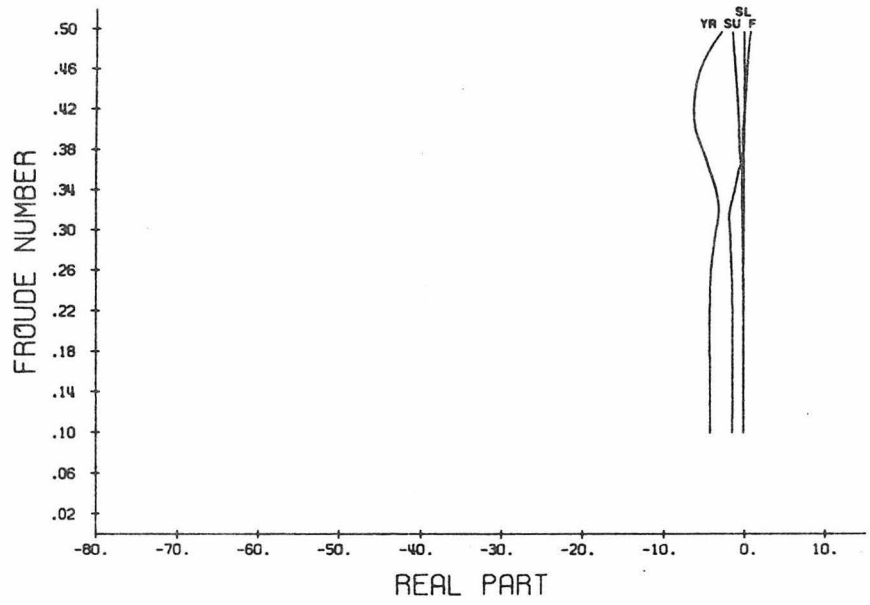


Figure C.1. $\gamma = 10^{o}$ (By-the-lee)



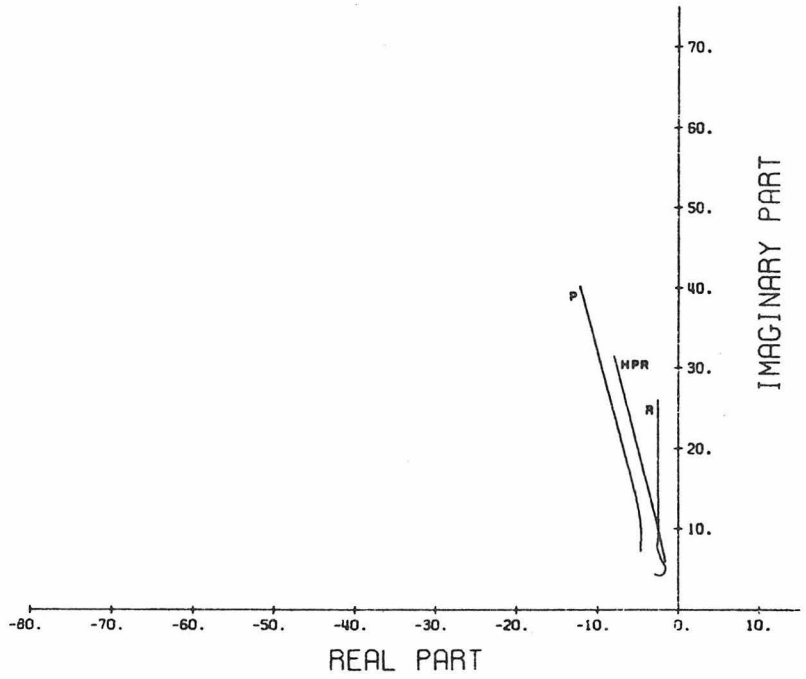


Figure C.2. $\gamma = 0^{o}$ (Run)

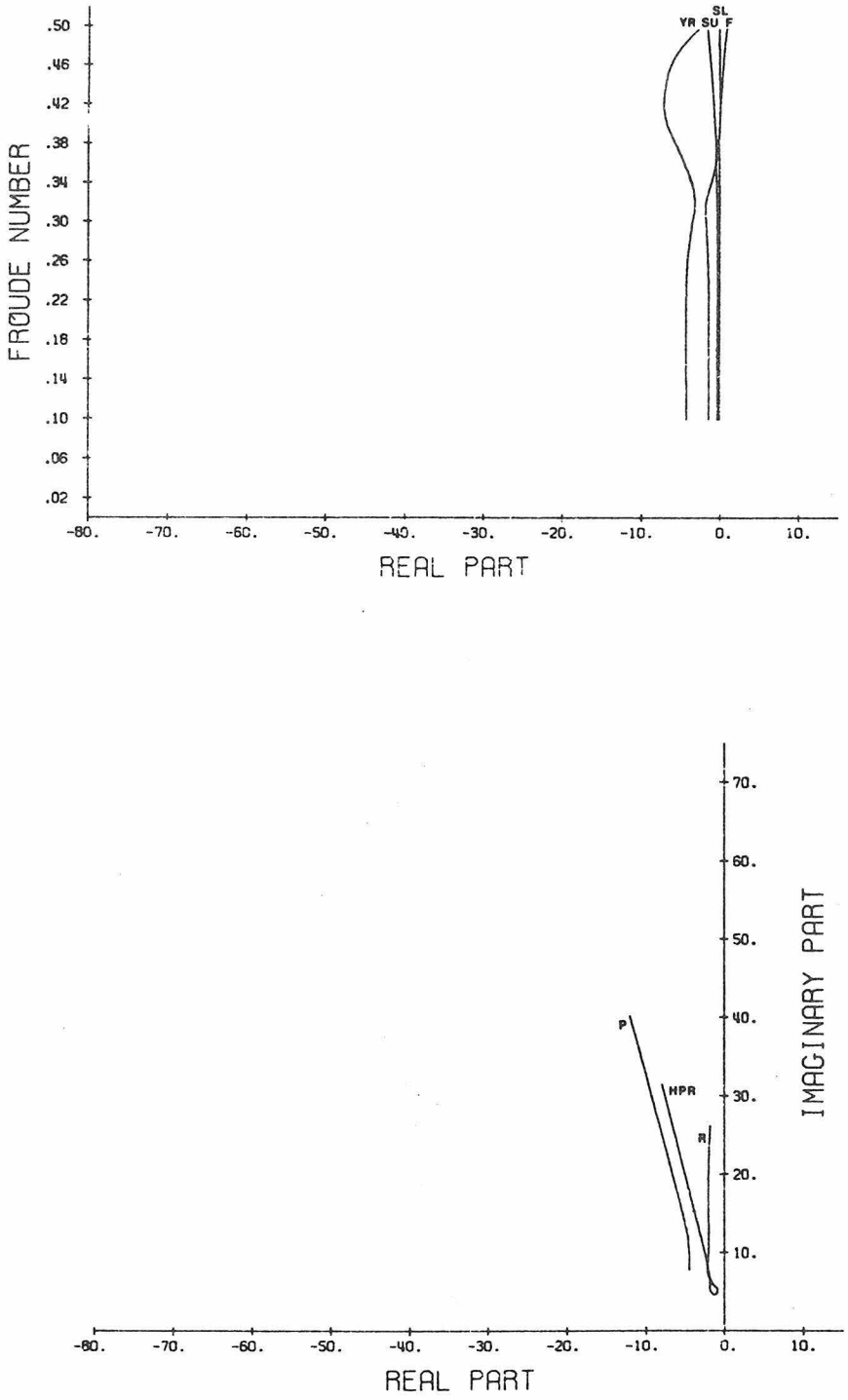
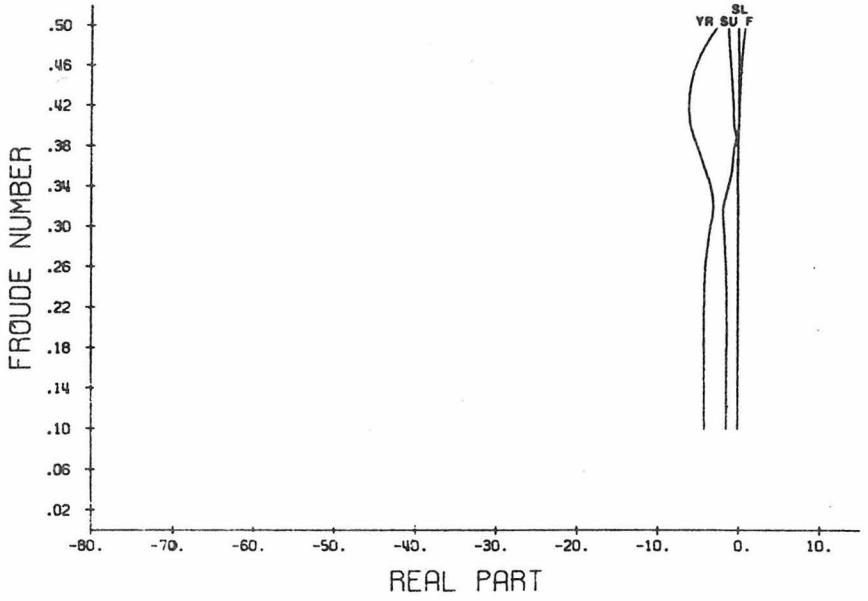


Figure C.3. $\gamma = -10^{o}$ (Run)



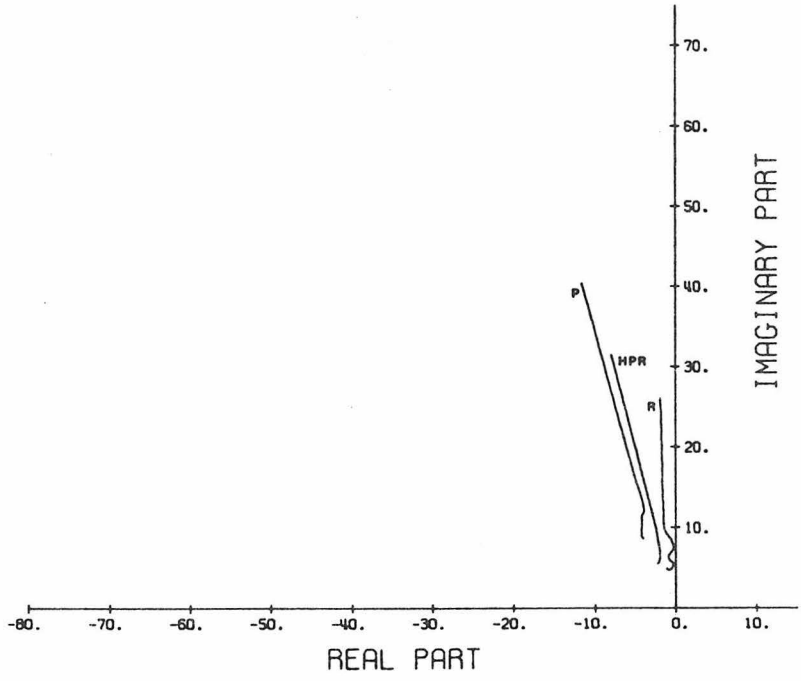


Figure C.4. $\gamma = -20^{o}$ (Broad Reach)

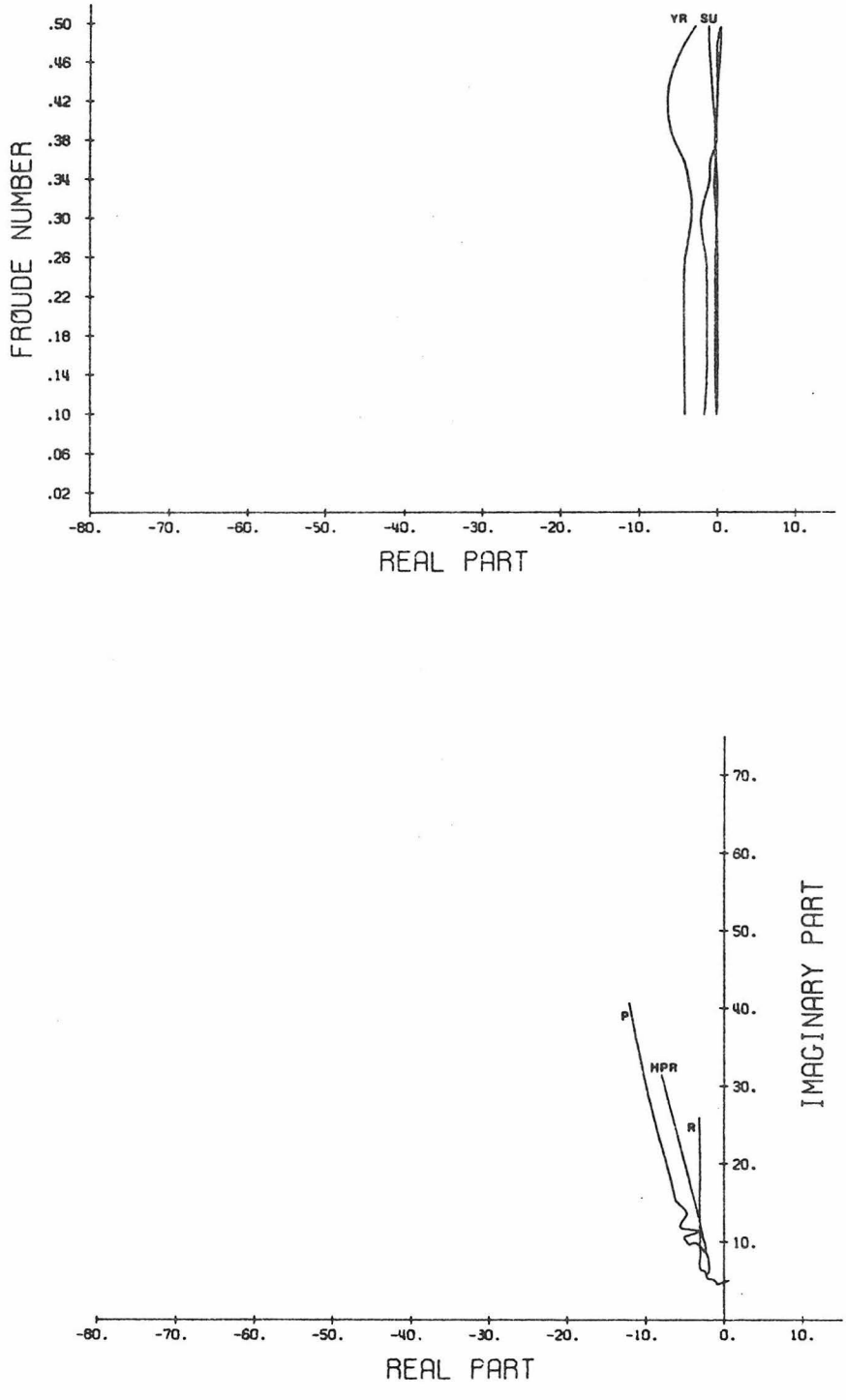
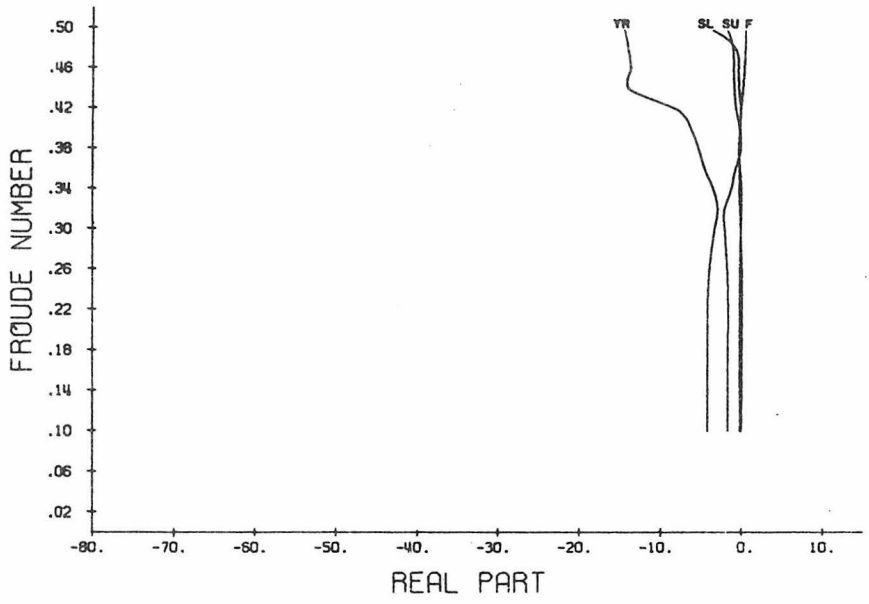


Figure C.5. $\gamma = -30^{o}$ (Broad Reach)



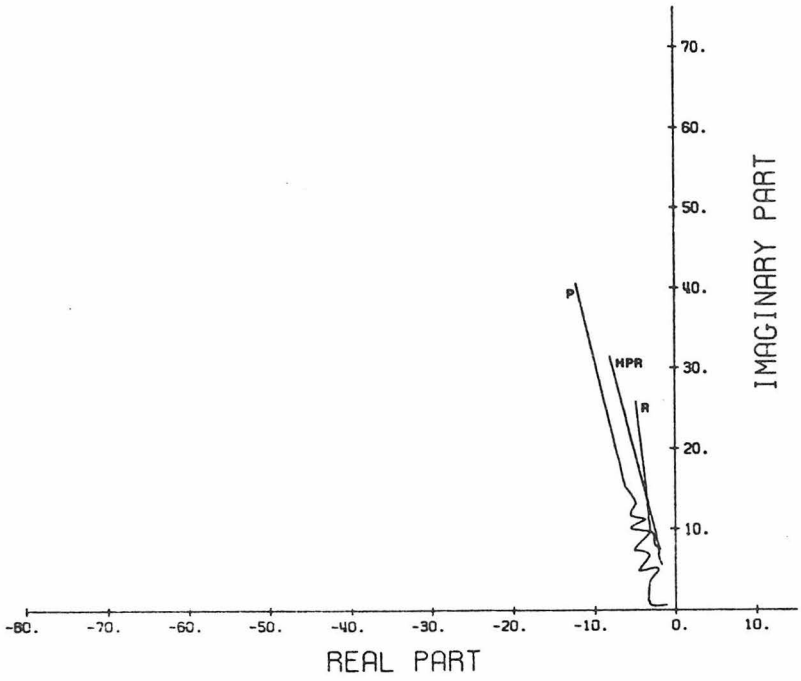


Figure C.6. $\gamma = -40^{o}$ (Beam-Broad Reach)

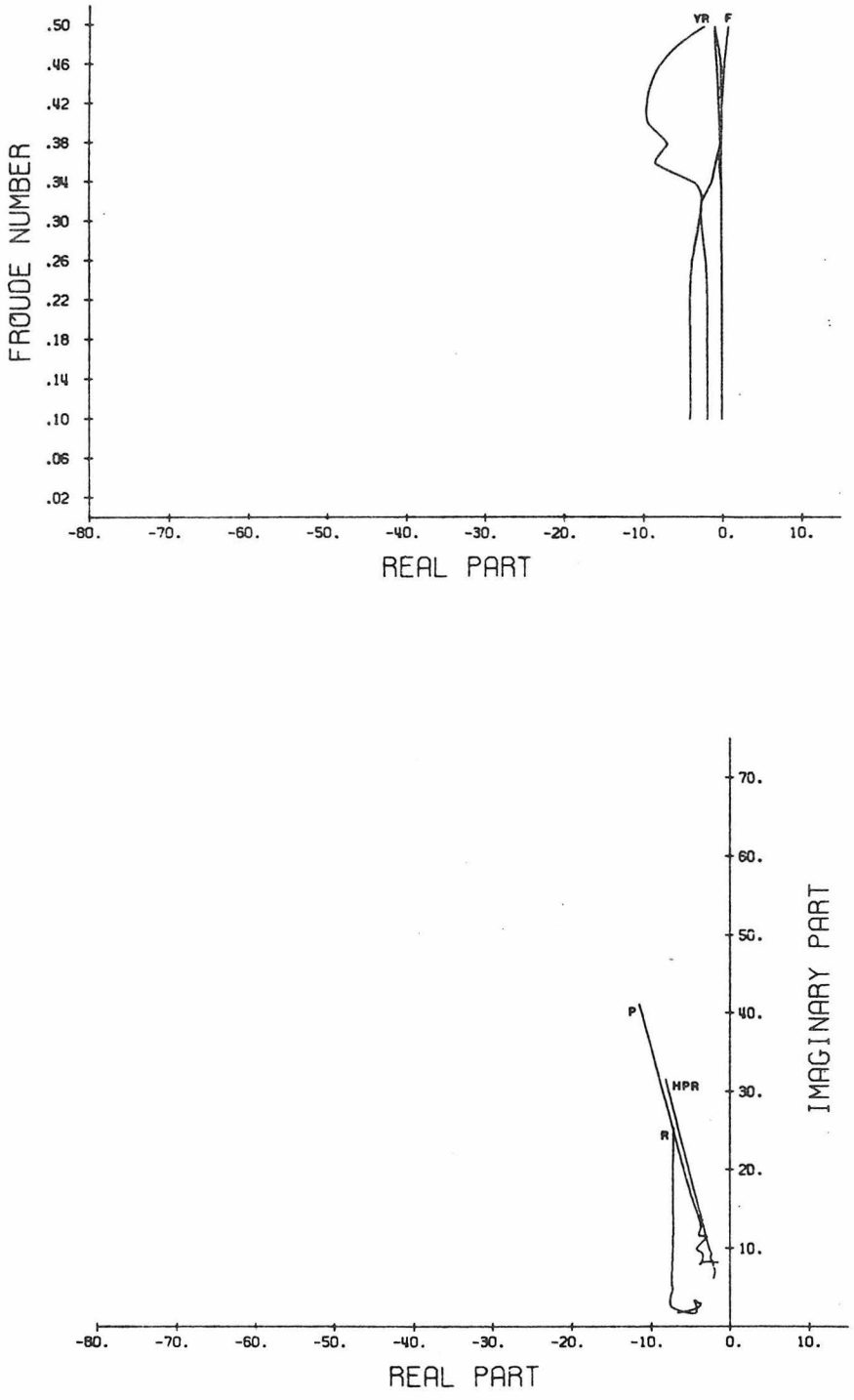


Figure C.7. $\gamma = -50^{o}$ (Close-Beam Reach)

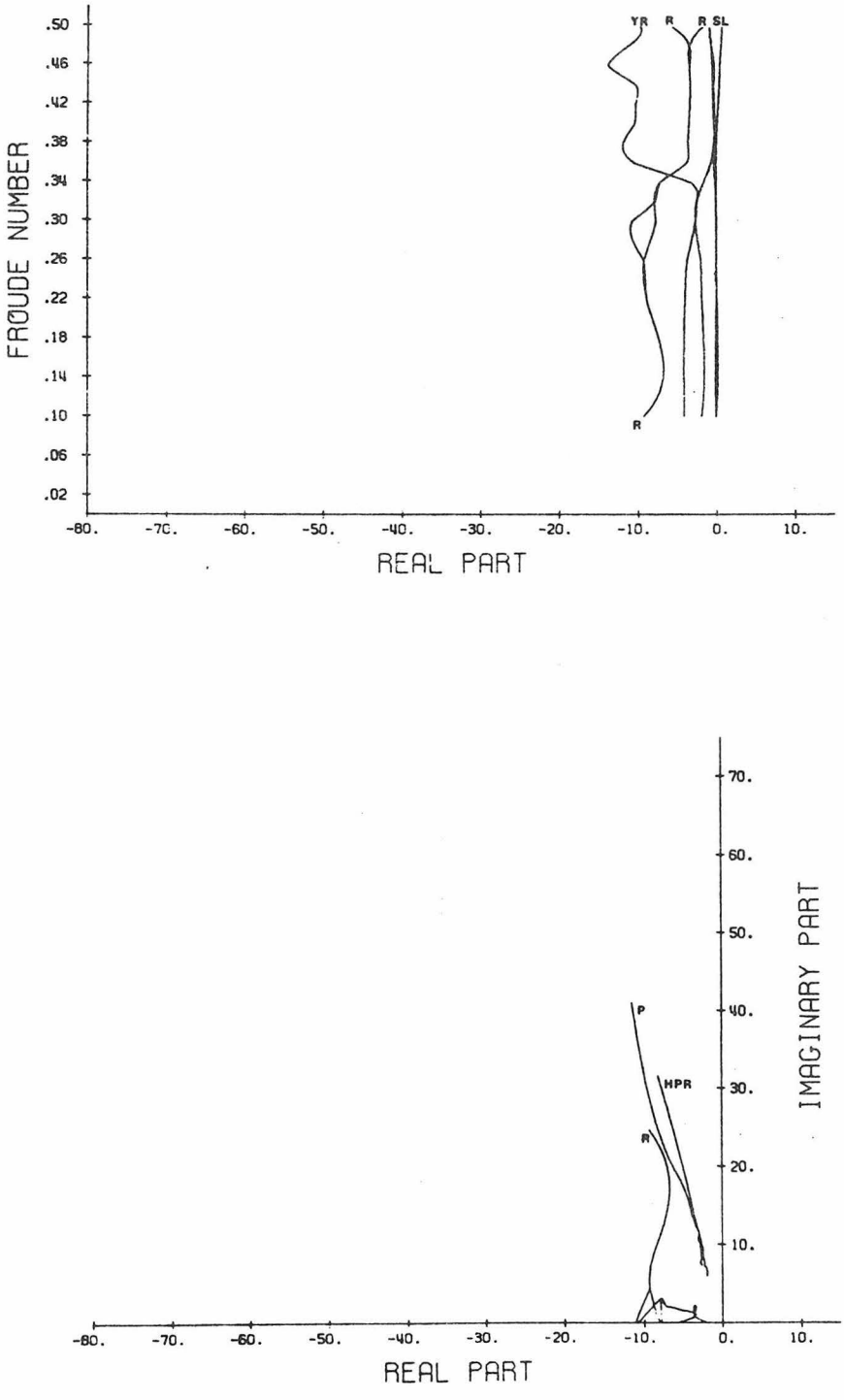


Figure C.8. $\gamma = -60^{\circ}$ (Close Reach)

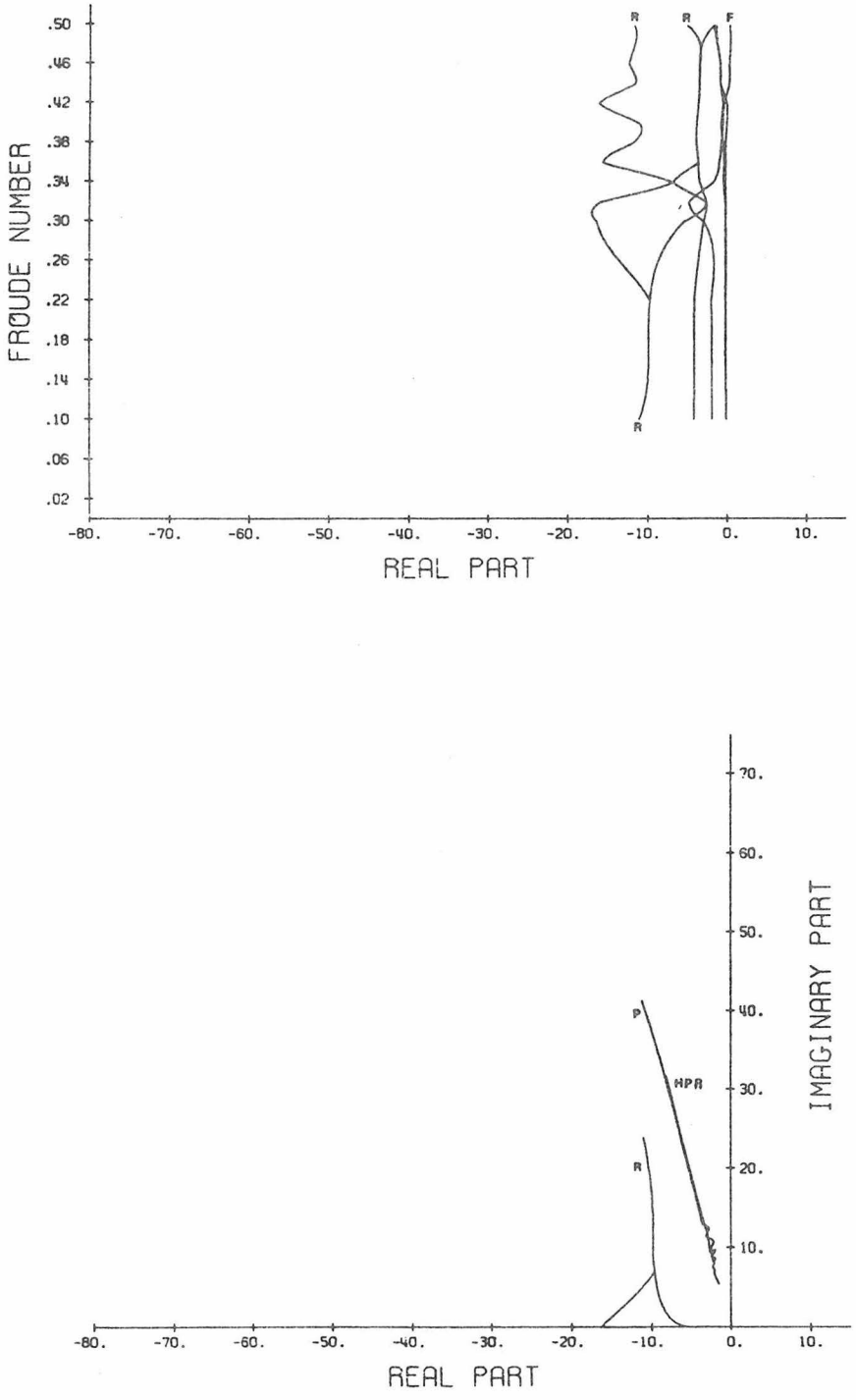


Figure C.9. $\gamma = -70^{o}$ (Close Reach)

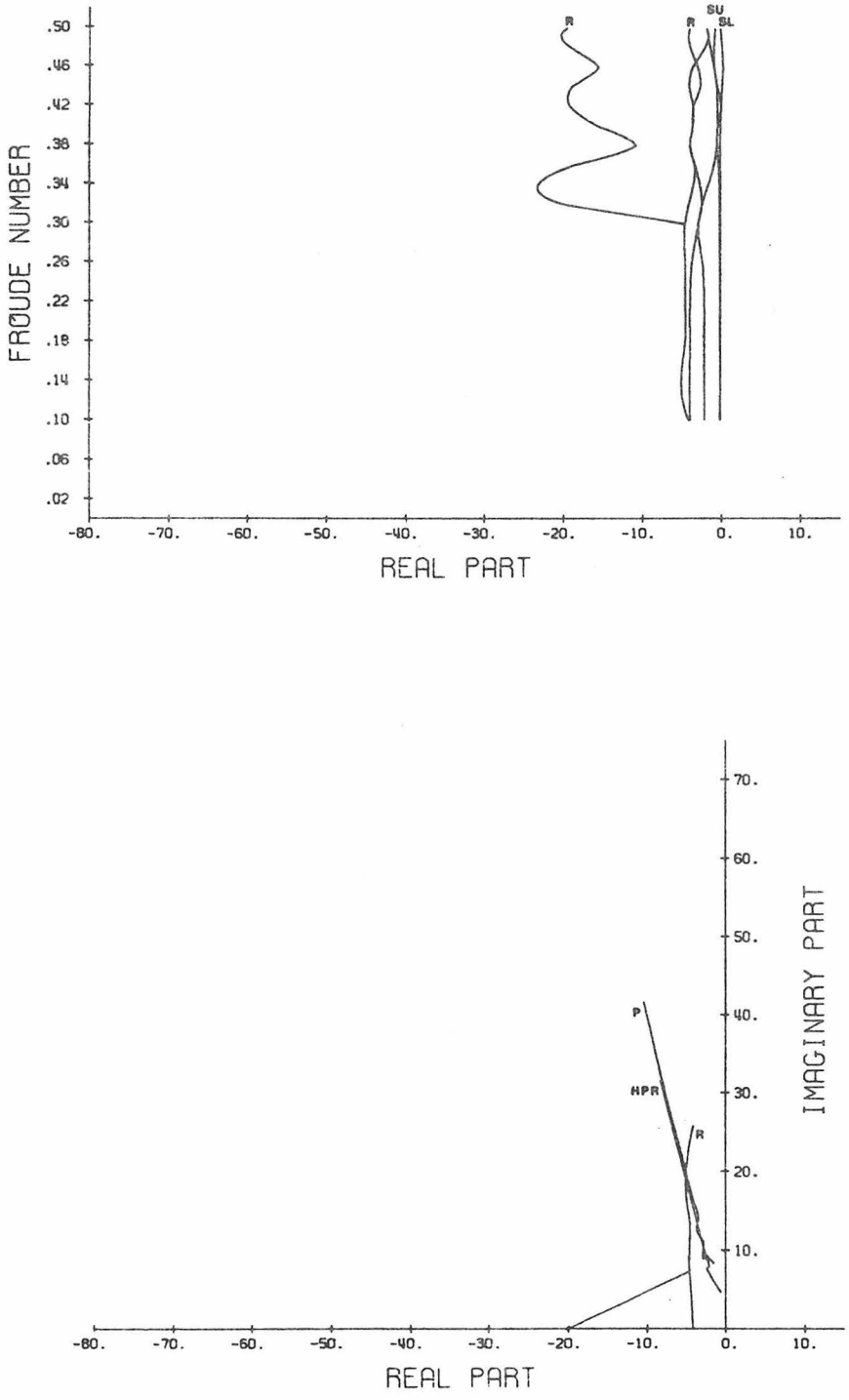


Figure C.10. $\gamma = -80^{o}$ (Beat-Close Reach)

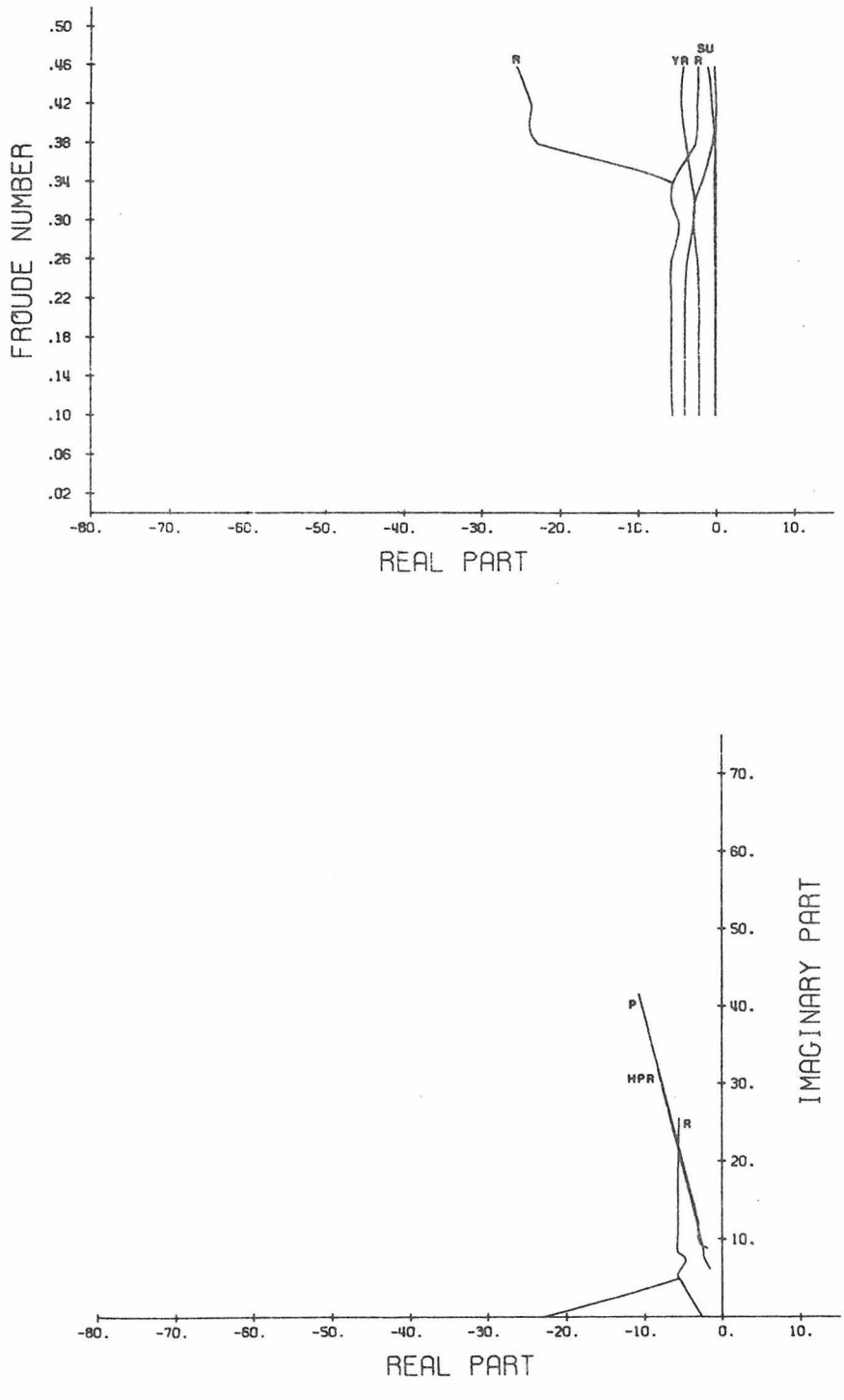
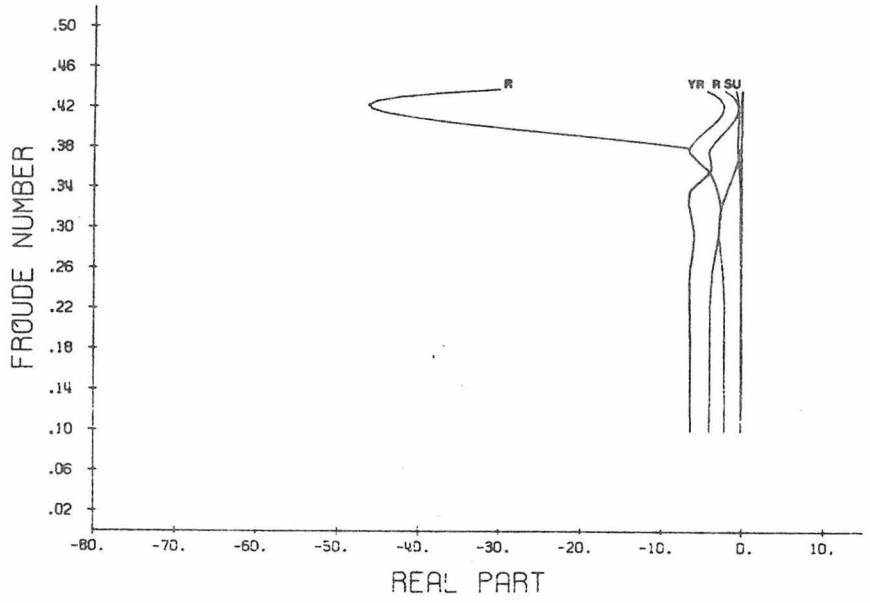


Figure C.11. $\gamma = -90^{o}$ (Beat-Close Reach)



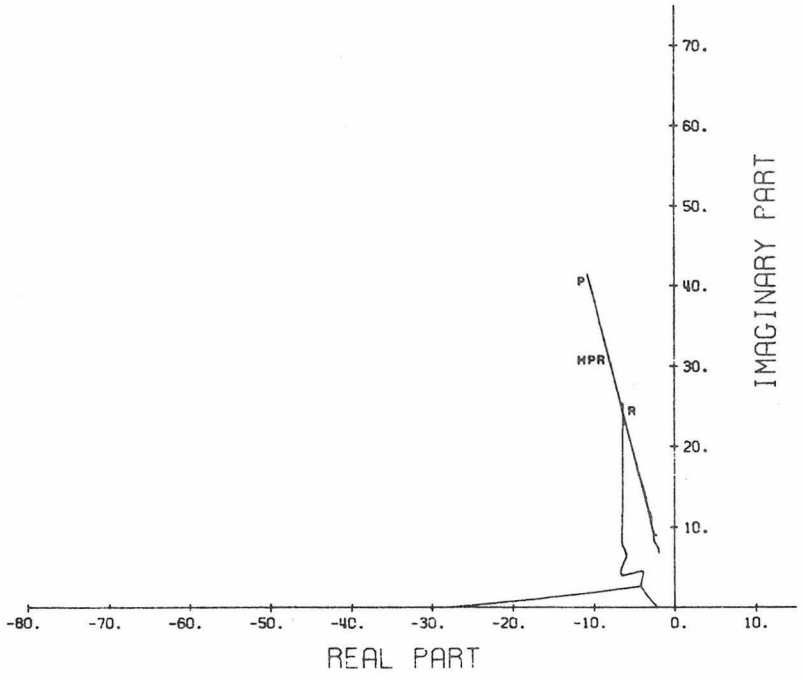


Figure C.12. $\gamma = -100^{o}$ (Beat)

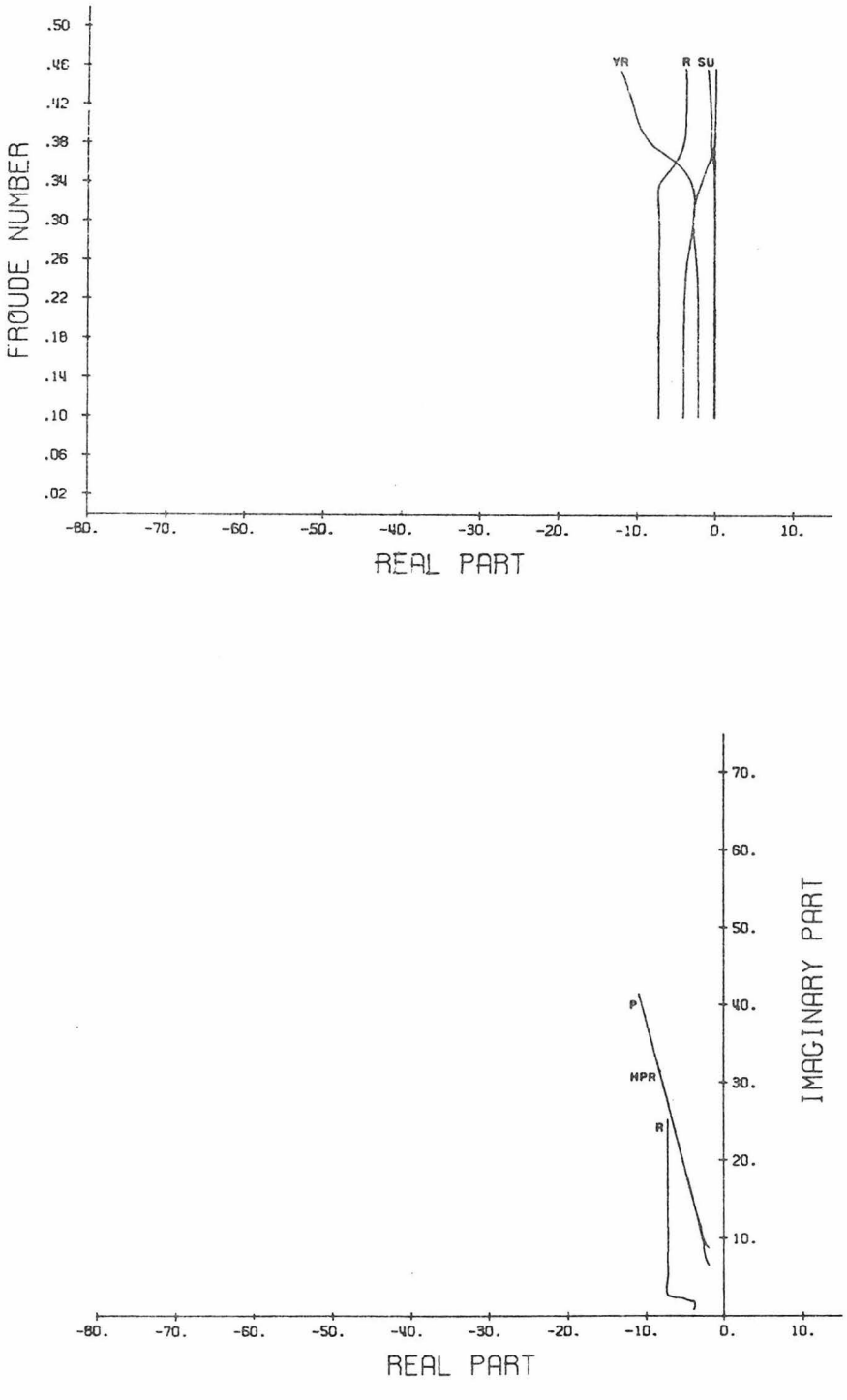
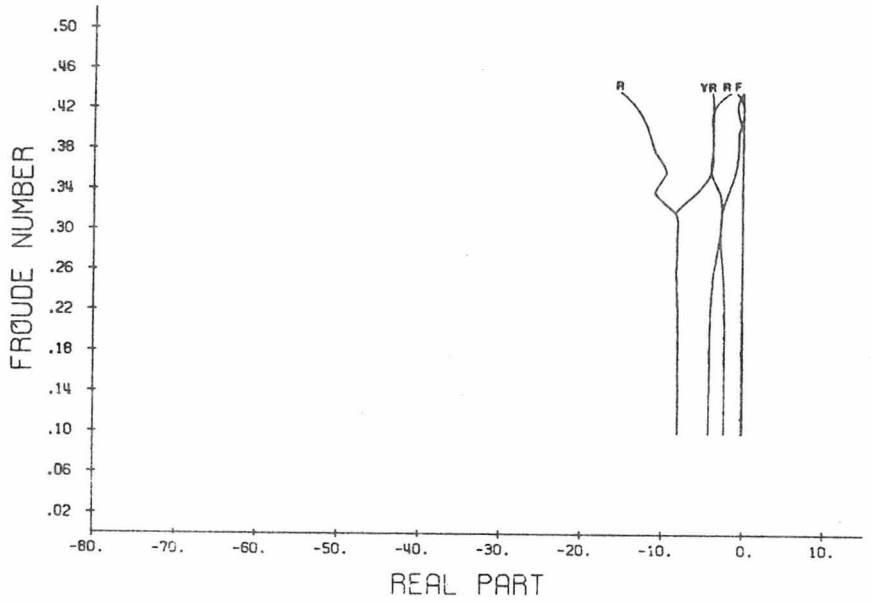


Figure C.13. $\gamma = -110^{\circ}$ (Beat)



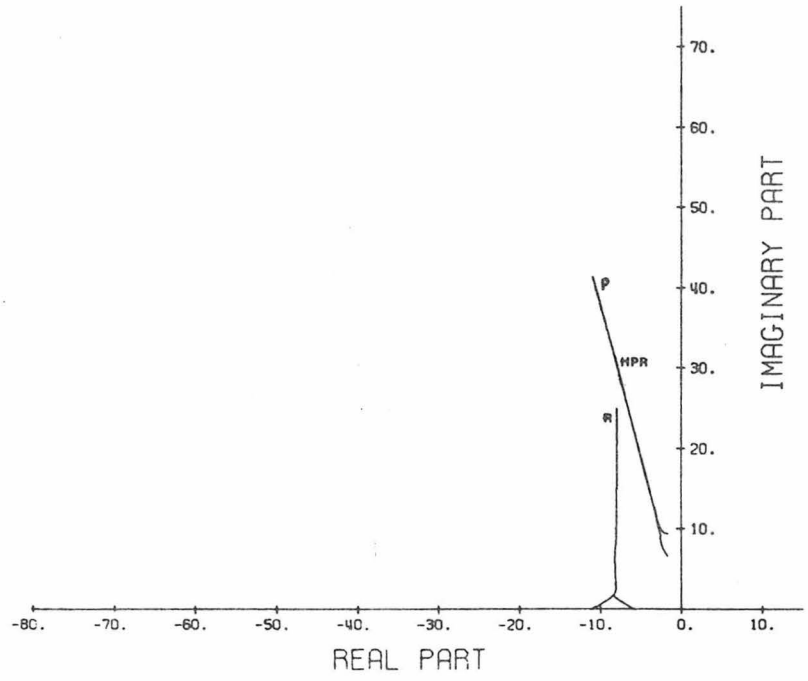


Figure C.14. $\gamma = -120^{o}$ (Beat)

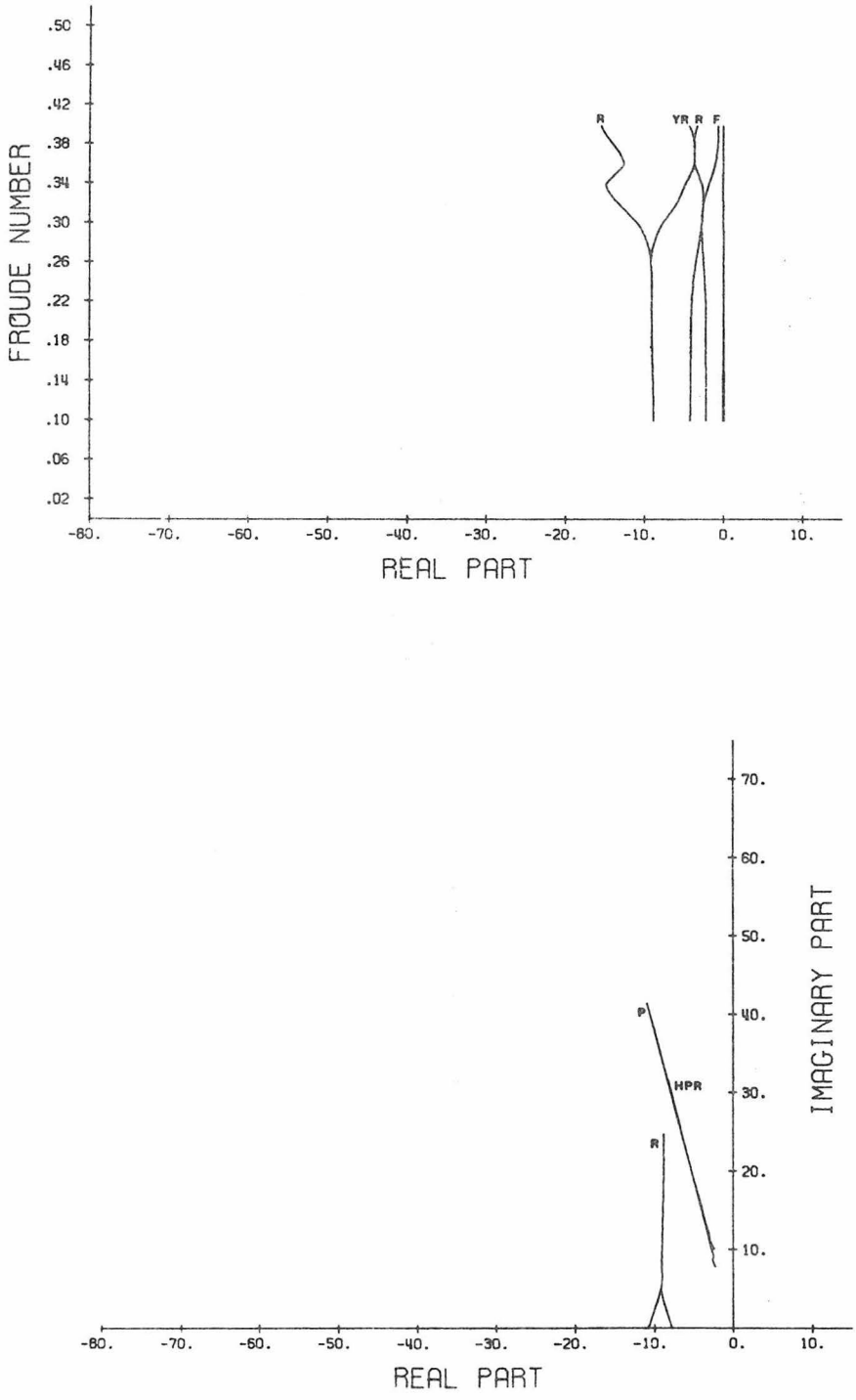


Figure C.15. $\gamma = -130^{\circ}$ (Beat)

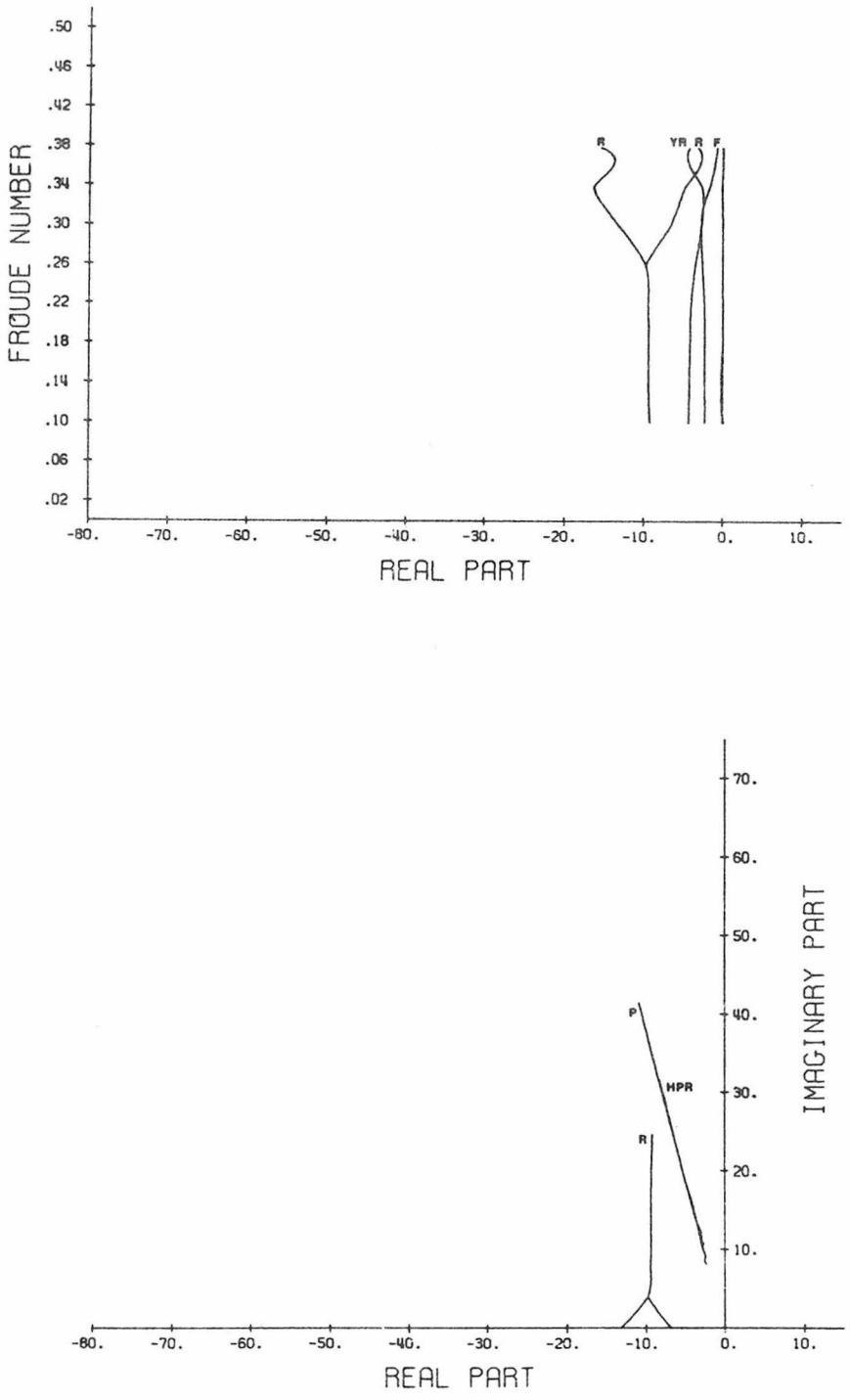


Figure C.16. $\gamma = -135^{o}$ (Beat)

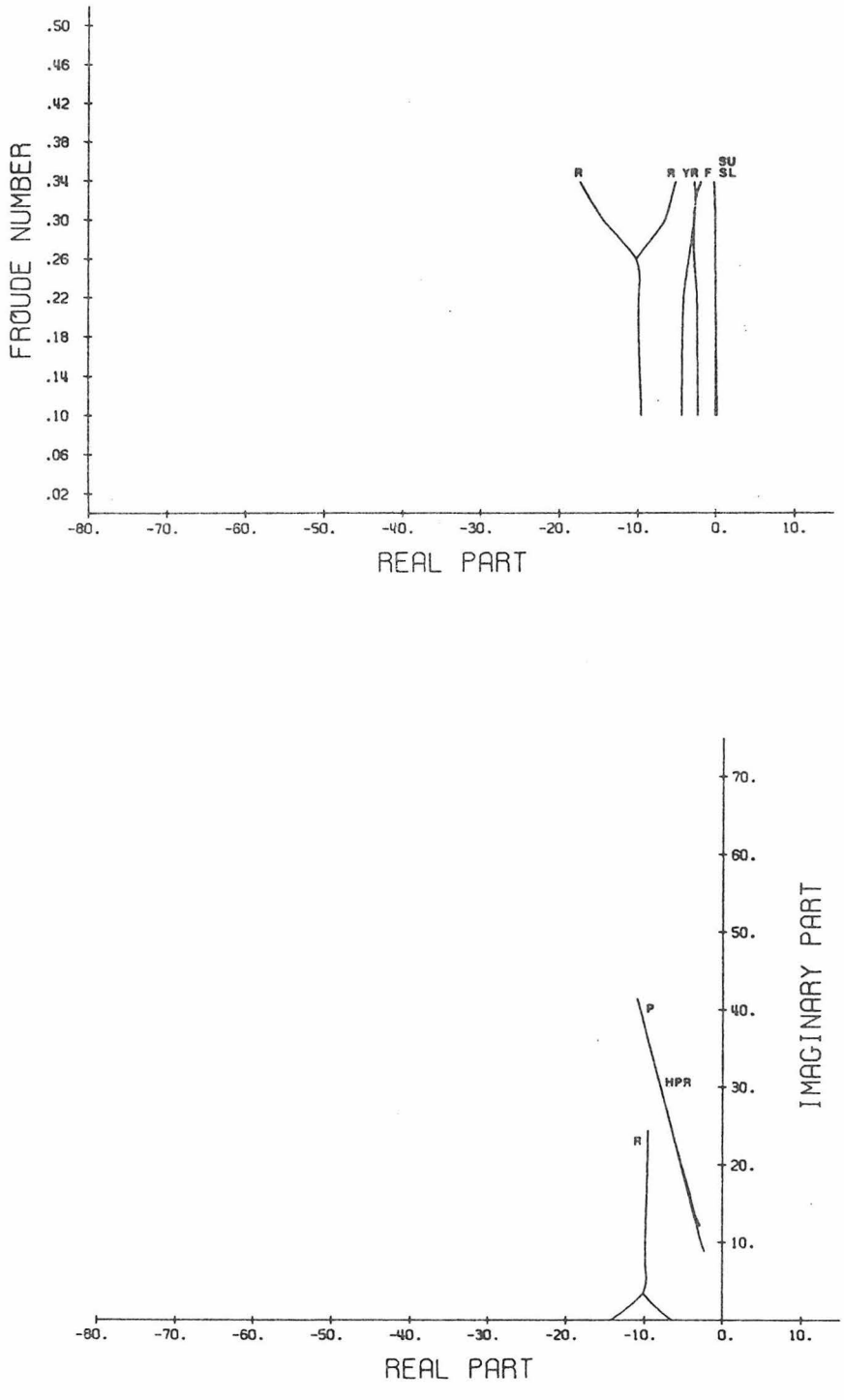


Figure C.17. $\gamma = -140^{o}$ (Beat)

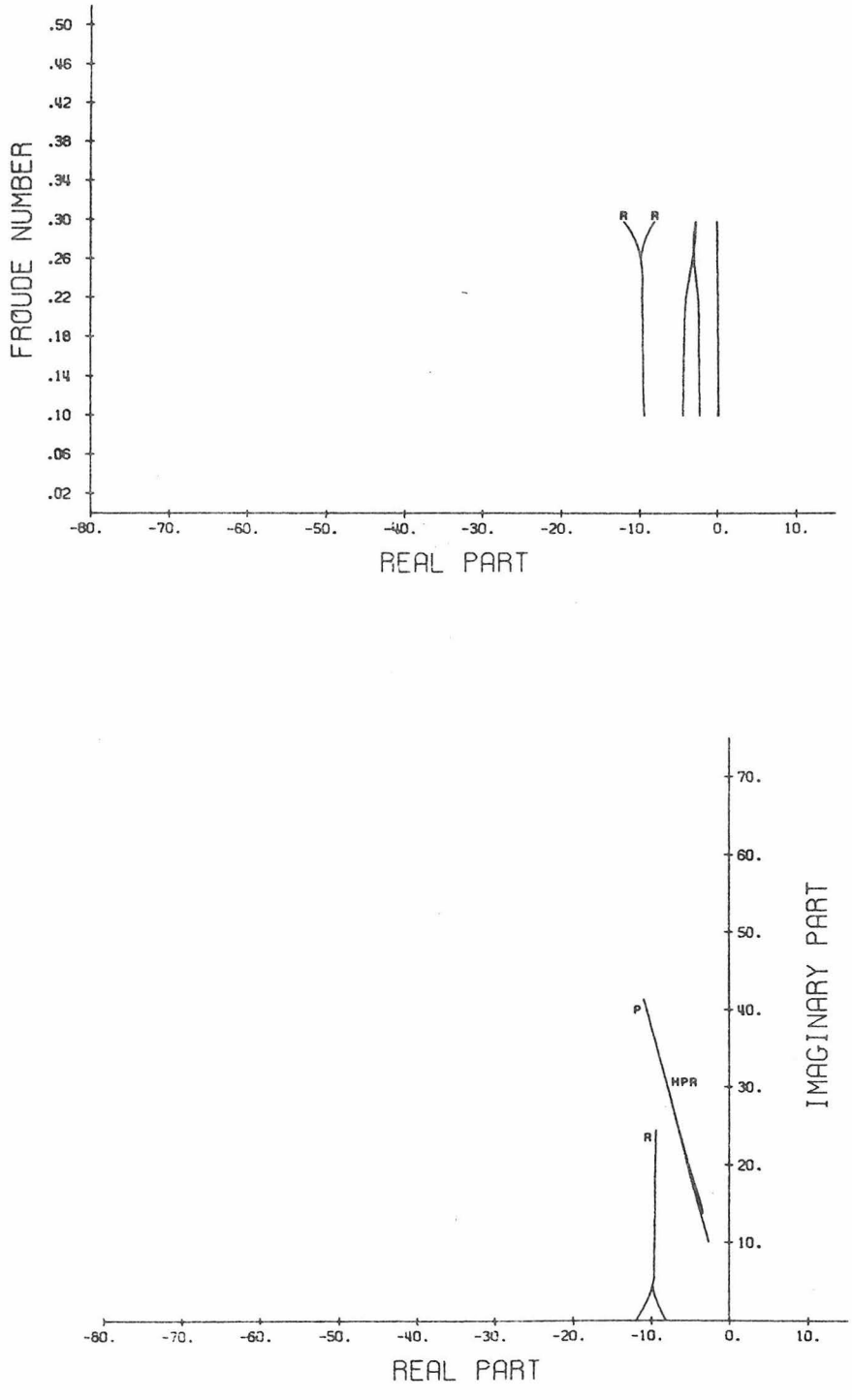


Figure C.18. $\gamma = -145^{\circ}$ (Beat)